VISCOELASTIC BEHAVIOR OF ARTICULAR CARTILAGE IN UNCONFINED COMPRESSION

A Thesis
Presented to
The Academic Faculty

by

Patrick A. Smyth

In Partial Fulfillment
of the Requirements for the Degree
Master of Science in the
Woodruff School of Mechanical Engineering

Georgia Institute of Technology
May 2013

VISCOELASTIC BEHAVIOR OF ARTICULAR CARTILAGE IN UNCONFINED COMPRESSION

Approved by:

Dr. Itzhak Green, Advisor
Woodruff School of Mechanical Engineering
Georgia Institute of Technology

Dr. Robert Jackson
School of Mechanical Engineering
Auburn University

Dr. Raymond Vito
School of Mechanical Engineering
Georgia Institute of Technology

Date Approved: 27 March 2013

ACKNOWLEDGEMENTS

The author would like to acknowledge the support and guidance of Dr. Itzhak Green, Dr. Robert Jackson, and Dr. Reid Hanson, whose direction and expertise has been invaluable. An extension of gratitude must also be made to the Auburn University School of Mechanical Engineering and College of Veterinary Medicine, and in particular to Hyeon Lee, Ryan Whitmore, Grant Kirkland, Hamed Ghaednia, Kelcie Theis, Chad Malpass, Hannah Young and Ashton Richardson. The author would also like to acknowledge the financial support of NSF Grant No. DGE-1148903.

TABLE OF CONTENTS

LIST OF TABLES

LIST OF FIGURES

NOMENCLATURE

CERF	Complementary error fractional derivative model
$E(t)$	Viscoelastic relaxation modulus
$\dot{E}(t)$	Time derivative of relaxation modulus
E_∞	Rubbery (equilibrium) modulus
E_0	Glassy (instantaneous) modulus
$E'(\omega)$	Storage modulus
$E''(\omega)$	Loss modulus
$E^*(\omega)$	Complex modulus
E_r	Reduced relaxation modulus
$erfc$	Complementary error function
GOF	Goodness of fit
i	Imaginary unit
∞	Long-term, steady-state
$\mathcal{F}$	Fourier domain
$\mathcal{L}$	Laplace domain
$norm$	Mathematical norm of vector
R^2	Coefficient of determination
s	Laplace variable
t	Time
TC	Time constant

Greek Symbols:

α	Fractional derivative constant
$\epsilon(t)$	Strain
$\dot{\epsilon}(t)$	Time derivative of strain

η	Dashpot time constant
Γ	Gamma function
μ	Complementary error function model material constant
ω	Frequency (rad/s)
$\sigma(t)$	Stress

SUMMARY

Previous decades of cartilage research have predominantly focused on decoupling the solid and fluid interactions of the mechanical response. The resulting biphasic and triphasic models are widely used in the biomechanics community. However, a simple viscoelastic model is able to account for the stress-relaxation behavior of cartilage, without the added complexity of solid and fluid interactions. Using a viscoelastic model, cartilage is considered a single material with elastic and dissipative properties. A mechanical characterization is made with fewer material parameters than are required by the conventional biphasic and triphasic models. This approach has tremendous utility when comparing cartilage of different species and varying healths. Additionally, the viscoelastic models can be easily extended in dynamic analysis and FEA programs.

Cartilage primarily experiences compressive motion during exercise. Therefore, to mimic biological function, a mechanical test should also compress the cartilage. One such test is a viscoelastic stress-relaxation experiment. The Prony and fractional calculus viscoelastic models have shown promise in modeling stress-relaxation of equine articular cartilage. The elastic-viscoelastic correspondence principle is used to extend linear viscoelasticity to the frequency domain. This provides a comparison of articular cartilage based on stored and dissipated moduli. The storage and loss moduli metrics are hypothesized to serve as benchmarks for evaluating osteoarthritic cartilage, and provide guidelines for newly engineered bio-materials.

The main goal of the current study is to test the applicability of modeling articular cartilage with viscoelastic models. A secondary goal is to establish a rigorous set of harvesting techniques that allows access to fresh explants with minimal environmental

exposure. With a complex substance like cartilage, it is crucial to avoid unnecessary *in vitro* environmental exposure. Additional areas of study include: determining the strain-dependency of the mechanical response, exploring the response of cartilage in different fluid mediums such as saline, synovial fluid, and synthetic substitutes, and studying the time-dependent properties of cartilage during stress-relaxation experiments. Equine stifle joints, which are mechanically analogous to human knees, are harvested and used for analysis in this study. It is believed that the proposed viscoelastic models can model other articulating joints as well. If viscoelastic theory can be used to characterize cartilage, then comparisons can be drawn between real and artificial cartilage, leading to better joint replacement technology.

CHAPTER I

INTRODUCTION

Cartilage provides compressive load support and facilitates near frictionless motion within articulating joints. This flexible substance must allow for motion within the joint while protecting the bone ends from grinding and wear. When this protection fails, the cartilage surface breaks down. This is known as osteoarthritis, which is a common degenerative disease that is painful and often debilitating in humans and other animals. For humans, artificial joint replacement is often the best option to remedy a degraded joint, at the cost of many thousands of dollars and lost-time during rehabilitation [1]. Although artificial joint technology is improving, a joint replacement has an average life of only 15 years [2], and is subject to catastrophic failure if the mechanical replacement becomes unseated in the joint capsule. It is desired to study cartilage to better understand the mechanics of an articulating joint, in hopes that degradation can be prevented or offset.

In healthy joints, cartilage transfers weight while experiencing little to no wear. If we characterize the structural properties of cartilage, we can create more effective mechanical connections, such as porous and/or flexible bearings. Cartilage is viscoelastic in nature, which allows for elastic and dissipative mechanisms to exist. This may contribute to the effectiveness of cartilage as a low-wear material. Studying cartilage could yield biomimetic advances, such as flexible bearings in rotordynamic systems [3, 4], or improved porous bearings in industrial applications [5].

Cartilage is a unique medium and has been the study of decades of research [6, 7]. Most of this work has focused on the interactions of the collagen matrix and the

lubricating synovial fluid that permeates the joint capsule [8, 9, 10, 11, 12]. In addition, many attempts have been made to develop constitutive relations for cartilage. The prevailing theories account for the biphasic (solid-fluid) and triphasic (solid-fluid-ionic) properties of cartilage. These models represent significant contributions to the constitutive equations of cartilage; however, the utility of a simple model that gives elastic and dissipative properties is apparent. From this model, mechanical comparisons between joints can easily be made, as well as between healthy and osteoarthritic cartilage.

1.1 Objectives

Viscoelasticity is fundamental to the unique nature of cartilage. For that reason, it is desired to characterize the viscoelastic response of cartilage. The viscoelastic properties of a medium can be determined from multiple methods, such as stress-relaxation, creep, and dynamic testing. The stress-relaxation experiment is particularly useful because it contains a wide spectrum of storage and loss properties. The primary objective of the current study is to apply classic viscoelastic models, such as the Prony series and fractional derivative, to experimental data from stress-relaxation experiments. The time-dependent material properties of cartilage can be characterized from this information.

Freshly harvested cartilage explants from horses are analyzed with a CETR-UMT-3 tribometer. The tribometer can perform precise stress-relaxation experiments, and measure the thickness of cartilage explants. This information is used to determine the storage and loss moduli of cartilage, which correlate to the stiffness and damping properties of mechanical systems. In the current study, multiple cartilage plugs are analyzed and a benchmark is established for healthy cartilage. A deviation from the benchmark may indicate osteoarthritis. Additional goals for the study include: determining an effective time constant for the relaxation behavior, and analyzing

multiple lubricating mediums for differences in mechanical response. Mow, Lai and others [13, 14] have shown that the mechanical properties of cartilage are strain-dependent. A final goal of the work is to propose a linear viscoelastic model that is also strain-dependent.

1.2 Scope

Healthy cartilage is an effective load support and motion facilitating medium. The current work aims to understand some of cartilage's mechanical properties. For medical applications, it is desired to develop a "macro" understanding of cartilage in healthy versus osteoarthritic situations. Additionally, the elastic and dissipative mechanisms in cartilage need to be understood. Artificial joint replacements might not match the storage and loss properties of real cartilage over the entire physiological spectrum of motion. It is possible that this contributes to the premature wearing of artificial joints. Mow [7] has shown that the ionic nature of cartilage and synovial fluid contributes to the mechanical response by drawing fluid into the porous cartilage matrix. In the current work, cartilage plugs are submerged in saline, synovial fluid, hyaluronic acid, and other mediums. The viscoelastic response is then compared between bathing mediums.

The overarching goal of the current study is to develop and apply viscoelastic models to cartilage samples. The main limitation of the work is a relatively small number of samples. The Student's t test is used to statistically analyze the experimental data, but like many biological studies, the number of samples is small and the variation is large. However, the viscoelastic nature of the individual samples is marked. The following chapter discusses the literature related to the mechanical characterization of articular cartilage.

CHAPTER II

LITERATURE SURVEY

This chapter is an overview of the fundamentals of cartilage mechanics. First, a general description of cartilage is given, followed by a chronological review of two leading theories of cartilage mechanics. Viscoelasticity is introduced, but not fully developed until the next chapter.

2.1 Cartilage

Cartilage provides compressive load support of articulating joints and cushions the impact of physical contact between bone surfaces. In healthy joints, cartilage is a nearly frictionless and low wearing substance. Cartilage functions with a variety of complex interactions between the solid collagen structure and the lubricating synovial fluid. A brief biological description of cartilage is included in the next section, with an emphasis on mechanical modeling.

2.2 Cartilage Composition

Articular cartilage appears smooth and white under macro observation (Fig. 2.1). However, high magnification shows that cartilage is rough on the order of micrometers. Its peaks and valleys trap and retain synovial fluid, which helps support joint function. Structurally, articular cartilage is composed of a porous web of chondrocytes. The chondrocytes produce the cartilage matrix, composed mainly of collagen fibers in four layers: the superficial, middle, deep, and calcified.

Cartilage is effective in part because it is flexible and durable. This flexibility facilitates motion and protects joints from impact and wear. In healthy joints, cartilage can retain function for the user's life; however, damaged joints can degrade to painful

Figure 2.1: View of cartilage from macro-scale

and debilitating conditions. Cartilage does not recover quickly (or at all) when damaged because there is negligible blood flow to the collagen structure. Instead, nutrients must be transferred to cartilage through diffusion, which is less effective and more time consuming. The mechanical functionality of cartilage, combined with poor recovery when damaged, has motivated many decades of study. However, physiological, mechanical, and rheological problems remain to be studied.

Cartilage is a four layer web of collagen fibers (Fig. 2.2). Each of the four layers contains a different orientation of collagen. Viewed in a cross-section (Fig. 2.2), the superficial layer contains fibers in a tangential orientation. These fibers resist shearing forces, while the deeper layers are oriented in a vertical direction to resist compression. The collagen fibers create a porous matrix that allows synovial fluid to absorb into the body. Synovial fluid is squeezed from the matrix during compression, resulting in energy dissipation. The vacated collagen body has a charge imbalance that draws fluid back into the matrix when the compressive force is released. The solid and fluid interactions have underpinned models that separate the contributions of the two phases. Viscoelastic theories characterize cartilage by assuming that it is

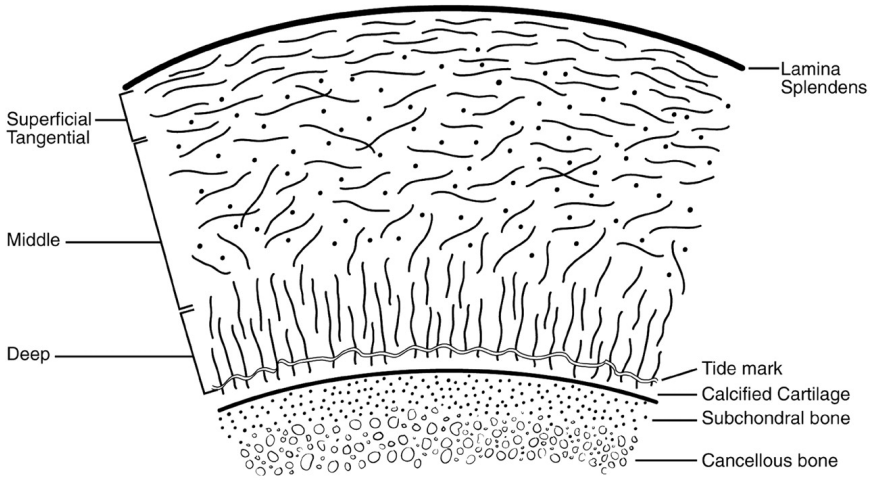

Figure 2.2: Schematic of the collagen structure of cartilage from the superficial to deep layers [15]

a homogeneous material that has dissipative capabilities.

Cartilage is particularly difficult to model because it is unique to the user. However, some important conclusions can be drawn and applied to the fields of mechanics, biomimetics, artificial replacements, and medicine. These include the amount of modulus retained and dissipated in the cartilage matrix, the time and frequency dependent behavior of cartilage for a range of physiological gaits, the relaxation behavior of cartilage in different lubricating mediums, and the response of cartilage to different strains. The listed items are objectives of the current study.

2.3 Cartilage Models: Foundation

Dating back to the 1940's, researchers have attempted to characterize the mechanical and lubricating nature of cartilage [6, 16]. Early researchers recognized that cartilage is unique in many ways. Not only does cartilage serve as the cushion for joint interactions, it also facilitates motion by excreting and retaining lubricant in the synovial capsule. Modern models attempt to obtain a mechanical characterization of cartilage that can explain, or at least acknowledge, the interactions of the solid matrix and fluid lubricant. However, cartilage continues to be difficult to characterize completely

and robustly.

In the 1960's and 70's researchers studied the nonlinear relationship of stress and strain in biological tissues. In work from 1967, Fung [17] shows the strong nonlinear behavior of tissue from rabbit explants. Although the work does not look at cartilage specifically, the viscoelastic nature of living tissue is described. Fung shows that the hysteresis loop of living tissue is nearly strain-rate independent, indicating nonlinear viscoelastic behavior. Fung's research is instrumental in developing the field of tissue mechanics, which is within the realm of continuum mechanics but deviates from standard solid mechanics. Biological tissues typically undergo much higher strains than classical materials, and are usually constitutively modeled differently. However, cartilage deviates less from solid mechanics than other biological substances such as arteries and ligaments. For this reason, many classical mechanics theories are utilized to characterize cartilage.

In 1971, Kempson et al. [18] pioneered a study of cartilage as a viscoelastic medium. Kempson et al. saw viscoelastic behavior in cartilage when performing indention and uniaxial tension tests. The samples were tested in a bath of Ringer's solution to maintain physiological conditions as closely as possible. The Poisson's ratio of cartilage was experimentally determined to be near 0.5, similar to rubber. Kempson et al. did not specifically correlate their findings to viscoelastic theory; however, the similarity of cartilage to rubber and the finding of a creep mechanism formed the basis of cartilage viscoelasticity. Many further attempts have been made to define constitutive equations that govern cartilage. The two leading categories of models are presented in the following sections.

2.4 Cartilage Models: Biphasic/Triphasic Theory

Mow and Mansour (1977) [19] are attributed with the first known stress-relaxation experiment on cartilage. They used a rigid confining chamber, porous indenter, load

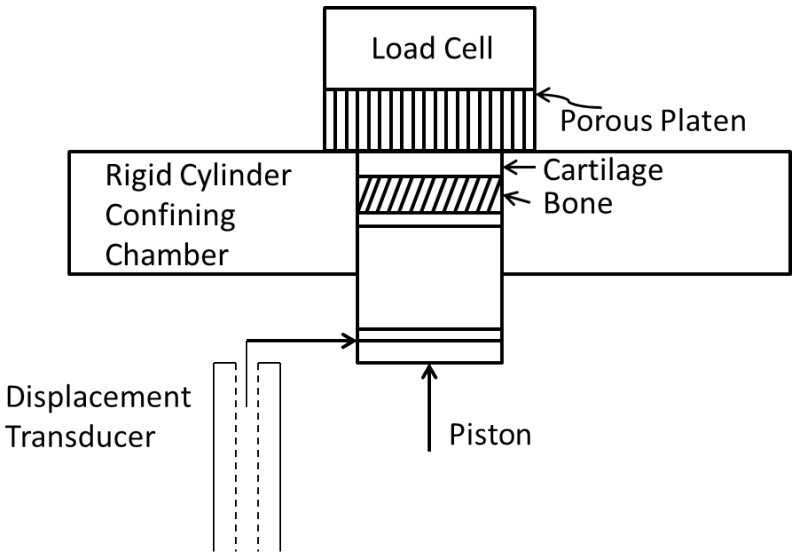

Figure 2.3: Reproduction of test setup used by Mow and others [13, 21, 19]

cell, and piston to perform relaxation experiments (Fig. 2.3). Lipshitz et al. [20] also used the test rig to perform stress-relaxation experiments on cartilage from bovine samples. A biphasic, rheological model consisting of a Kelvin-Voigt solid and an incompressible fluid was proposed to model the relaxation behavior. The model qualitatively describes the viscoelastic relaxation of cartilage, but conclusive results are not obtained. A confining cylinder is used in the experiments. The cylinder is intended to simplify the model; however, it makes the results difficult to interpret because the stress in the cartilage matrix is complex at the boundaries, rather than uniaxial. Additionally, the experimental procedure involves loading the cartilage in phases, which allows for relaxation between data collection sets. An instantaneous, or near instantaneous, displacement must be imposed for a stress-relaxation experiment to truly capture all of the dissipation.

In 1978, Eisenfeld, Mow and Lipshitz [21] mathematically describe the stress-relaxation behavior of cartilage in confined compression, and qualitatively validate their biphasic model [19]. In the model, a nonlinear, permeable, Kelvin-Voigt viscoelastic solid is assumed to interact with an incompressible fluid. These interactions

are governed by a consolidation mechanism and a Darcy type nonlinear permeability relationship. This is a fundamental advance in the biphasic theory.

The first major biphasic model is attributed to Mow et al. [13] in 1980. The model describes the coupled solid (20% by weight) and fluid (80% by weight) contributions of cartilage. The solid and fluid phases are assumed incompressible and non-dissipative, so the relaxation (dissipative) mechanism is attributed to the frictional interactions between the solid and fluid phases. Similar to previous tests by Mow and Lipshitz [22], the cartilage specimens are placed in a confining chamber and compressed with a porous filter. Recall that this type of testing creates complex stress fields. The stress-relaxation experiments are performed with a ramp displacement, where the ramp time, t_0, is approximately 2 seconds. Some mismatch between the model and experiment is introduced here because the relaxation model is derived with an instantaneous displacement (Heaviside unit step). Although Mow's model has some shortcomings, it is the fundamental articular cartilage model in the biomechanics community.

In 1981, Lai, Mow and Roth [14] address the permeability of cartilage and its effect on cartilage stress response. The biphasic model used considers the solid matrix as linear elastic; however, the experimental data shows strain-dependency (nonlinearity). The authors propose that permeability is non-linear and accounts for the viscoelastic-like behavior seen. Additional studies also attempt to resolve the appearance of viscoelasticity in the solid cartilage matrix. The biphasic model must satisfy infinitesimal strain theory, which is one limitation of this study. For fast compression tests, the biphasic model is unable to track the material behavior. This explains the ramp input that is used consistently in stress-relaxation experiments. Physiologically however, a ramp input is an unlikely loading scenario during normal exercise.

Armstrong (1984) [23] extends the biphasic theory of Kuei, Lai, and Mow (KLM) [13] for the case of stress-relaxation in unconfined compression. The experiment is

designed with rigid plates in place of porous indenters. The relaxation results show marked differences between confined and unconfined compression experiments. Not only does the solid portion of the cartilage experience a different stress field, the direction of fluid movement is different between tests. In unconfined compression, fluid moves laterally away from the plates, whereas in confined compression the fluid excretes in the direction of displacement. Therefore, a porous indenter is required in confined compression experiments. In physiological joints, both mechanisms exist simultaneously. For modeling purposes, one direction of fluid transfer is typically chosen to reduce complexity.

In 1986, Mak [24] extends the biphasic model to include viscoelasticity in the bulk and shear deformations of the cartilage matrix. The interstitial fluid is considered inviscid and incompressible. Mak determined that viscoelasticity in the solid phase of cartilage is an important driver in the mechanical response. The revised model mimics relaxation behavior from confined compression, rate-controlled experiments. However, a "true" relaxation experiment, with an instantaneous displacement imposed on an unconfined sample, is not compared in this work.

Many additions and modifications to the biphasic theory are made in the 1990's and 2000's. In 1990, Holmes and Mow [25] extend the biphasic theory to include finite deformations (hyperelastic biphasic theory). Ateshian et al. [12] corroborate this theory in 1997 with experimental results. In 1999, Suh and DiSilvestro [26] perform short ramp time stress-relaxation experiments to test the biphasic theories of Mow et al. [13] and Mak [24]. The unconfined compression results show that Mow's biphasic theory is unable to capture short-term (less than 50 seconds) relaxation behavior, although it is excellent in describing long-term (longer than 50 seconds) behavior. Mak's biphasic model is better suited for describing relaxation mechanisms. DiSilvestro, Zhu and Suh [27] validate this in 2001.

Lai et al. [28] show that the ionic properties of cartilage effect the mechanical response. The significance of the ionic charge in cartilage and its effect on the material response is noted; however, quantification is understandably difficult. The triphasic nature of cartilage explains how fluid is drawn back into the cartilage matrix after being excreted during compression. The biphasic and triphasic models both separate the solid and fluid components of cartilage and attempt to characterize the interactions between each phase. While this is a physically intuitive way to model cartilage, it is also very complex. The complexity does not necessarily increase the model's fidelity, which is why the current research models cartilage as a single viscoelastic material.

The experimental procedures used by Mow, Mak and others remain the predominate means for testing cartilage today. It is important to note some differences in confined and unconfined compression. An instantaneous displacement cannot be readily imposed on the cartilage plugs in confined compression. The confining chamber creates very high stresses in the cartilage plugs when a fast displacement is imposed (assuming that the porous filter allows negligible fluid flow during compression). Additionally, the confining chamber creates a 3D stress field on the cartilage plug throughout. This is because the cartilage is restrained by the rigid walls of the chamber. Consider an isotropic, elastic material- the stress and strain relations are determined as follows in cylindrical coordinates [29]:

$$\{\sigma\} = \begin{Bmatrix} \sigma_r \\ \sigma_\theta \\ \sigma_z \end{Bmatrix} = \frac{E}{(1+\nu)(1-2\nu)} \begin{bmatrix} 1-\nu & \nu & \nu \\ \nu & 1-\nu & \nu \\ \nu & \nu & 1-\nu \end{bmatrix} \begin{Bmatrix} \epsilon_r \\ \epsilon_\theta \\ \epsilon_z \end{Bmatrix} \tag{2.1}$$

or for strain in terms of stress:

$$\{\epsilon\} = \begin{Bmatrix} \epsilon_r \\ \epsilon_\theta \\ \epsilon_z \end{Bmatrix} = \frac{1}{E} \begin{bmatrix} 1 & -\nu & -\nu \\ -\nu & 1 & -\nu \\ -\nu & -\nu & 1 \end{bmatrix} \begin{Bmatrix} \sigma_r \\ \sigma_\theta \\ \sigma_z \end{Bmatrix} \tag{2.2}$$

Referencing Eq. 2.1, Poisson's ratio is needed in the confined compression case ($\epsilon_r = \epsilon_\theta = 0$) to obtain stress in the z (vertical) direction (σ_z):

$$\sigma_z = \left[\frac{E}{(1-\nu^2)(1-2\nu)} \right] \epsilon_z \tag{2.3}$$

Poisson's ratio must be assumed or determined experimentally, which adds an additional parameter to the models using confined compression experiments. It is likely that Poisson's ratio is also time and frequency dependent, and is difficult to determine. Poisson's ratio is *not* needed for the unconfined compression case ($\sigma_r = \sigma_\theta = 0$) because stress and strain are related only by E (refer to Eq. 2.2):

$$\sigma_z = E\epsilon_z \tag{2.4}$$

In summary, the stress fields for confined and unconfined compression experiments are theoretically related by Poisson's ratio for linear elasticity and viscoelasticity. However, the determination of Poisson's ratio is difficult and adds an additional parameter to cartilage models. For this reason, unconfined compression experiments are used in the current study. It should also be noted that the relationships above are spatial in nature, not temporal, so they remain valid for linear viscoelasticity.

2.5 Cartilage Models: Standard Linear Solids

An alternative way of modeling cartilage is to consider the solid and fluid interactions as part of a total mechanical response. The goal is to model the total response of cartilage as a single material. Viscoelasticity is well-suited for this type of analysis because it already includes a mechanism for dissipation. This dissipation can come

from frictional drag between the solid and fluid phases, compressibility of the solid matrix, or other mechanisms. A viscoelastic material only considers the total (net) dissipation. There is a risk that viscoelasticity will not have enough fidelity to accurately model cartilage. However, the use of fewer material parameters allows for an extremely convenient comparison between samples for any number of metrics, such as health, age, weight, use, breed, etc. The following review encompasses the highlights of cartilage modeling with viscoelastic theory.

Coletti et al. [30] drew a correlation between articular cartilage and standard viscoelastic models in 1972. Uniaxial tension tests were performed on cartilage specimens from rabbits. The observed creep behavior was then compared to a Kelvin-Voigt solid model in series with another spring. The authors found that articular cartilage exhibits non-linear viscoelastic behavior dependent on strain.

In 1976, Woo et al. [31] used Fung's exponential stress/strain relationship to model articular cartilage. The authors studied the elastic properties of articular cartilage in uniaxial tension. The goal was to find the material properties of cartilage at various depths and orientations. Woo found a similar non-linear stress/strain response in cartilage that Kempson [18] and others had noted. Woo also saw different responses based on the orientation of the collagen fibers, and the depth of the test.

In separate research in 1977, Parsons and Black [32] study the viscoelastic creep response of cartilage in shear. The tests were performed with a cylindrical ram while the samples were immersed in saline at physiological temperatures. The viscoelastic model uses three Kelvin solid elements in series with an additional spring. Parsons and Black discuss the difficulty of extracting intrinsic mechanical properties of cartilage from indention data. Aside from different testing procedures among researchers, the difficulty of obtaining intrinsic parameters is also due to a lack of a robust theoretical solution that accounts for the complexity of cartilage. The proposed equation to realize the properties of cartilage is based on creep compliance (J), which is the

inverse of the shear modulus. The results show decent agreement with the literature available at the time. Parsons and Black recognize the importance of finding the intrinsic properties of cartilage, which can be used to compare between joints and among species.

In an additional paper, Parsons and Black [33] discuss the ionic concentration of the lubricating fluid. The concentration plays an important role in the mechanical response of articular cartilage. This is an early attempt to describe the triphasic nature of cartilage. The study shows that cartilage must be immersed in a fluid to prevent dehydration, and *in vitro* testing should consider the ionic properties of the lubricating medium.

At the same time as the biphasic model is being developed in 1980, Woo et al. [34] looks at cartilage samples in tension, performing stress-relaxation experiments. The results are connected to viscoelastic theory. Fung's model [17] for soft tissue is utilized in the work. The experiments compare favorably to the compression relaxation experiments of Mow and others [22].

Extending the model proposed by Fung [17], Simon et al. [35] performs relaxation experiments on cartilage specimens. The biphasic and the standard viscoelastic solid models are compared. Simon's work shows the advantage of viscoelastic theory- it looks at the macro-scale response of cartilage. This is also the disadvantage of the viscoelastic model if it is desired to separate the biphasic contributions. Viscoelasticity does not separate contributions of the solid matrix and interstitial fluid.

In 2000, Ehlers and Markert [36, 37] propose using a generalized Maxwell model (Prony series) to characterize cartilage. No empirical data is provided, but finite-element models (FEM) are created as examples. Wilson et al. (2004-2005) [38, 39] use a modified viscoelastic solid to model the fibril part of cartilage. The spring in the Maxwell element is taken to be strain-dependent (non-linear). This is a modification of the linear model proposed by Wang [40]. The poroviscoelastic fibril reinforced

model developed by Wilson et al. considers the local morphology of collagen fibers and their apparent strong influence on stress and strain. The work compares to DiSilvestro and Suh's [41] favorably. Garcia et al. [42] use a similar model to Wilson's [38, 39] to describe the solid portion of the nonlinear biphasic model. Julkunen et al. [43] corroborate the work of Wilson et al. [38, 39] with a FEM study, finding good agreement between experiment and model in stress-relaxation applications.

A recent paper from June et al. [44] discusses the stress-relaxation behavior of cartilage at varying compressive stresses. June at al. found that the time constant of relaxation experiments changes with strain. Specifically, relaxation occurs more slowly under higher compressive strains. These results are consistent with theories from polymer dynamics. A second paper from June et al. [45] shows that the ionic concentration of the fluid bath the influences stress-relaxation response. This finding is concomitant to the idea of a triphasic response in cartilage.

Many models exist to characterize the mechanical behavior of cartilage. The sheer number of theories proves that a satisfactory model for cartilage does not exist yet. The biphasic and standard solid theories have distinct advantages and disadvantages. For a larger-scale analysis based on total mechanical response, viscoelastic theory is much easier to employ and interpret. When evaluating the predictive capabilities of a model, viscoelastic theory is readily implemented in full-scale motion studies. This is a distinct advantage over the biphasic theories. For that reason, viscoelastic models are used in the current study. The next chapter introduces two viscoelastic models that are used in this work.

CHAPTER III

VISCOELASTIC THEORETICAL BACKGROUND

The mechanical properties of cartilage can be linked to viscoelastic theory. A brief overview of viscoelasticity is useful for the rest of the work. Viscoelasticity describes a material behavior that is time-dependent, or retains memory of the material history. This is in contrast to an elastic material, which is time invariant. The current work is concerned with uniaxial loading only, in which linear elastic materials obey Hooke's Law, where stress is linearly proportional to strain:

$$\sigma = E\epsilon \tag{3.1}$$

In Eq. 3.1, σ is the stress, ϵ represents strain, and E is Young's modulus. Each of these quantities is independent of time. However, for a material that retains memory of the past, the material "history" must be accounted for. In 1962, Gurtin and Sternberg [46] developed a constitutive law accounting for material history. This law relates stress, strain and the relaxation modulus using Boltzmann's superposition principle:

$$\sigma\left(t\right) = \epsilon\left(0\right) E\left(t\right) + \int_0^t \dot{\epsilon}\left(\tau\right) E\left(t-\tau\right)\, \mathrm{d}\tau. \tag{3.2}$$

where $\sigma\left(t\right)$ is the stress, $\epsilon\left(t\right)$ is the strain, and $E\left(t\right)$ is the relaxation modulus. Typically, $\sigma(t)$ and $\epsilon(t)$ are either set or measured during experimentation, while $E\left(t\right)$ is obtained from a fixed strain input $\epsilon = \epsilon_{step}, E(t) = \sigma(t)/\epsilon_{step}$. In comparison to Eq. 3.1, the parameters of stress, strain, and elastic modulus in Eq. 3.2 are now time-dependent. It should be noted that Eq. 3.2 describes linear viscoelasticity, i.e. there is a linear relationship between the strain history and the current stress. Transferring Eq. 3.2 into the Laplace domain allows for simple treatment of the convolution

integral:

$$\sigma(s) = sE(s)\,\epsilon(s) \tag{3.3}$$

Equation 3.3 is similar to Hooke's Law (Eq. 3.1) in the Laplace domain. This provides the foundation for the viscoelastic-elastic correspondence principle. The elastic element, E, in Eq. 3.1 has simply been replaced with a viscoelastic element, $sE(s)$, in Eq. 3.3. For a physical understanding of the viscoelastic-elastic correspondence principle, see Appendix A.

To transfer between the Laplace and frequency domains, the s in Eq. 3.3 can simply be replaced with $i\omega$, where i is defined as $\sqrt{-1}$ and ω is the frequency in rad/s. The analytical forms of the Laplace and Fourier domains show the relationship between s and $i\omega$:

$$\mathcal{L}\{g(t)\} = G(s) = \int_0^\infty g(t)e^{-st}\,\mathrm{d}t. \tag{3.4}$$

$$\mathcal{F}\{g(t)\} = G(\omega) = \int_{-\infty}^\infty g(t)e^{-i\omega t}\,\mathrm{d}t. \tag{3.5}$$

Hence, applying $s \to i\omega$, Eq. 3.3 becomes:

$$\sigma(\omega) = (i\omega)\,E(\omega)\,\epsilon(\omega) \triangleq E^*(\omega)\epsilon(\omega) \tag{3.6}$$

where:

$$E^* = (i\omega)\,E(\omega) \tag{3.7}$$

E^* is the complex modulus, which has two components- a real and an imaginary:

$$E^*(\omega) = E'(\omega) + iE''(\omega) \tag{3.8}$$

The real component (E') is known as the storage modulus, while the imaginary component (E'') is known as the loss modulus. Both measures describe the dynamic behavior of viscoelastic materials, in this case cartilage. The correspondence principle

is powerful because one constitutive formulation determines the amount of modulus retained (stored) or lost (loss). Stress-strain constitutive equations must be formed that accurately model the experimental data. Two such models will be discussed later in this chapter. Before analyzing the constitutive models used to characterize a viscoelastic material, a physical description of viscoelasticity is provided.

As mentioned, a viscoelastic material has a time-dependent nature. Consider a uniaxial experiment- if a fixed force (or stress) is imposed on the material, a phenomenon known as creep occurs, where the material continues to change dimension (length, or strain) over time. Alternatively, if a fixed displacement (strain) is placed on the material, the phenomenon of stress-relaxation occurs. This can be seen in Fig. 3.1, where the relaxation behavior, $E(t) = \sigma(t)/\epsilon_{step}$, occurs as time progresses. As indicated above, in the frequency domain, a viscoelastic material has two components, the storage and loss moduli, as shown in Fig. 3.2.

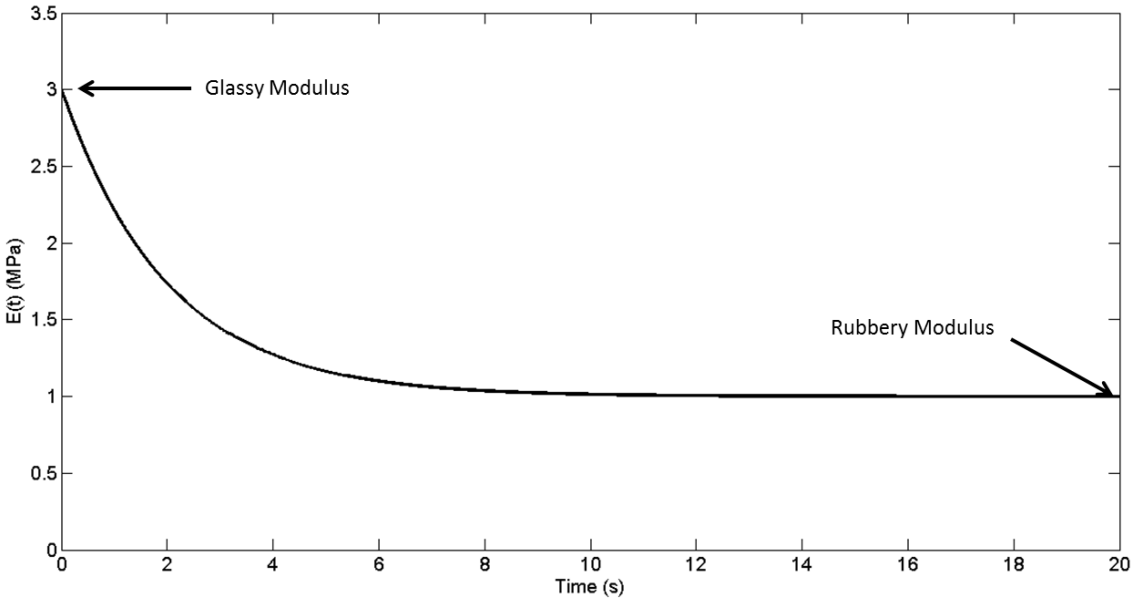

Figure 3.1: Stress relaxation experiment output

For discussion purposes, assume that the relaxation curve can be described by the equation: $E(t) = 1 + 2e^{(-1/2t)}$ (MPa). Two definitions will be used throughout this work: the glassy and rubbery moduli. These definitions are historically used in viscoelasticity, but should not be considered as literal explanations of material behavior. An example of viscoelastic behavior is seen in glass. At room temperature, glass acts like a brittle material, and will fracture if brought to failure accordingly. However, at high temperatures, glass flows like rubber when acted upon. These historic definitions describe the time-dependent behavior of a viscoelastic material as well. The glassy modulus occurs at time $t = 0$, which corresponds to the highest frequencies or lowest temperatures, as shown in Fig. 3.2. Here, a viscoelastic material acts like a brittle material (glass). For the said example case, the value of the glassy modulus is $E_0 = 3\ MPa$. The rubbery modulus is at the opposite end of the spectrum from the glassy modulus. At the large time-scales (low frequencies), or high temperatures, a viscoelastic material flows like a rubber. For the example case, the rubbery modulus is $E_\infty = 1\ MPa$. The rubbery modulus can be zero; however, most viscoelastic materials have a non-zero rubbery modulus. The glassy and rubbery modulus will be used extensively throughout the current work, sometimes with the designation instantaneous and equilibrium modulus, respectively. For behavior between the glassy and rubbery modulus, the material is in a transition region, seen in Fig. 3.2. Notably, higher energy dissipation (indicated by the loss modulus) occurs in the transition region.

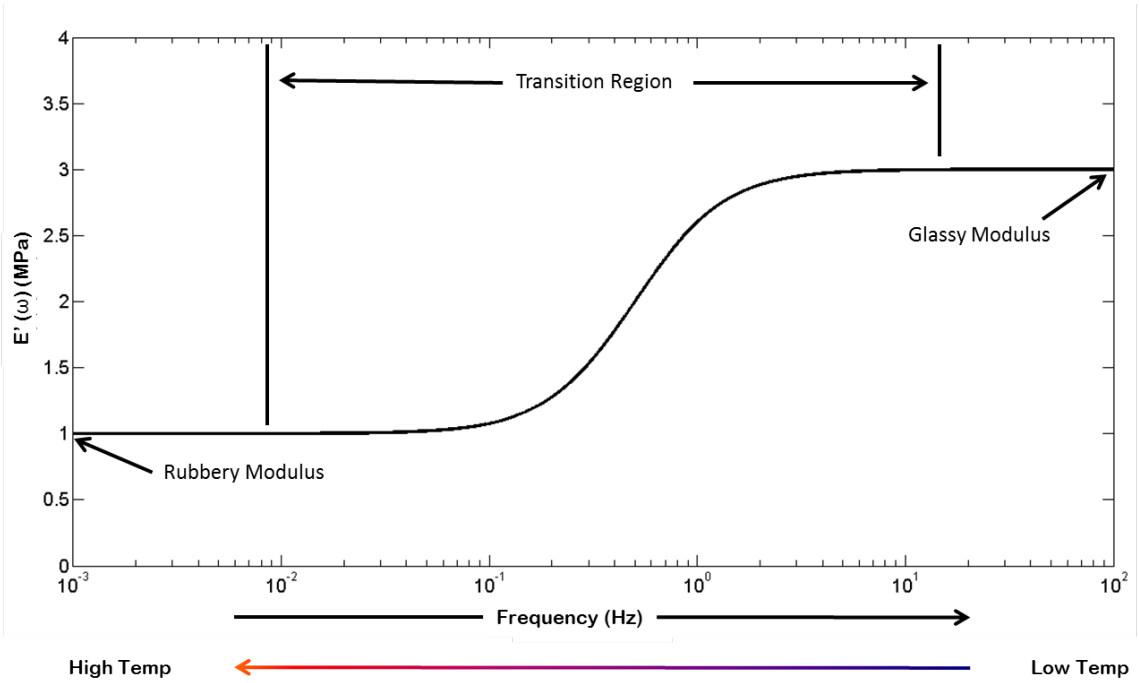

(a) Storage moduli of sample viscoelastic material (semi-log scale)

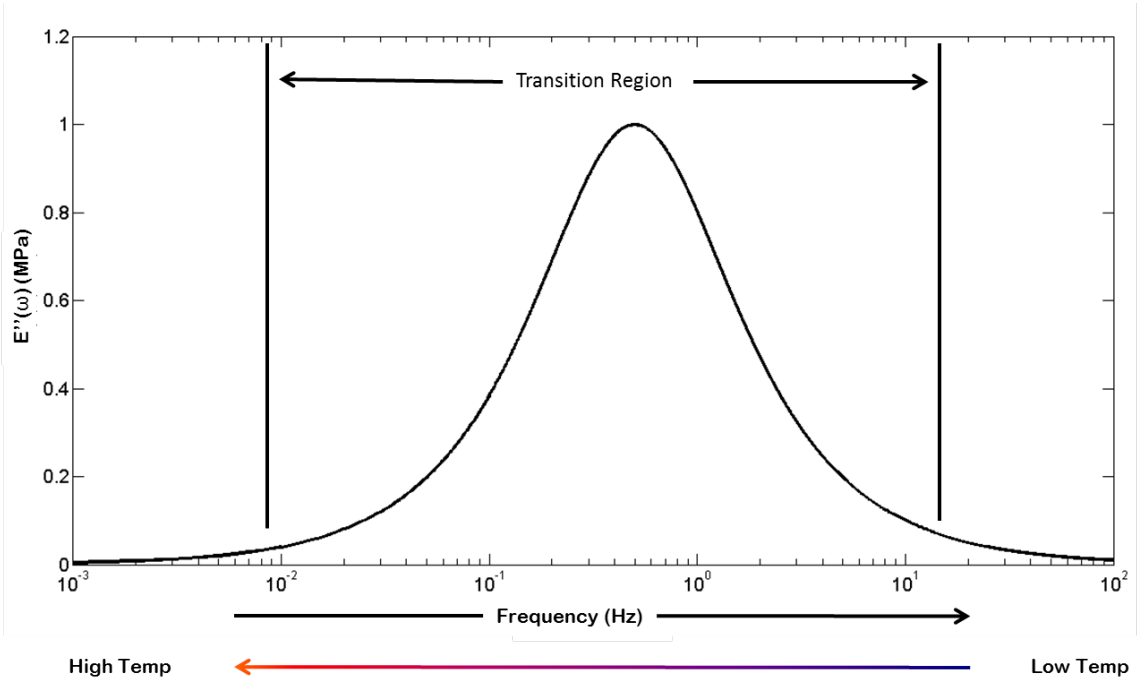

(b) Loss moduli of sample viscoelastic material (semi-log scale)

Figure 3.2: Sample viscoelastic material in the frequency domain, during a stress-relaxation experiment

3.1 Prony and Fractional Derivative Stress-Strain Constitution Laws

3.1.1 Prony Model

A viscoelastic material displays both elastic and dissipative mechanisms simultaneously [46, 47, 48]. This behavior is shown in Figs. 3.1-3.2 for a relaxation experiment. The dissipative mechanisms are rate dependent, much like a dashpot or damper in physical systems. In fact, many common models for viscoelasticity consider springs and dashpots in various configurations. The Prony series, Fig. 3.3, is one such model (See Appx. B for derivation). The Prony series model is composed of a free spring and an infinite series of Maxwell elements in parallel. Each Maxwell element is an individual spring and dashpot in series.

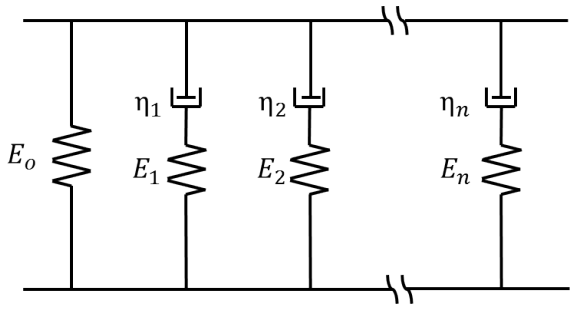

Figure 3.3: Prony series for modeling viscoelastic behavior

The Prony series captures the viscoelastic behavior described in the previous section- at high frequencies the dashpots will "lock," and become rigid. Here, only the springs contribute to the mechanical response. At low frequencies, the individual Maxwell elements have no contribution to the overall load support. The dashpots that are in series with the springs transmit negligible force, rendering the Maxwell elements ineffective. Therefore, the only load support comes from the free spring, E_0. The Prony series combines multiple exponentially decaying functions:

$$\sigma_T = \left(E_0 + \sum_{n=1}^{\infty} E_n e^{\lambda_n t} \right) \epsilon_0, \tag{3.9}$$

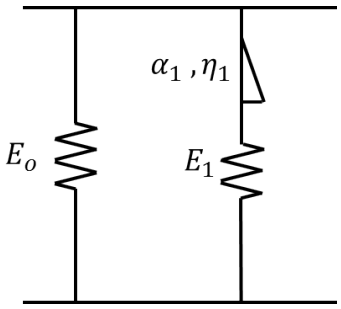

Figure 3.4: Fractional calculus model for viscoelasticity

which satisfies viscoelastic relaxation. The infinite sum in Eq. 3.9 allows for different decades of relaxation. For instance, a material that rapidly expels energy may require many short-lived decay terms, which the Prony model accommodates easily. Although the Prony series is a robust viscoelastic model, it may require a large number of Maxwell elements to fully capture material behavior. The additional terms in the Prony series expand the eigenvalue problem, and make extrapolation more difficult. A model that contains few terms, but remains accurate, is desired. The fractional derivative model is one-such model.

3.1.2 Fractional Derivative Model

The fractional derivative model reduces the number of elements, and terms, needed to robustly model viscoelasticity. The model replaces the dashpot of the Maxwell element with a fractional spring-pot, as seen in Fig. 3.4. The spring-pot interpolates between spring and dashpot behavior, giving the fractional model more flexibility. Mathematically, this is described as:

$$\sigma_P = \eta \frac{d^\alpha \epsilon_p}{dt^\alpha} \tag{3.10}$$

where α is a rational number between 0 and 1, and η is a material parameter similar to a damping coefficient. The interpolative nature of the spring-pot element is clear- if $\alpha = 0$ then the element becomes a spring. If $\alpha = 1$ then the element becomes

a dashpot. For any α between 0 and 1, the element has both spring and dashpot behavior. The relaxation modulus can be found in the frequency domain (see Appx. C for derivation):

$$E(\omega) = \frac{E_0}{i\omega} + \sum_{n=1}^{\infty} \frac{E_n (i\omega)^{\alpha}}{\left((i\omega)^{\alpha} + \frac{E_n}{\eta_n}\right)} \left(\frac{1}{i\omega}\right) \tag{3.11}$$

In the time-domain, the fractional relaxation modulus is [49, 50]:

$$E(t) = E_0 + \sum_{n=1}^{\infty} E_{\alpha} \left(-\frac{E_n}{\eta_n} t^{\alpha_n}\right) \tag{3.12}$$

Where E_{α} is the Mittag-Leffler function [51]:

$$E_{\alpha,\beta}(z) = \sum_{k=0}^{\infty} \frac{z^k}{\Gamma(\alpha k + \beta)} \tag{3.13}$$

In Eq. 3.13, Γ in the gamma function: $\Gamma(x) = (x-1)!$

The fractional model is difficult to fit in the time-domain. To be practical in modeling, a finite number of terms must be used in the summation in Eq. 3.13. If the parameter (η) is very small, k must be very large, and convergence issues arise. Typically, the fractional model is fit in the frequency domain, where the Mittag-Leffler function is not used. However, for the special case where $\alpha = 1/2$, the Mittag-Leffler function reduces and the fractional derivative model becomes the complementary error function model (CERF) [52]. The complementary error function model is a robust and convenient model for viscoelasticity. It has the advantage of a concise time-domain solution in the form of the complementary error function multiplied by an exponential function, as shown in Eq. 3.14:

$$E(t) = E_0 + \sum_{n=1}^{\infty} E_n e^{\left(\mu_n{}^2 t\right)} erfc\ (\mu_n \sqrt{t}) \tag{3.14}$$

Where E_n and μ_n are material properties and:

$$\mu_n = \frac{E_n}{\eta_n} \tag{3.15}$$

The complementary error function decays at a faster rate than the exponential increases, giving a relaxation behavior. The behavior described is shown in Appx. C. Models with time-domain representations have utility in fitting, which is discussed in Chapter 4.

The complementary error function can be computed by most engineering software packages; however, the function can be reduced with an expansion given by Abramowitz and Stegun [53]:

$$erfc(t) = (a_1 y + a_2 y^2 + a_3 y^3 + a_4 y^4 + a_5 y^5) e^{-t^2} \tag{3.16}$$

$$y = \frac{1}{1 + pt} \tag{3.17}$$

where p = 0.3275911, a1 = 0.254829592, a2 = −0.284496736, a3 = 1.421413741, a4 = −1.453152027, a5 = 1.061405429. The maximum error of this expansion is $1.5 \cdot 10^{-7}$. The expanded complementary error function in Eq. 3.16 can be used in Eq. 3.14. The result is a polynomial expression:

$$E(t) = E_0 + \sum_{n=1}^{\infty} E_n (a_1 y + a_2 y^2 + a_3 y^3 + a_4 y^4 + a_5 y^5) \tag{3.18}$$

With Eq. 3.18, fitting the time-domain relaxation modulus is straightforward. A least-squares algorithm will easily fit the polynomial expression in Eq. 3.18 to relaxation data from experiments. The CERF model has the advantages of the fractional model, with a time-domain analogue.

Models such as the modified Bessel [52] and Kelvin-Voigt also describe viscoelasticity. However, the Prony and fractional models are the most robust and reliable models for the present study. In fact, the Kelvin-Voigt model, which is used predominantly to model creep, is unable to describe relaxation without modification. In particular, the Prony and reduced fractional models are used for their time-domain fitting capabilities. These linear, viscoelastic models reduce the complexity of cartilage modeling. If viscoelastic theory can accurately model cartilage with sufficient fidelity, the biphasic or triphasic theories may not be necessary. The current work studies the applicability of viscoelastic modeling of cartilage. Additionally, the viscoelastic models can be modified as the study progresses.

3.2 Summary

A longstanding interest in cartilage research has produced a large number of models and theories. The supplied review gives a brief history of the leading constitutive models governing articular cartilage. The biphasic model separates the mechanical contributions of the fluid and solid phases of cartilage. Different equations govern the interactions of the two mediums. Some biphasic models consider porosity and permeability as well. The standard solid models do not decouple the solid and fluid interactions of cartilage, instead focusing on energy retained and dissipated. Viscoelasticity is a macro-scale approach that is easier to implement and apply from a dynamics perspective. The standard models are used in this study to characterize the relaxation behavior of cartilage. The experimental methods developed for this study are presented in the next chapter.

CHAPTER IV

EXPERIMENTAL DESIGN

This chapter highlights the unique aspects of the experimental design. The availability of equine cartilage samples comes from a partnership between the Auburn University College of Veterinary Medicine and the College of Engineering. The partnership allows for rapid access to sample explants, which reduces environmental effects on the cartilage. The final harvesting is performed in the same laboratory as the mechanical testing equipment, yielding efficient and controlled experimentation. Cartilage is very sensitive to environmental factors, so controlled experimentation is important. The harvesting and testing techniques are as minimally invasive as possible, so that the cartilage is not altered unnecessarily.

4.1 Theoretical Framework

In general, cartilage is a heterogeneous, non-linear, viscoelastic, compressible, and anisotropic material. Unlike muscle tissue, cartilage has relatively no growth remodeling or contractile behavior. The theoretical framework of the current study depends primarily on the viscoelastic nature of cartilage. On the micro-scale, cartilage displays heterogeneity in the collagen fibers and synovial fluid mixture. However, on the macro-scale, cartilage can be approximated as homogeneous in its mechanical response. Cartilage is generally anisotropic, but often considered transversely isotropic. However, for strains in a limited range, cartilage is typically considered linear and isotropic. The initial theoretical framework for cartilage is therefore linear viscoelasticity, although strain-dependency can be introduced in the elastic response with slight modification. The experiments are run in a fluid bath at room temperature, so isothermal conditions are maintained.

4.2 Materials and Methods

This section describes the specimen harvesting and mechanical testing routines used. Articular cartilage samples are harvested from the right stifle joints of horses that are euthanized for other reasons. Equine samples are used for multiple reasons: the cartilage surfaces are large and allow for "macro-scale" analysis, the joints have large load to size ratios (meaning that there are typically higher stresses within the joints), the availability of samples is suitable, and the expertise of the team members from the Auburn University College of Veterinary Medicine is in equine surgery and medicine. In addition, equine and human articular cartilage have similar structural features and collagen organization [54].

After euthanasia, the horses are taken to the Alabama State Necropsy facility where intact joints for this and other studies are removed. The joints remain sealed in their native joint capsule during this time. The samples are brought to the Multiscale Tribology Lab in the Mechanical Engineering Department of Auburn University. In the lab, the cartilage is harvested by dissection of the surrounding tissue, and resized with an industrial bandsaw (Appx. D). Figure 4.1 shows the area of interest in the stifle joint. The cartilage surface is hydrated with a biological solution to prevent drying.

The medial condyle of the right rear stifle is used for study. The stifle joint is mechanically analogous to the human knee, and the condyle contains an area of thick and relatively flat cartilage. The condyle is advantageous because large, relatively flat, samples can be obtained. The similarity between equine stifle joints and human knees is also of interest. It is hoped that the equine results can eventually be extrapolated to human studies, where artificial knee replacements are the second most common type of surgical replacement, behind hip joint replacements.

After bulk harvesting and resizing of the condyle, a 10 mm plug is created with a hollow punch. The punch is driven into the sample with an arbor press, depicted

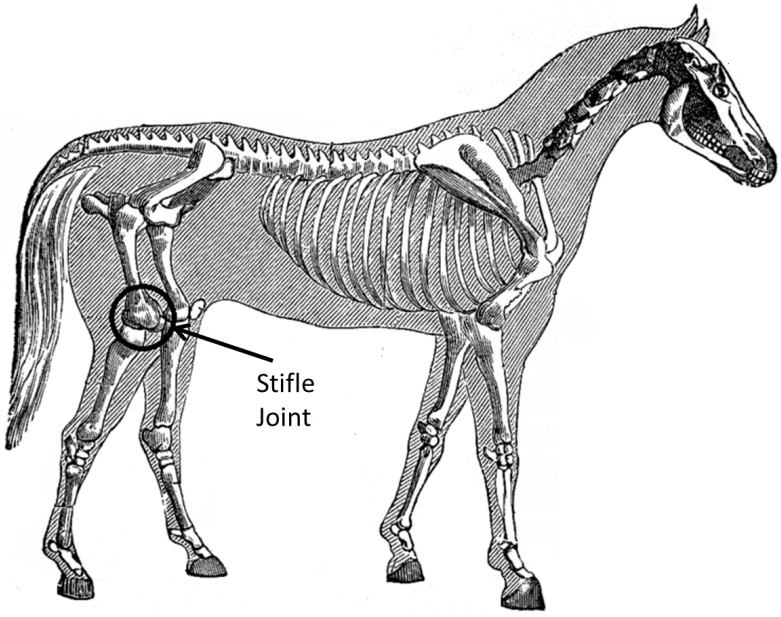

(a) Side schematic of stifle joint in horse skeleton

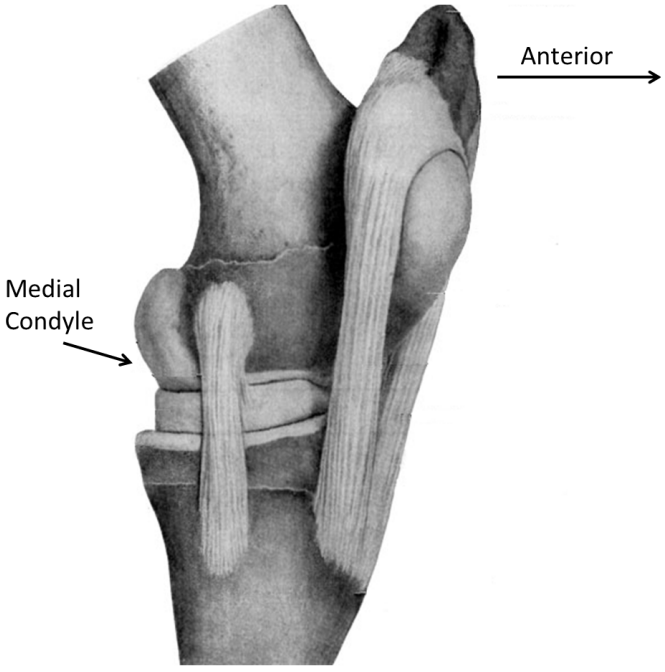

(b) Side view of medial condyle in the stifle joint

Figure 4.1: Location of the stifle joint and the associated cartilage surface that is sampled

in Fig. 4.2. With the punch embedded in the cartilage and subchrondial bone, the surrounding cartilage is removed with a Dremel and wire brush attachment. The punch has an access hole to allow for hydration of the sample. After the plug is created, it is immersed in a biological medium. The average time from the beginning of dissection to immersion is less than 20 minutes. The joint capsule is open for approximately 10 minutes during the process. As was previously stated, the samples are continuously hydrated with a biological medium to prevent dehydration.

4.2.1 Relaxation Experiments

The cartilage plugs are placed in a UMT CETR (Appx. D) tribometer. The tribometer imposes a nearly instantaneous (approximately 30 ms) displacement on the cartilage surface, while tracking the force generated in the cartilage matrix. By design, this is a stress-relaxation experiment. The tribometer holds a 12 mm rigid aluminum cylinder attached to a load cell, as shown in Fig. 4.3. Initially, the cylinder contacts the cartilage surface with a preload of 0.5 N. The preload ensures that the cylinder makes complete contact with the cartilage surface. In effect, the cylinder is flattening out any curvature in the cartilage. At time $t = t_0$, a downward displacement is imposed on the cartilage and the resulting force is measured. After approximately 180 seconds of measurement, the rigid cylinder is withdrawn from the surface. The cartilage is allowed two minutes to recover between tests, and the procedure is repeated. The typical test includes four runs at a lower strain, followed by four runs at a higher strain.

Typically, displacements of 0.25 mm and 0.35 mm are imposed on the cartilage matrix. The cartilage thickness is measured after the relaxation experiment, so *a priori* strains can not be determined. However, the displacements are designed to strain the cartilage matrix 5-15%. The relaxation behavior usually reaches an equilibrium by the test's conclusion. In all cases, the bulk of the relaxation behavior

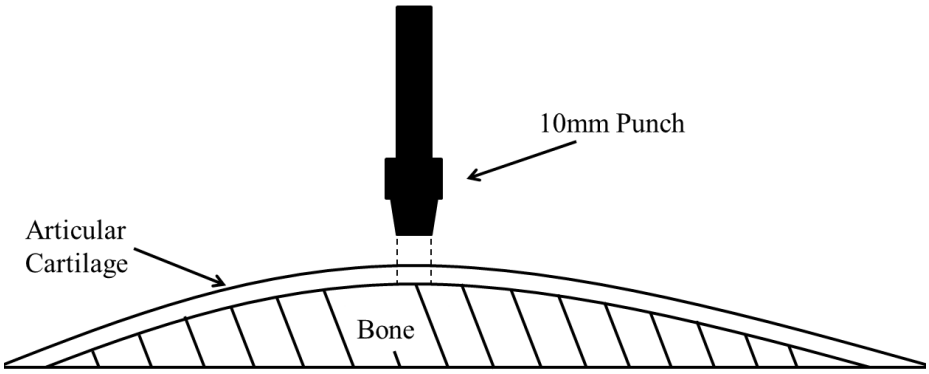

(a) Side schematic of stifle joint before plug is created

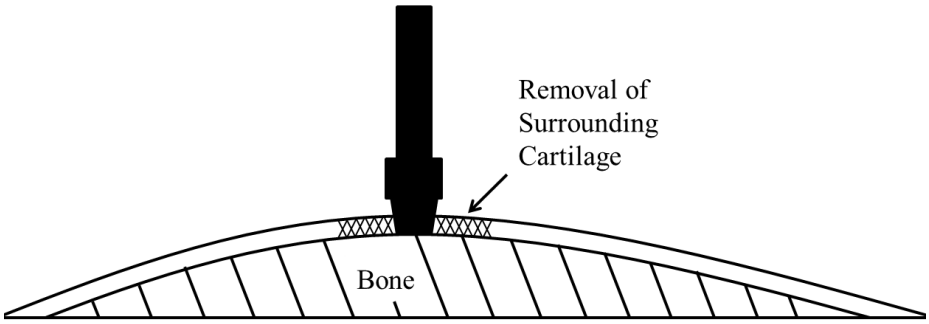

(b) Punch embedded in the cartilage as the surrounding structure is removed

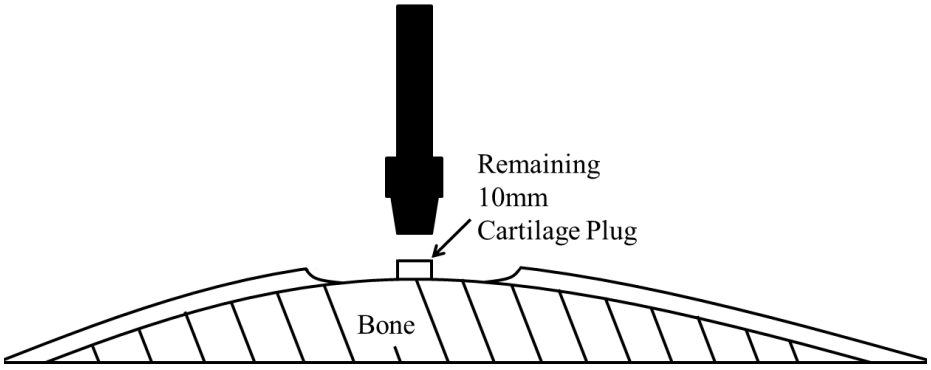

(c) The remaining cartilage plug

Figure 4.2: Schematic of the 10 mm plug creation process

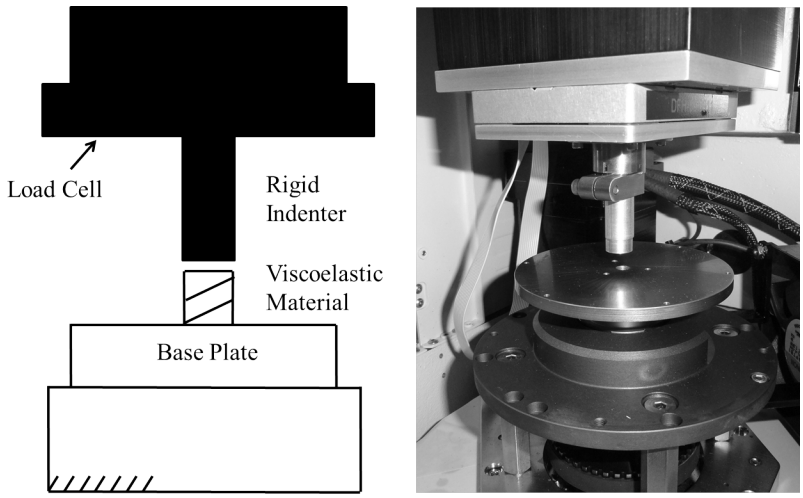

Figure 4.3: CETR UMT3 Tribometer fitted with a 12 mm rigid indenter

has occurred by 180 seconds, and the steady-state (rubbery modulus) information can be extrapolated with the proposed viscoelastic models. Additional information regarding the testing procedure, including deviations for particular experiments, is included in Appendix E.

4.2.2 Determination of Cartilage Thickness

The diameter and thickness of the cartilage plugs is needed to find the relaxation modulus. Recall that the modulus is $E(t) = \sigma(t)/\epsilon_{step}$. The diameter and thickness determine stress and strain, respectively. The harvesting techniques set the diameter of the cartilage plug; however, the thickness of the plug is unknown. Needle probe testing is developed to find thickness. After the relaxation experiments are run, a hypodermic needle is installed on the tribometer, as shown in Fig. 4.4. The needle is lowered vertically into the cartilage body until it hits the subchondral bone. A sharp rise in the force response indicates that bone has been reached. Figure. 4.5 shows an example of the force response from needle tests. The starting and stopping points are denoted in Fig. 4.5 with A and B, respectively. Initially, force rises as the needle deforms the cartilage. In this region, the cartilage resists puncture. The dashed

Figure 4.4: CETR UMT3 Tribometer fitted with a 20 gauge hypodermic needle

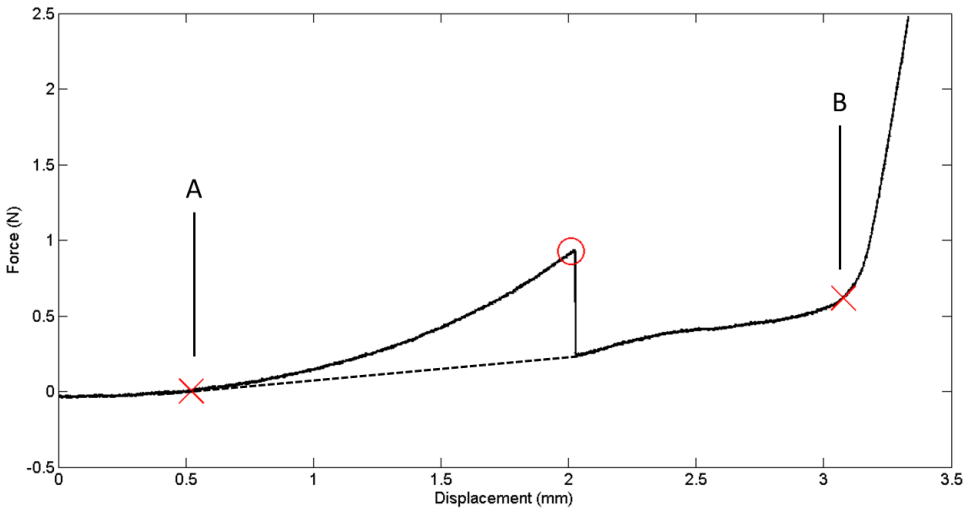

Figure 4.5: Determination of the cartilage thickness with needle probe testing

line is a hypothetical path that the force would follow if puncture was immediate. At the point where the force releases (circled in Fig. 4.5), the needle pierces the cartilage surface and begins traveling through the collagen matrix. The clear spike in force seen on the right side of Fig. 4.5 is the location where the needle encounters the subchondral bone. The absolute difference between the beginning and ending points gives the thickness of the cartilage plug. This method is inherently subjective, but repeatable patterns are seen between samples. The thickness measurements are obtained for each sample with the aid of a Matlab algorithm. A mean thickness for each sample is found by averaging the individual tests. Each plug is considered to have a uniform thickness, which is a simplification of the actual geometry. However, since the strain levels are relatively low (5%-15%), the effect of this variation is considered negligible. The result is an average thickness and average strain throughout the cartilage matrix. After testing, the samples are frozen for later analysis if required.

CHAPTER V

TIME DOMAIN ANALYSIS

This chapter discusses the time-domain modeling of the experimental data obtained from 11 horses. Six samples were hydrated with a saline solution (0.9%), and two samples were immersed in pooled synovial fluid from multiple horse specimens. The three remaining samples were immersed with Hylartin, Polyglycan, and Adequan respectively. These synthetic substances are used in surgical applications and mimic the biological function of synovial fluid. The analysis is grouped based on fluid bath composition; however, some comparisons will be made between samples in different mediums. Also, an effective time constant of relaxation is created using the Prony series.

5.1 Motivation for Modeling in the Time-Domain

The nature of viscoelasticity is time-dependent. Stress-relaxation tests are performed in the time-domain, and depend on material history. Therefore, a viscoelastic model that is applied in the time-domain is desired. However, the frequency dependent behavior of cartilage is also important. In the frequency domain, the storage and dissipation mechanisms of cartilage can be found as a function of gait. These metrics help analyze whether cartilage has a natural structure that helps facilitate motion. The correspondence of the time and frequency domains necessitates a model that transfers without loss of generality. A model that is fit to relaxation data, and analyzed in the frequency domain is needed. The two models proposed, the Prony and complementary error function, have the desired quality.

5.2 Data Reduction

A typical series of data is shown in Fig. 5.1 for a given sample. Interestingly, the cartilage stiffens during subsequent tests at the same strain. In the lower four tests (8.04% Strain), the time-dependent relaxation nature of the cartilage stays relatively constant, while the rubbery modulus stiffens. The same phenomenon appears at higher strains (11.27%) as well, where the relaxation behavior stays relatively the same as the cartilage stiffens. It was initially thought that the cartilage needed more time to recover between tests; however, further testing showed that this is not the case. It is foreseeable that fluid is leaving the cartilage during compression and not returning quickly enough, or at all, during the recovery phase. Additional testing would then cause more stress in the solid collagen structure, likely resulting in higher stiffness. The tests could also vary because damage from the harvesting techniques or testing procedures is causing fluid exodus, and/or the tests are replacing synovial fluid in the plugs with the bathing medium. For simplicity in analysis, all of the tests at a given strain were averaged to produce one dataset per strain level, as shown in Fig. 5.2.

5.3 Prony Series

The Prony series model is fit in the time-domain, and analytically transferred into the frequency domain with a Fourier transform. This is advantageous because the experimental data is particularly noisy from the tribometer. Transferring the raw experimental signal from the time-domain to the frequency domain is difficult even with filtering and smoothing algorithms, as will be discussed later. Therefore, having a model that can be fit in the time-domain and transferred to the frequency domain is necessary. The tribometer samples at 1000 Hz, which yields approximately 180,000 data points for a typical experiment. A least squares fitting routine is implemented in Matlab to parse the combined relaxation data. The norm metric is used in least-square

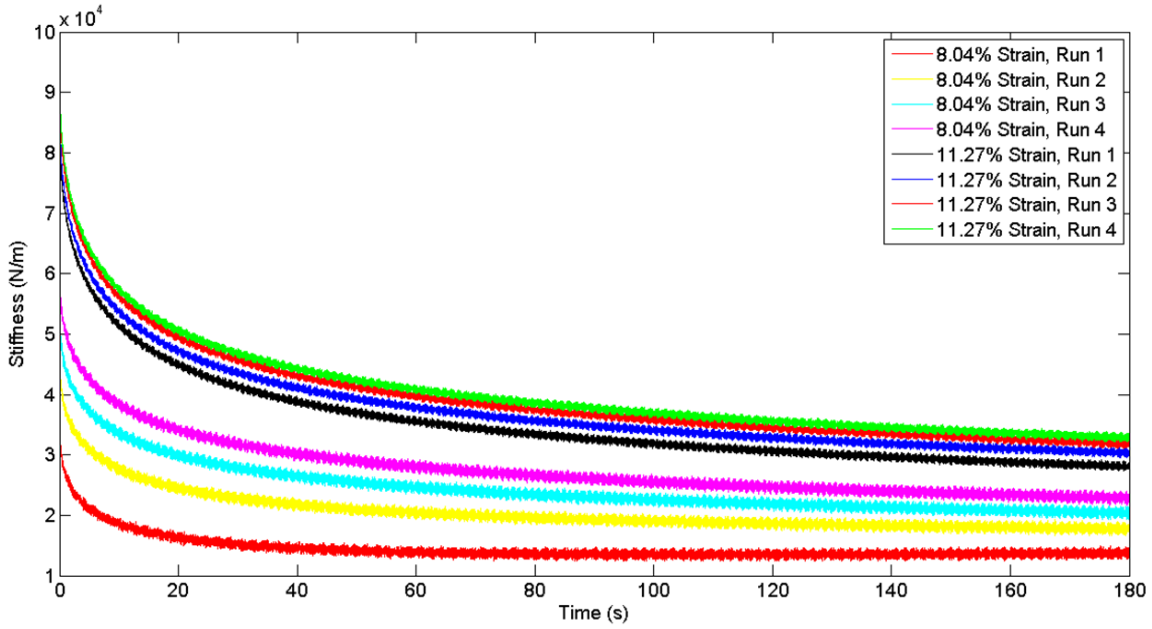

Figure 5.1: Sample data from relaxation experiment Saline (d)

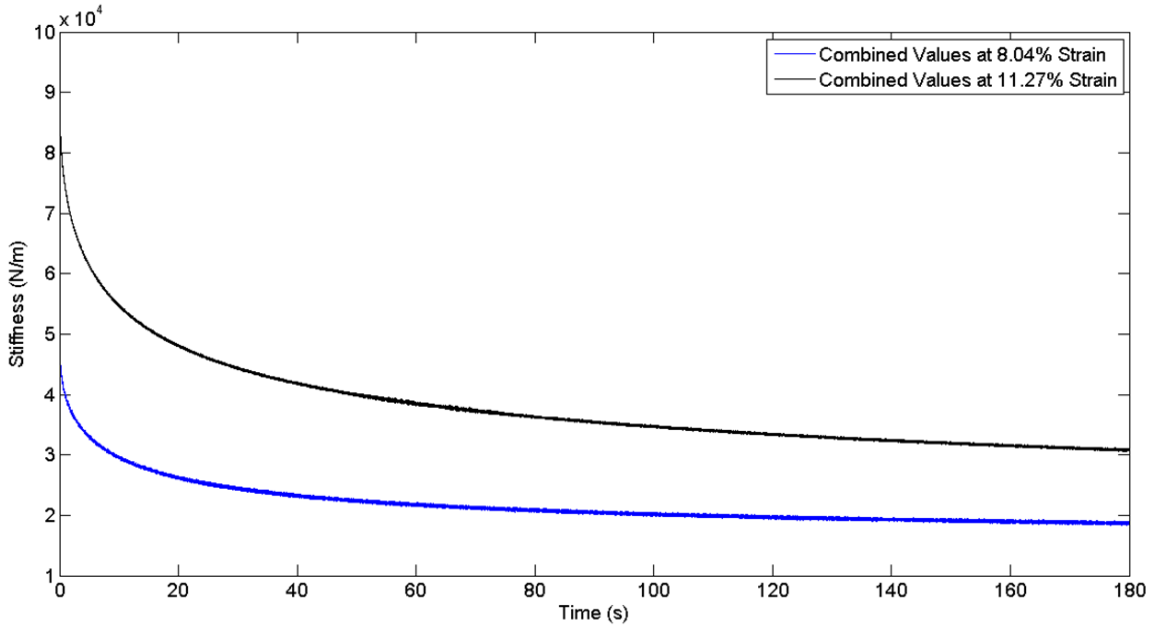

Figure 5.2: Sample reduced data from relaxation experiment Saline (d)

Table 5.1: Reduced norm of sample data (Saline (d))

# of Prony Terms	Reduced Norm (10^5)
1	159.1600
2	39.7383
3	16.0992
4	10.2755

fits to determine the goodness of fit (GOF) between the model and experimental data.

$$GOF = \frac{norm}{\#_{pts} - \#_{parameters}} \tag{5.1}$$

For data sets with a large number of points, the goodness of fit and norm are closely related. Therefore, the norm will be used to determine the quality of the fit.

The eigenvalue problem is minimized by fitting the relaxation data with as few terms as possible. However, more terms typically describe viscoelastic behavior better. An example of this is seen in Table 5.1 (Saline (d), 05/30/12 (1)), where the reduced norm decreases as the number of terms increases. The consequence of increasing the number of terms is that the model develops "wiggles" in the frequency domain. These wiggles are not material based, but rather a figment of the modeling. In this regard, the fewer Prony terms that can be used, the better. The model also begins to fail to converge when the number of Prony terms gets too high ($n \geq 5$). The convergence issues are due to the least squares algorithm becoming ill-conditioned. When this occurs, the Prony terms are more difficult to uniquely define. Four Prony terms is the maximum that can be fit reliably to the experimental data.

The Prony series is fit to the experimental data presented in Fig. 5.2. The fit is shown in Fig. 5.3. A four-term Prony series is used to capture the relaxation behavior, which is pronounced in the initial seconds of the experiment. In general, the four-term Prony series does an excellent job fitting the relaxation behavior. In Fig. 5.4, which shows a zoom-in of the information from Fig. 5.3 in the initial decay period ($1s$),

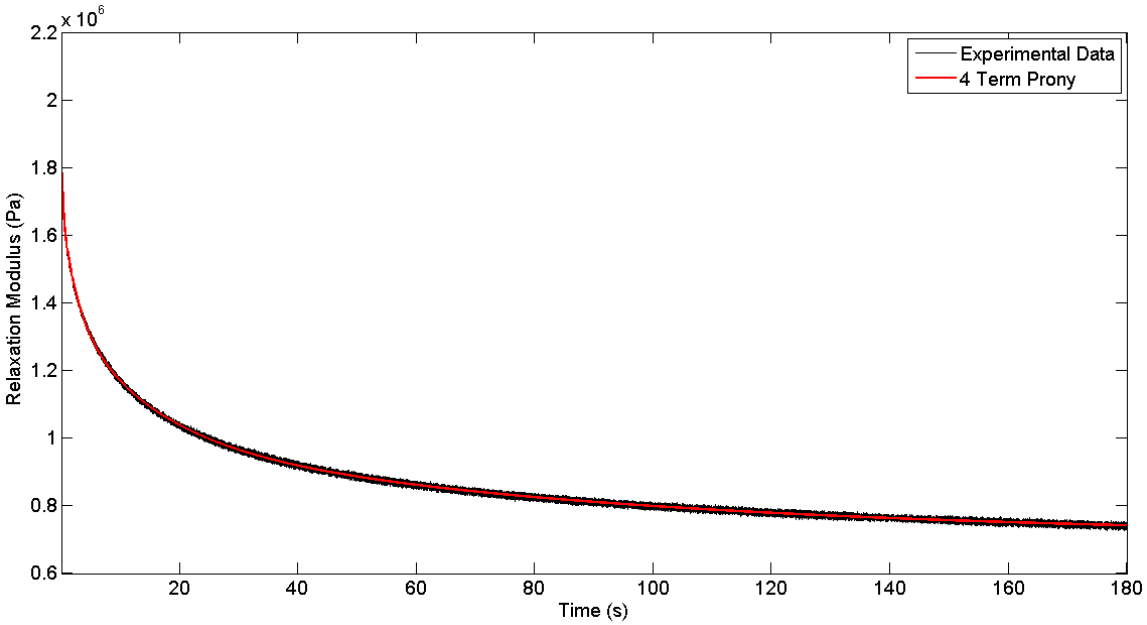

Figure 5.3: Example of a four-term Prony fit to experimental data (Saline (d))

some deviation between the fit and the actual data is seen. The deviation between the model and experimental data corresponds to the highest frequency information. For horses (and humans), frequency ranges greater than 5 Hz are not accessed during even the most strenuous exercises. Therefore, it is less important to accurately capture this region of the relaxation. The physiological region of the relaxation occurs from $t = 0.25s$ and on. The Prony series is able to robustly model these decades of relaxation behavior (shown in Fig. 5.5 using a semi-log scale), which makes its utility apparent for analysis between samples.

5.3.1 Application of the Prony Model to Determine the Effective Time Constant

The empirical data indicates that the decay properties of cartilage are strain-dependent. Cartilage exhibits greater stiffness with higher strain, and appears to decay more slowly. An effective time constant is created to quantify this observation. In exponential decay, the time constant represents the time it takes for the response to reach $\left(\frac{1}{e}\right)$ of the initial value. This is typical of a first-order system that mimics the

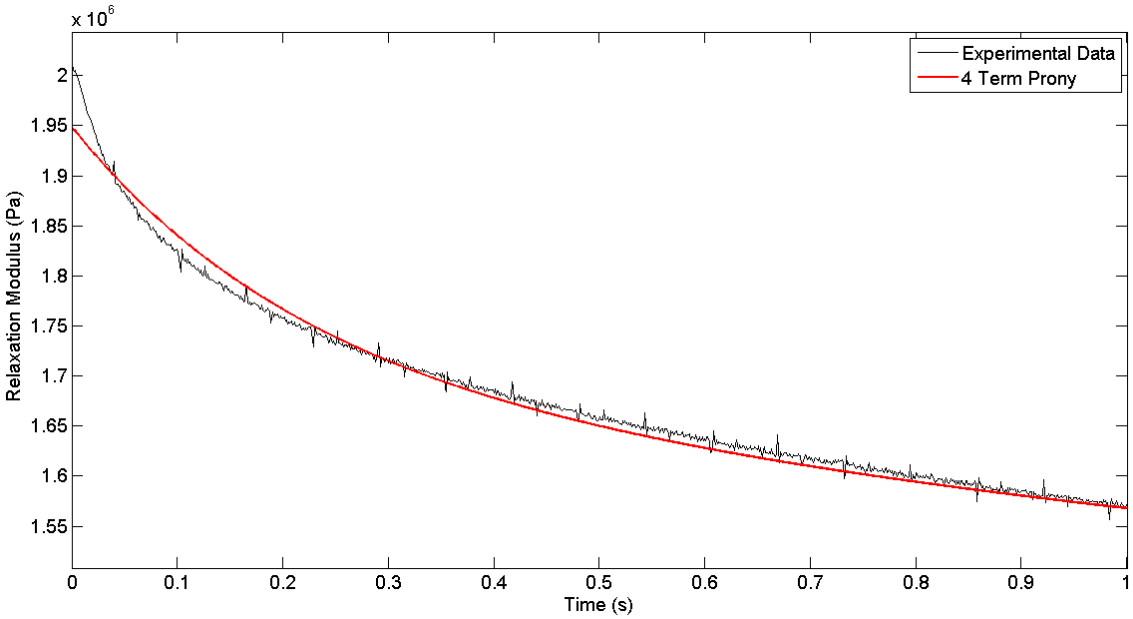

Figure 5.4: Four-term Prony series fit in the initial time period (Saline (d))

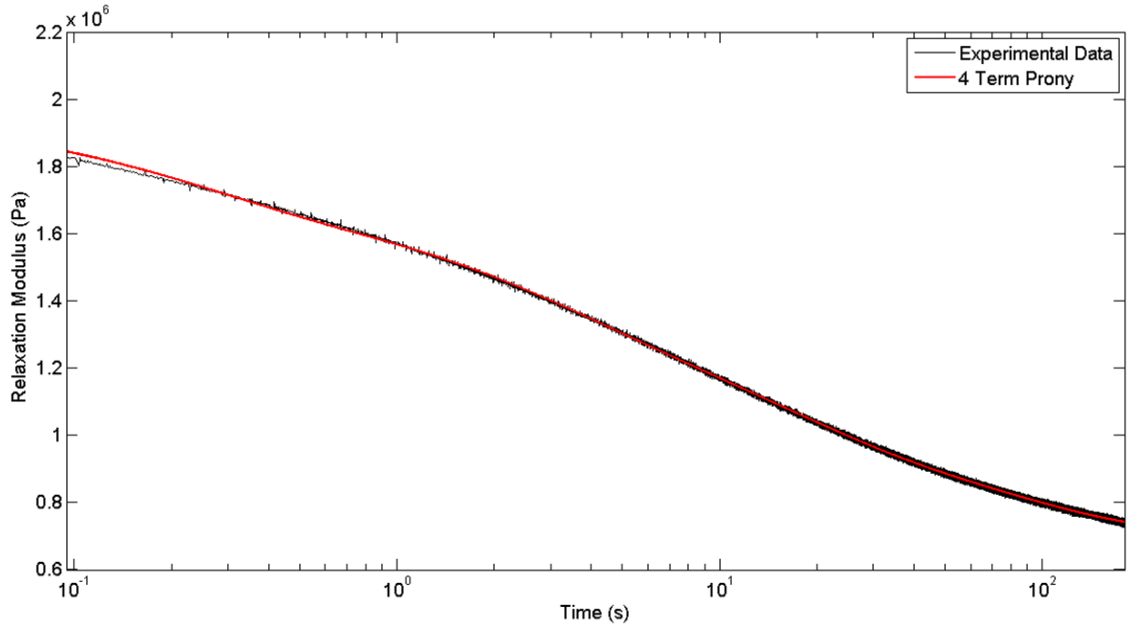

Figure 5.5: Four-term Prony series fit, displayed on a semi-log scale (Saline (d))

relaxation behavior. For a series of exponential decays (a Prony series), the effective time constant can be found by locating the time when 63.2% of the relaxation has occurred. This means means 0.368 = 36.8% of $E(t)$ remains. The time constant is found numerically with Matlab. The flowchart shown in Fig. 5.6 outlines the process taken to locate the time constant. When the relaxation threshold is reached, the program records the time and exits the loop.

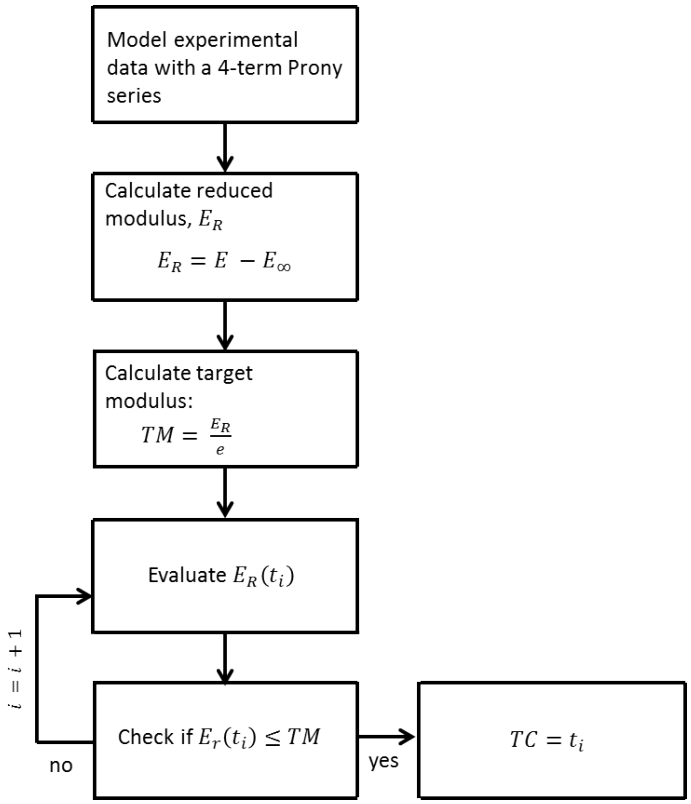

Figure 5.6: Flowchart depicting the steps taken to locate the time constant

The time constant information is presented in Table 5.2 for the six cases in saline. With one exception (Saline (d)), the time constant is greater for the higher strain tests. Cartilage takes longer to dissipate energy at higher strains, proportional to the initial value of the response. This finding is significant because higher strains probably occur during periods of high activity. In effect, cartilage has a higher modulus during periods of higher strain, which likely allows for a more fluid joint motion. This finding

Table 5.2: Time constant information for cases immersed in saline

Name	Test Date	Lower Strain (s)	Higher Strain (s)	Viscosity (mPa s)
Saline (a)	5/22/2012	1.57	1.98	0.890 [55]
Saline (b)	5/24/2012	6.38	8.36	0.890
Saline (c)	5/29/2012	5.00	10.06	0.890
Saline (d)	5/30/2012 (1)	10.28	15.36	0.890
Saline (e)	5/30/2012 (2)	17.06	13.23	0.890
Saline (f)	6/26/2012	15.71	19.37	0.890

Table 5.3: Time constant information for cases immersed in alternative fluids

Name	Test Date	Lower Strain (s)	Higher Strain (s)	Viscosity (mPa s)
Synovial (a)	06/13/2012	2.99	5.37	33.6 [56]
Synovial (b)	06/19/2012	7.89	11.54	33.6
Hylartin	06/20/2012 (1)	28.07	14.08	Unspecified
Polyglycan	06/20/2012 (2)	5.07	4.64	Unspecified
Adequan	06/21/2012	12.06	11.90	Unspecified

agrees with the work of June [44]. The results are mixed when different lubricants are used. Table 5.3 shows this difference. The two studies where synovial fluid is used have the same trend as saline. However, for the case of Hylartin, Polyglycan, and Adequan, the results are reversed. It is likely that the lubricant significantly influences the time constant. Not enough data exists to definitively determine the effects of the fluid bath. However, the saline and synovial fluid cases appear to express the same trend of higher compressive strain to higher time constant. The correlation of strain and time constant is physiologically reasonable, and could be a factor in cartilage's adaptivity and durability.

The viscosity of the synovial fluid used in this study is presented in Table 5.3. The data for Hylartin, Polyglycan, and Adequan is not listed on the respective manufacturer's material safety data sheet (MSDS). All three fluids appear to be more viscous than water or saline, but additional study should accurately quantify the viscosities of each fluid.

The time constant varies largely between cartilage samples. The time constant information can be normalized by taking the integral of the reduced relaxation curve, from the initial time $t = t_0$ to the time constant $t = t_{TC}$. When compared to the total area under the curve, the integral from t_0 to t_{TC} gives a quantitative idea of the amount of relaxation that occurs before the time constant is reached. To determine this quantity, the "equilibrium area" is removed from the total area under the relaxation curve, as shown in Fig. 5.7a. In effect, the rubbery modulus is subtracted from the relaxation curve so that the response decays to zero. The remaining curve is called the "reduced relaxation curve." The "time constant area" is found by integrating the reduced relaxation curve from $t = t_0$ to $t = t_{TC}$ (Fig. 5.7b). Dividing the time constant area by the total area of the reduced relaxation curve gives an "area ratio." The area ratio is more stable than the time constant itself, but initial tests do not show a significant trend for cartilage. Additional study is required to determine the applicability of the area ratio.

5.4 Fractional Derivative Model

The fractional model is a robust viscoelastic constitutive formulation. In the full fractional case, the parameter α, which interpolates between spring and dashpot behavior, gives the fractional model more flexibility than the Prony model. Typically, the flexibility of the fractional model means that fewer elements are needed to fully characterize a viscoelastic material. The fractional model has obvious utility in modeling applications. However, due to the Mittag-Leffler function, the fractional model is challenging to implement in the time-domain without modification. It is desired to perform the majority of the cartilage analysis in the frequency domain, where the fractional model can be fit without major problems. However, transforming the experimental data from the time to frequency domain is difficult without excessive

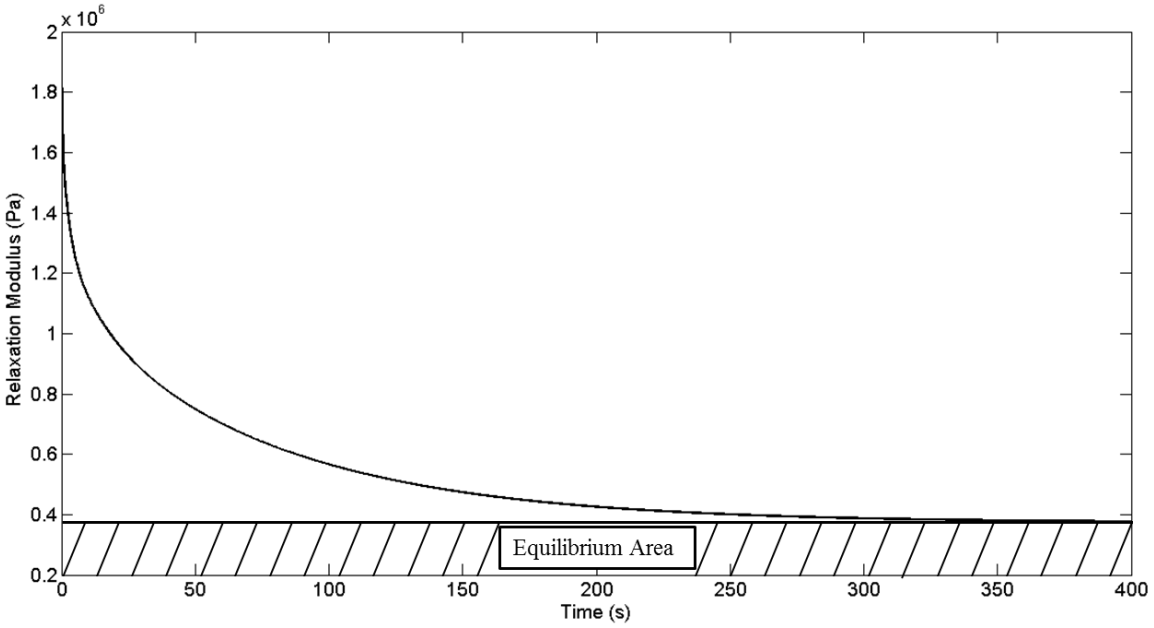

(a) Example of a relaxation curve with the equilibrium area marked

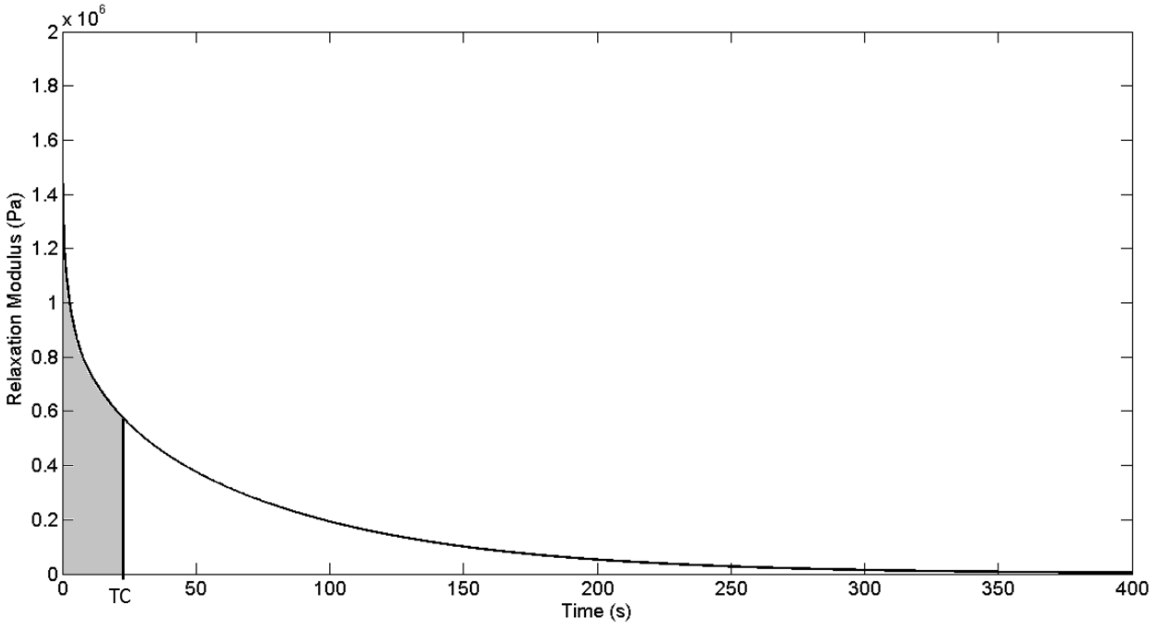

(b) Example of a reduced relaxation curve with the time constant area in gray

Figure 5.7: Graphical depiction of the process used to determine the area ratio time constant information

manipulation of the empirical data. The original material behavior is often compromised during the transformation. This is discussed in the following section, with a remedy proposed later in the chapter.

5.4.1 Fractional Model Shortcomings in the Time-Domain

The time-domain representation of the fractional model contains the Mittag-Leffler function. The function requires a relatively large number of terms to converge for cartilage applications. In some instances, the Mittag-Leffler function does not converge at all. Therefore, the full fractional model does not have a stable time-domain representation, and is better suited for analysis in the frequency domain. However, the time-domain to frequency domain transition requires manipulation that may compromise the experimental data. For example, the fast Fourier transform (FFT) is a typical routine for transforming from the time-domain to the frequency domain. The experimental data is noisy, and applying an FFT leads to unreadable information at the highest frequencies (Fig. 5.8). Although the majority of the severe noise occurs at frequencies that are out of the physiological realm for horses and humans (greater than 4-5 Hz), more than half of the narrow band of physiologically appropriate frequencies contains noise. Techniques such as zero padding, numerical reduction of aliasing, filtering, and smoothing are used to reduce noise; however, the higher frequency information is distorted enough to render the FFT data unacceptable for analysis.

Another method for finding the frequency representation of the experimental data is used by Miller [48, 57]. The storage and loss moduli can be found with the following equations:

$$E'(\omega) = E_0 + \int_0^\infty \dot{E}\,(t)\, cos(\omega t)\,\mathrm{d}t \tag{5.2}$$

$$E''(\omega) = -\int_0^\infty \dot{E}\,(t)\, sin(\omega t)\,\mathrm{d}t \tag{5.3}$$

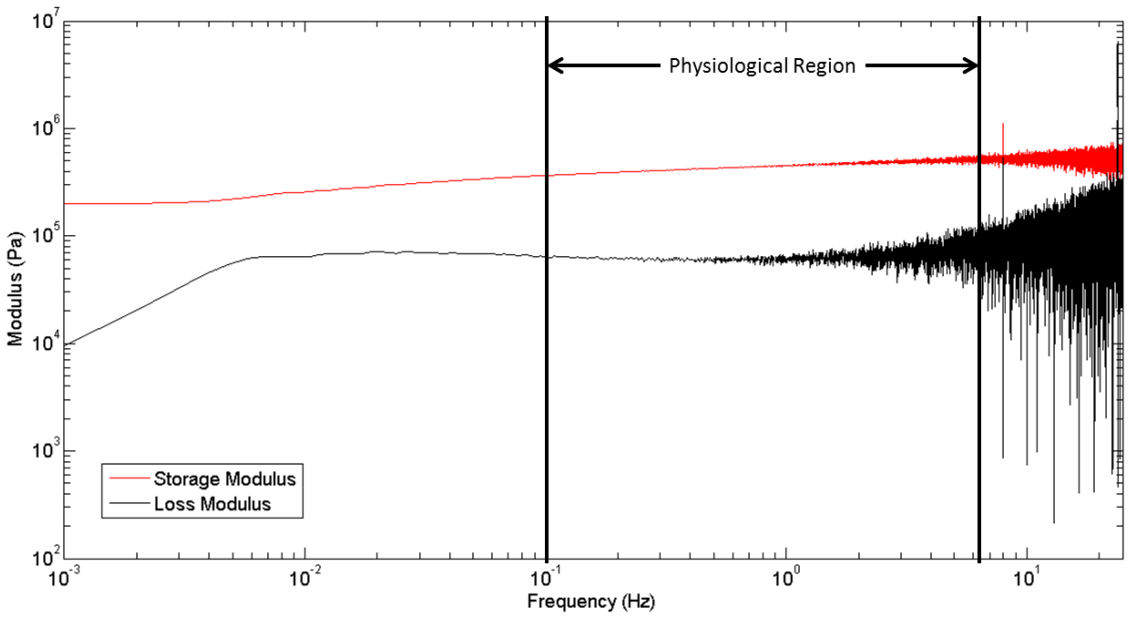

Figure 5.8: Example of the FFT routine applied to experimental data (Saline (c))

Here, the relaxation term E is related to the experimental data. The problem of signal noise is exacerbated by the derivative of the relaxation term, $\dot{E}$. Even a high accuracy numerical derivative, which has a tendency to smooth the data (see Hildebrand [58]), does not reduce the noise sufficiently. The data is so disjointed that it is not useful for analysis, as shown in Fig. 5.9. The storage and loss information is obviously devoid of significant meaning using derivative techniques.

Green [59] developed a method to remove the derivative term in Eqs. 5.2 and 5.3 with integration by parts. The result gives a form of the storage and loss moduli that does not involve the derivative of the relaxation modulus:

$$E_r = E - E_\infty \tag{5.4}$$

$$E'(\omega) = E_\infty + \int_0^\infty \omega E_r\,(t)\, sin(\omega t)\,\mathrm{d}t \tag{5.5}$$

$$E''(\omega) = \int_0^\infty \omega E_r\,(t)\, cos(\omega t)\,\mathrm{d}t \tag{5.6}$$

This form of the Fourier transform reduces the effects of signal noise. However, as

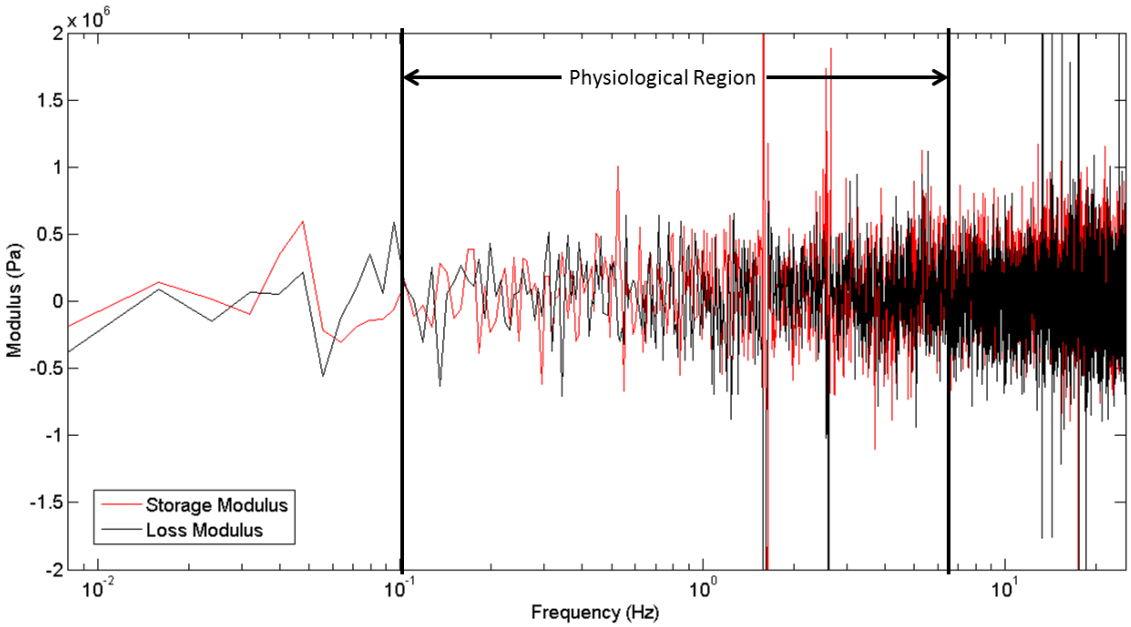

Figure 5.9: Example of the derivative routine applied to experimental data (Saline (c))

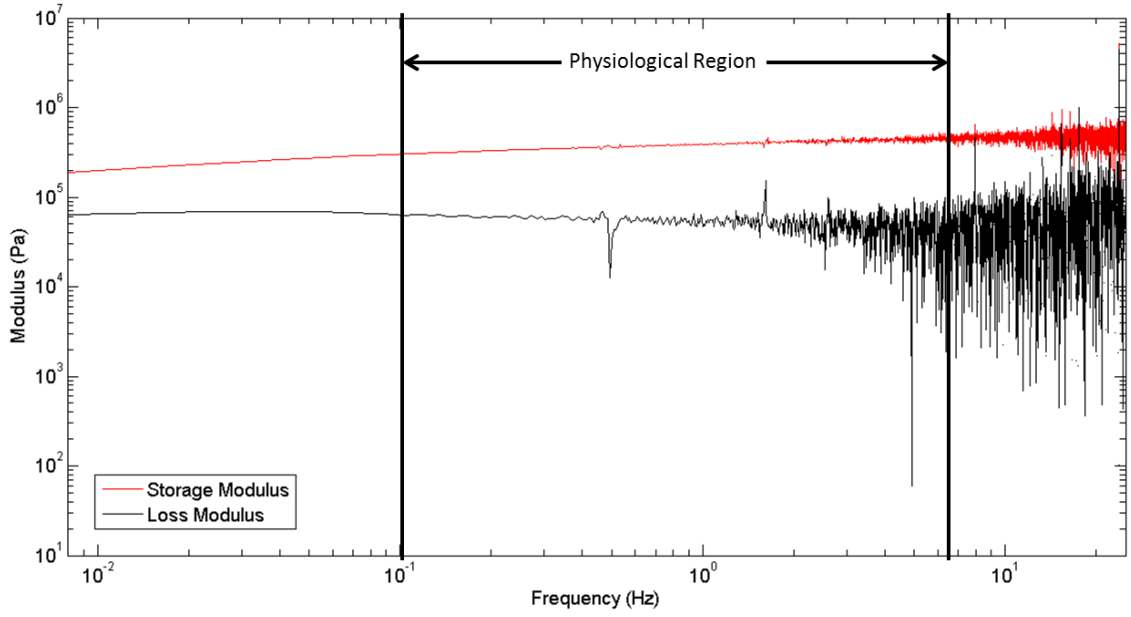

Figure 5.10: Example of the integral routine applied to experimental data (Saline (c))

shown in Fig. 5.10, the noise reduction is not sufficient for the experimental data. Apart from the noise, the transformations also introduce waviness in the signal. The waviness is due to the cyclic nature of the functions used to transform the experimental data. The wavy behavior is an unfortunate pitfall of these techniques, and is not a material characteristic. It is computationally intensive to get the required fidelity in the frequency domain with the integral techniques.

The techniques presented allow the experimental data to be transferred to the frequency domain. However, the transformations do not satisfactorily allow for analysis in the frequency domain. One remedy is to smooth the time-domain information. Smoothing the relaxation data removes the majority of noise from the signal. The smoothed signal can be transformed to the frequency domain, where the storage and loss data is obtained. The problem with smoothing is that the data is biased by the smoothing function. Even relatively impartial functions, like a moving average, alter the data. Relaxation data is particularly susceptible to bias because there is rapid mobility in the early decades, but not at longer time intervals. The experimental data is often manipulated excessively to become a monotonically decreasing function. The largest deviation between the smoothed curve and the experimental data occurs in the first ten seconds, as shown in Fig. 5.11. This period is very significant physiologically, as most movement occurs at frequencies in this range (0.25 - 4 Hz, or 0.25 - 4s). Therefore, a moving average algorithm is not the best choice of functions to smooth the data. Other smoothing functions can be used well, such as a Vogel function, and variations of it:

$$f(t) = a_1 e^{\frac{a_2}{(t-a_3)}} \tag{5.7}$$

$$f(t) = \frac{b_1}{(t+b_2)^{b_3}} \tag{5.8}$$

$$f(t) = \frac{c_1}{(t+1)^{c_2}} + c_3 \tag{5.9}$$

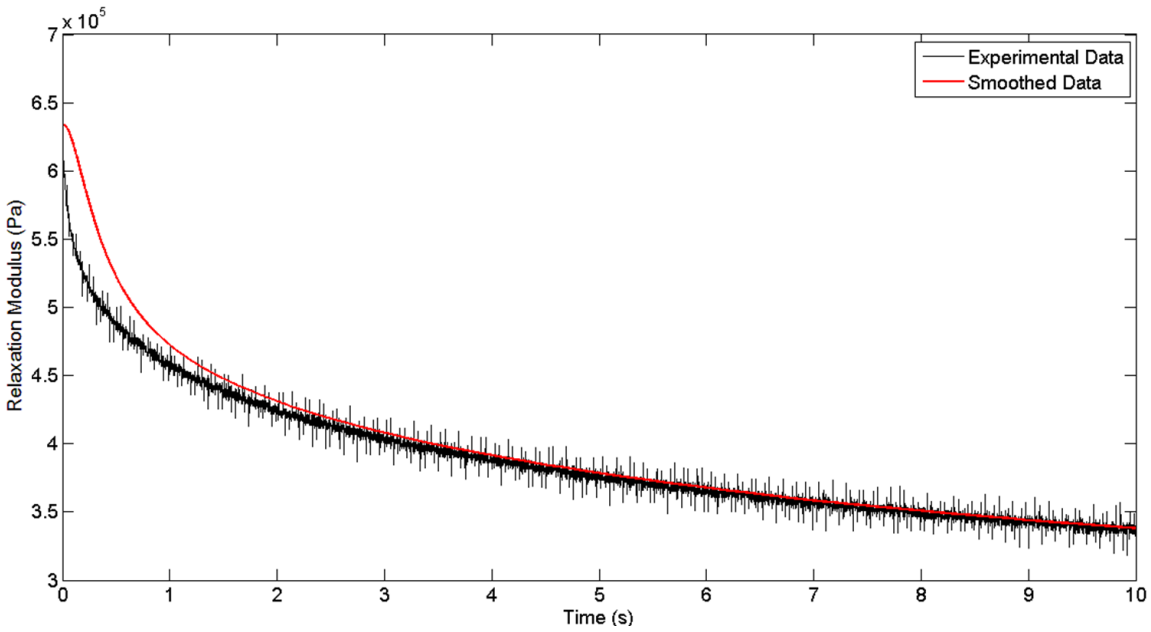

Figure 5.11: Example of deviations introduced by smoothing with a moving average filter

The fundamental problem remains with any smoothing function- the data will be manipulated before the viscoelastic models are applied. Each equation is able to fit and smooth the experimental data, but the result are manipulated enough to justify discarding these routines.

5.4.2 Complementary Error Function- Resolution of Fractional Model Problems

The problem of filtering and smoothing data in the time-domain is avoided by restricting the fractional model to $\alpha = 1/2$. As discussed, this case degenerates to the complementary error function model. The relaxation data from the tribometer can be fit with the CERF model, and analytically transferred to the frequency domain. The CERF model offers the advantages of the fractional model, while satisfying the requirement of time-domain fitting. The utility of the CERF model is apparent in the frequency domain, where a one-element function is used to model cartilage viscoelasticity. This yields a completely smooth function, which is indicative of the actual

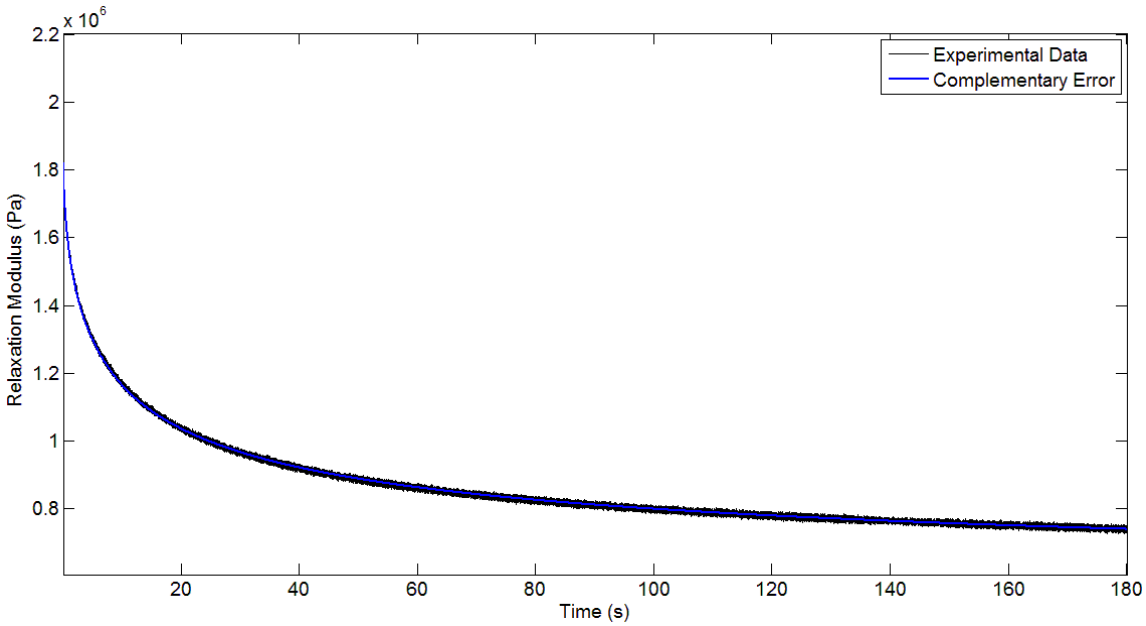

Figure 5.12: Relaxation data fit with the complementary error function (Saline (d))

material behavior. A one-element model is convenient for future dynamic analysis and modeling as well.

The CERF model is fit in the same way as the Prony model. A least squares approach is utilized to fit the CERF model to relaxation data. An example fit for Saline (d) is shown in Fig. 5.12. Once again, the early decades of time information show the largest deviations between the model and experimental data (Figs. 5.13 and 5.14). However, these initial time frames do not represent physiological capabilities of horse or human, and the modeling error is within approximately 3% at its maximum for the Saline (d) case. The CERF model displays robust capabilities in modeling cartilage stress-relaxation. The CERF model is advantageous compared to the Prony model because fewer terms are used to characterize the viscoelastic behavior. Using fewer modeling parameters results in a smooth curve in the frequency domain, which more realistically describes the material behavior of cartilage. Additional discussion of this is included in Chapter 6, where the higher-term Prony series models are shown to develop "wiggles."

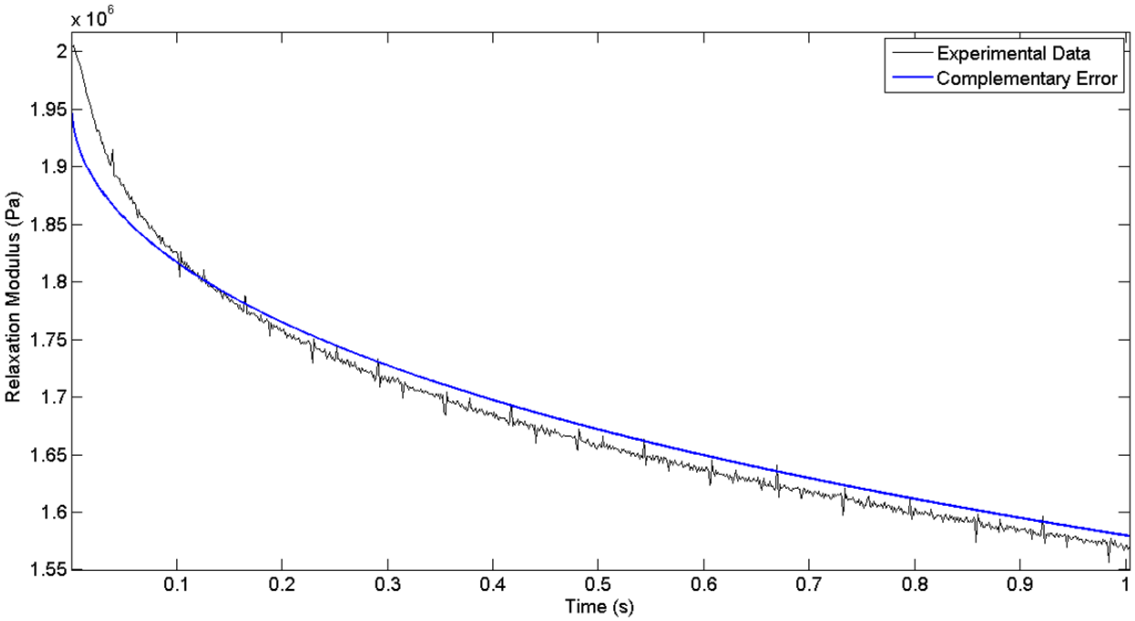

Figure 5.13: Complementary error function fit in the zoomed-in initial time period (Saline (d))

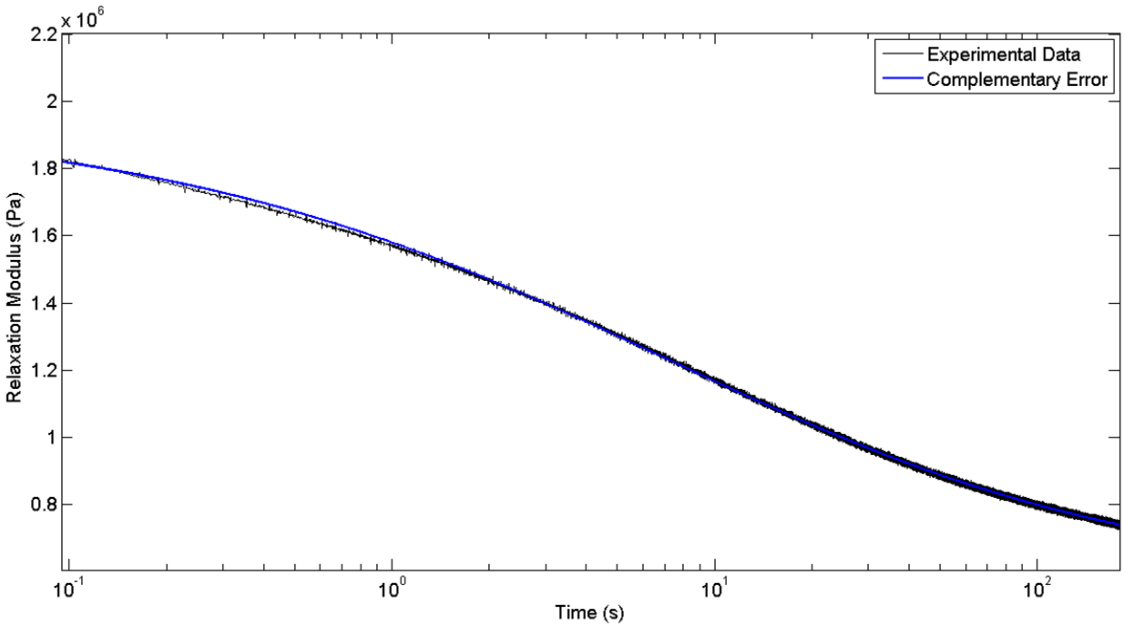

Figure 5.14: Complementary error function fit, displayed on a semi-log scale (Saline (d))

The Prony series and complementary error function models are both adept at capturing the viscoelastic behavior seen in the cartilage samples. Both models are monotonically decreasing in the time-domain, and thermodynamically permissible in general [47]. The CERF model is more flexible for describing viscoelastic behavior of cartilage with fewer terms, which is important for future analysis. However, both models are well-suited for use on articular cartilage in the equine stifle. Relatively few mechanical differences exist between the joints in the equine carpus and human cartilage [54]. It is proposed that the techniques described can be used to analyze human cartilage as well. In the next chapter, the two models will be compared in the frequency domain.

CHAPTER VI

FREQUENCY DOMAIN ANALYSIS

The frequency domain offers a different analytic tool for analyzing viscoelastic materials. Ultimately, the goal of characterizing articular cartilage is to understand how cartilage responds in dynamic situations, such as during normal walking or strenuous exercise. The elastic-viscoelastic correspondence principle transfers time-dependent information to the Laplace and frequency domains without loss of generality. In the frequency domain, a stress-relaxation experiment shows the storage and dissipation moduli as a function of frequency, ω. For articular cartilage, the storage and loss moduli are functions of the animal's gait. Studying cartilage as a function of gait offers insight into the adaptive nature of biological mediums. As discussed in Chapter 3, viscoelastic materials have three main characteristic regions: the glassy, transition, and rubbery. The physiological range of cartilage might fall within the transition region, where higher frequencies approach the glassy region and lower frequencies approach the rubbery region. Cartilage can then adjust to stimulus by storing and dissipating different amounts of energy, depending on the frequency of protuberance. The following sections discuss the frequency domain analysis of cartilage.

6.1 Data Reduction

In the previous chapter, the Prony and complementary error function models are fit in the time-domain and analytically transferred to the frequency domain via the elastic-viscoelastic correspondence principle. The models are compared over a range of gaits that are physiologically obtainable in horses. The goal is to study the storage and loss moduli of cartilage in multiple samples and draw broad conclusions about articular

cartilage viscoelasticity. If possible, a benchmark for healthy (not osteoarthritic) cartilage will be established. The two viscoelastic models are compared in the following sections.

6.2 Prony Model

One advantage of the Prony series is that the model can be easily analytically transferred between the time and frequency domains. Recall the form of the Prony series given in Chapter 3:

$$\sigma_T = \left(E_0 + \sum_{n=1}^{\infty} E_n e^{\lambda_n t} \right) \epsilon_0 \tag{3.9}$$

In the frequency domain, the Prony series is (see Appx. B.1 for derivation):

$$E(\omega) = \frac{E_0}{i\omega} + \sum_{n=1}^{\infty} E_n \left(\frac{\lambda_n - i\omega}{\lambda_n^2 + \omega^2} \right) \tag{6.1}$$

For the Prony series, the storage and loss moduli are:

$$E' = E_0 + \sum_{n=1}^{\infty} \omega^2 \left(\frac{E_n}{\lambda_n^2 + \omega^2} \right) \tag{6.2}$$

$$E'' = \sum_{n=1}^{\infty} \left(\frac{E_n \lambda_n \omega}{\lambda_n^2 + \omega^2} \right) \tag{6.3}$$

6.2.1 Prony Model Behavior for Different Number of Elements

The Prony series is a robust model because of the theoretically infinite number of terms that can be used. Each Maxwell element defines a decay characteristic that is fit to the experimental data. The problem with using additional Prony terms is threefold: (1) the time-domain curve fitting fails to converge as the number of terms increases, (2) additional Prony terms develop waviness in the frequency domain, and (3) the eigenvalue problem increases in dynamic modeling. A comparison of a 1, 2, 3, and 4-term Prony series is presented in Fig. 6.1a for the storage modulus, and Fig. 6.1b for the loss modulus. The development of waviness, or "wiggles," is

a construct of the model, *not* a material property. Additionally, the wiggles only appear with significance in the loss modulus.

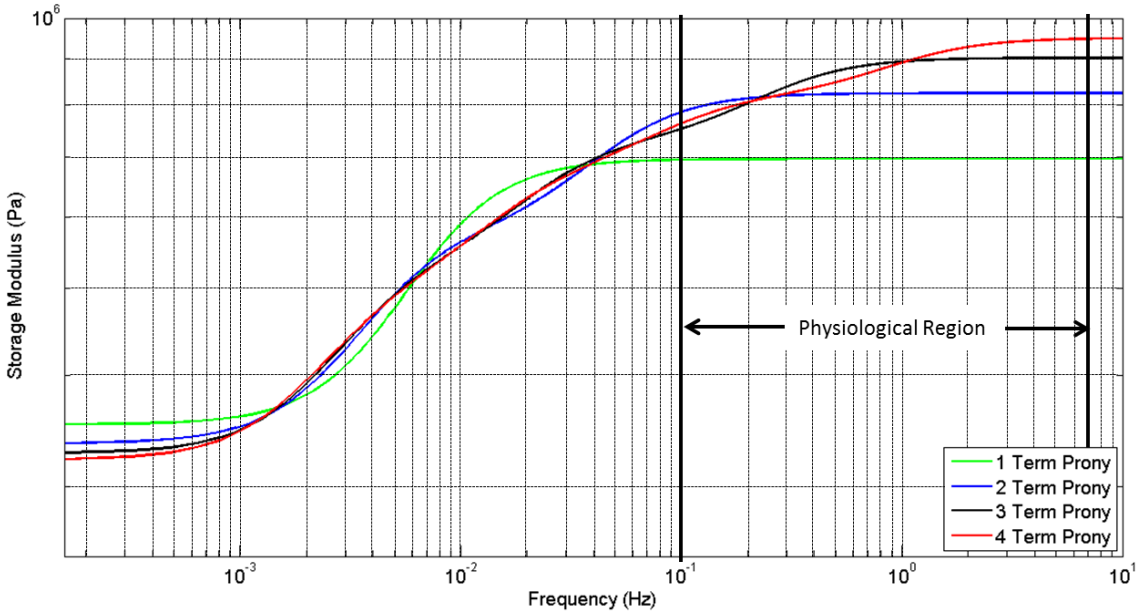

(a) Comparison of the storage information

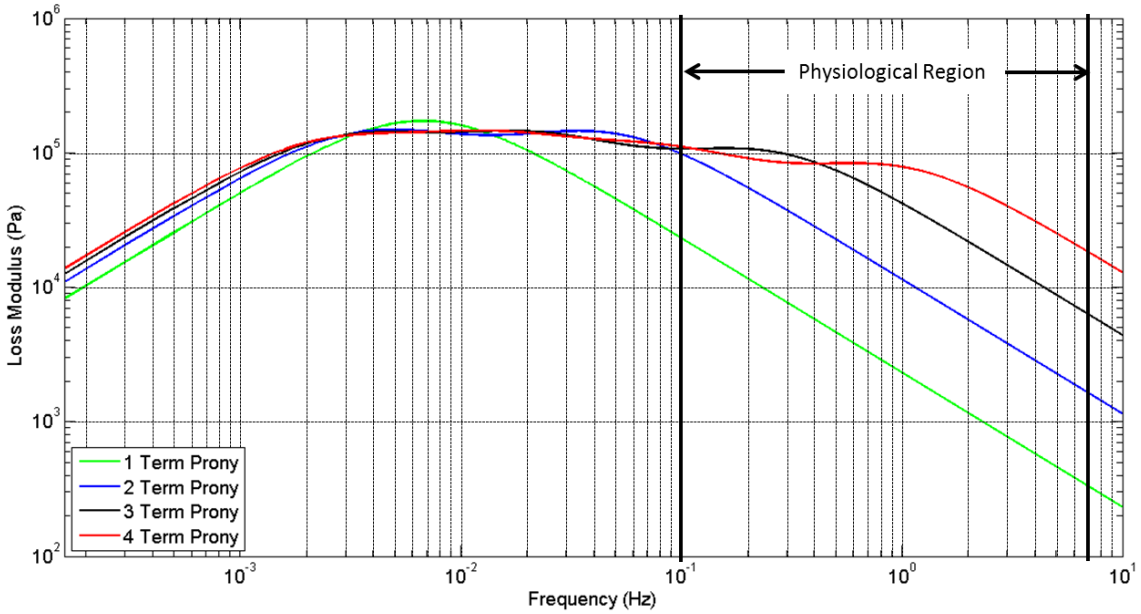

(b) Comparison of the loss information

Figure 6.1: Storage and loss comparison of different Prony models (Saline (c))

A trade-off exists between better fitting in the time-domain, and wiggles in the frequency domain. The one and two-term Prony models do not satisfactorily model the rapid decay characteristics of cartilage during stress-relaxation, and are unable to fully capture the material behavior in the frequency domain. These models are disregarded for that reason. However, the increase in fidelity of the four-term model over the three-term model is relatively minor when considering the norm values of the fits (recall Table. 5.1). A judgment call must be made as to which model provides the best combination of fitting in the time and frequency domains. In contrast to the Prony model, the CERF model uses fewer terms to characterize viscoelasticity. It is therefore less susceptible to the problem of wiggles in the frequency domain.

6.3 Fractional Model

A similar approach to that shown for the Prony series is taken to find the storage and loss components of the CERF model (Appx. C):

$$E' = E_0 + \sum_{n=1}^{\infty} \frac{E_n \left(\frac{\sqrt{2\omega}}{2}\right) \mu_n + \omega}{\mu_n^2 + \mu_n \sqrt{2\omega} + \omega} \tag{6.4}$$

$$E'' = \sum_{n=1}^{\infty} \frac{E_n \left(\frac{\sqrt{2\omega}}{2}\right) \mu_n}{\mu_n^2 + \mu_n \sqrt{2\omega} + \omega} \tag{6.5}$$

The functional forms of the storage and loss equations are nearly the same, except that the storage modulus contains the free term E_0 and additional dependency on ω. The one-term fractional model is perfectly smooth over the entire frequency domain, which is an advantage it has over the higher-term Prony models. The storage and loss moduli are shown for the fractional fit in Fig. 6.2. As expected, the storage and loss moduli show the rubbery, transition, and glassy regions of viscoelastic behavior. The additional mathematical complexity of the fractional model is tolerated because

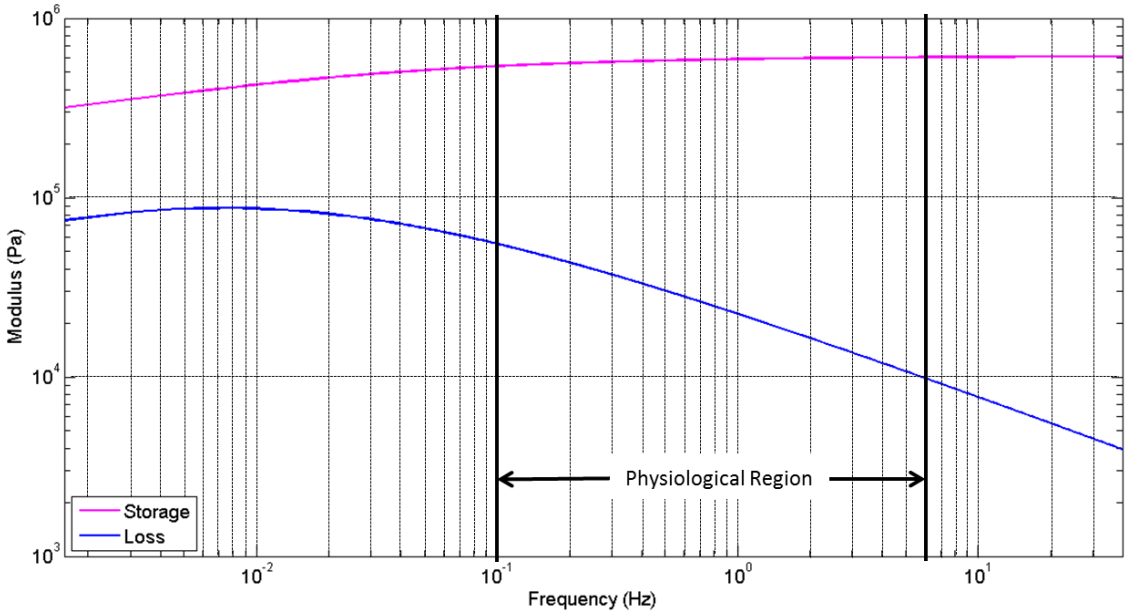

Figure 6.2: The storage and loss moduli of a one-term fractional mode (Saline (c))

fewer fractional elements are typically required to characterize viscoelasticity, as compared to the Prony model. Although the fractional model can use more elements to model viscoelasticity, the need for additional fractional elements is not necessary for cartilage.

Recall that the complementary error function also has a time-domain representation. Therefore, both the Prony series and CERF models can be fit in the time-domain and analytically transferred to the frequency domain. This eliminates any biasing that is done with smoothing procedures, and allows for an equivalent comparison of the two models.

6.4 Comparison

The Prony and CERF models are compared for some of the cartilage samples to demonstrate their capabilities. For a sample explant immersed in saline (Saline (c)), the two models are compared in Figs. 6.3a and 6.3b. The results for both models show relatively few differences. The CERF model has a slightly higher storage modulus

at low frequencies, but both models converge to nearly identical values for high frequencies (approaching the glassy modulus). In the loss modulus, both models exhibit similar behavior. However, the four-term Prony model fluctuates due to the larger number of terms. The fractional model is smooth for the entire frequency domain. There are small differences between the models, but the majority of the viscoelastic behavior is captured by either model. Both models will be used to compare the cartilage samples in further detail.

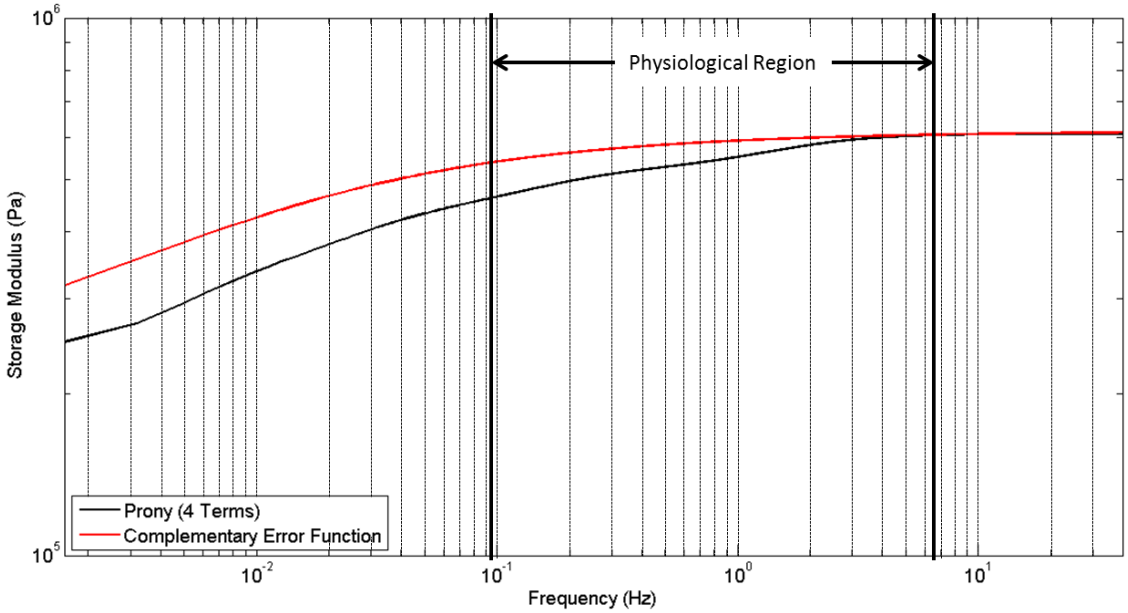

(a) Comparison of the storage information

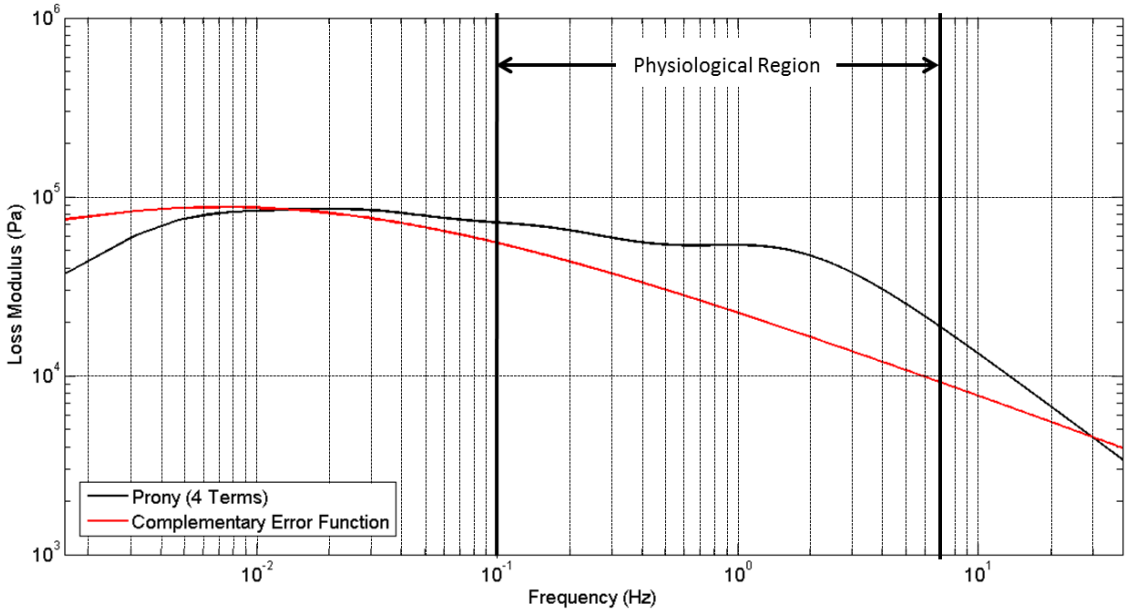

(b) Comparison of the loss information

Figure 6.3: Comparison of the storage and loss moduli of the complementary error function model and the four-term Prony series (Saline (c))

CHAPTER VII

STATISTICAL SIGNIFICANCE OF EXPERIMENTAL RESULTS

Viscoelasticity in cartilage has been established in the previous chapters, and two mechanical models have been introduced and tested. The eleven cartilage samples from the equine stifle joint remain to be compared. The information provided is intended to be a platform for additional study of viscoelastic behavior in cartilage.

7.1 Fractional and Prony Model Analysis

With biological tissues, large variations are expected between samples. It is not surprising since each cartilage explant is unique. Genetics, weight, age, diet, gender, and use can influence the mechanical properties of cartilage. Therefore, the model parameters obtained from experiments are expected to have large variations. One trend that appears ubiquitously is that the viscoelastic transition period of cartilage coincides with the physiological range of exercise. At lower frequencies, cartilage dissipates more energy than at higher frequencies, where additional elasticity is available in the joints. As shown in Fig. 6.3, the transition range of cartilage occurs in the middle of the common frequencies of motion (0.25 - 4 Hz). It is possible that the adaptive nature of cartilage is biologically designed for this purpose. A viscoelastic characterization of cartilage brings us closer to a more complete understanding of cartilage mechanics.

7.2 Moduli and Time Constant Analysis

One challenge in determining the glassy and rubbery moduli of cartilage is the thickness of the samples is not known *a priori*. The testing procedure imposes a predetermined displacement on the cartilage sample. The strain is determined by the thickness of the sample. Therefore, results obtained from the relaxation experiments are inherently over a range of strains. Attempts were made to limit the strains to 5-15%; however, there are a few cases where 15% is exceeded. Figure 7.1a shows the glassy modulus for the saline cases. Taken together, the six cases seen in Fig. 7.1a do not display a correlation of strain and instantaneous modulus. Of course, the individual samples typically have a larger glassy moduli at higher strains; however, a general trend for cartilage is not substantiated. The average glassy modulus is obtained by combining all of the samples, and statistical bounds are determined with a Student's t test. This information is presented in Table 7.1.

On a smaller scale, the rubbery modulus mimics the behavior of the glassy modulus, as shown in Fig. 7.1b. The two cases that show higher moduli in the rubbery data also correspond to higher moduli in the glassy data. Neither sample had known physiological differences from the others in the group. A very weak positive correlation ($R^2 = 0.112$) exists between the strain and rubbery moduli information. It is expected that the glassy and rubbery moduli will increase (on average) with higher strains. Physiological limits may dictate if the increase is pronounced or not. The combined rubbery modulus information is included in Table 7.1.

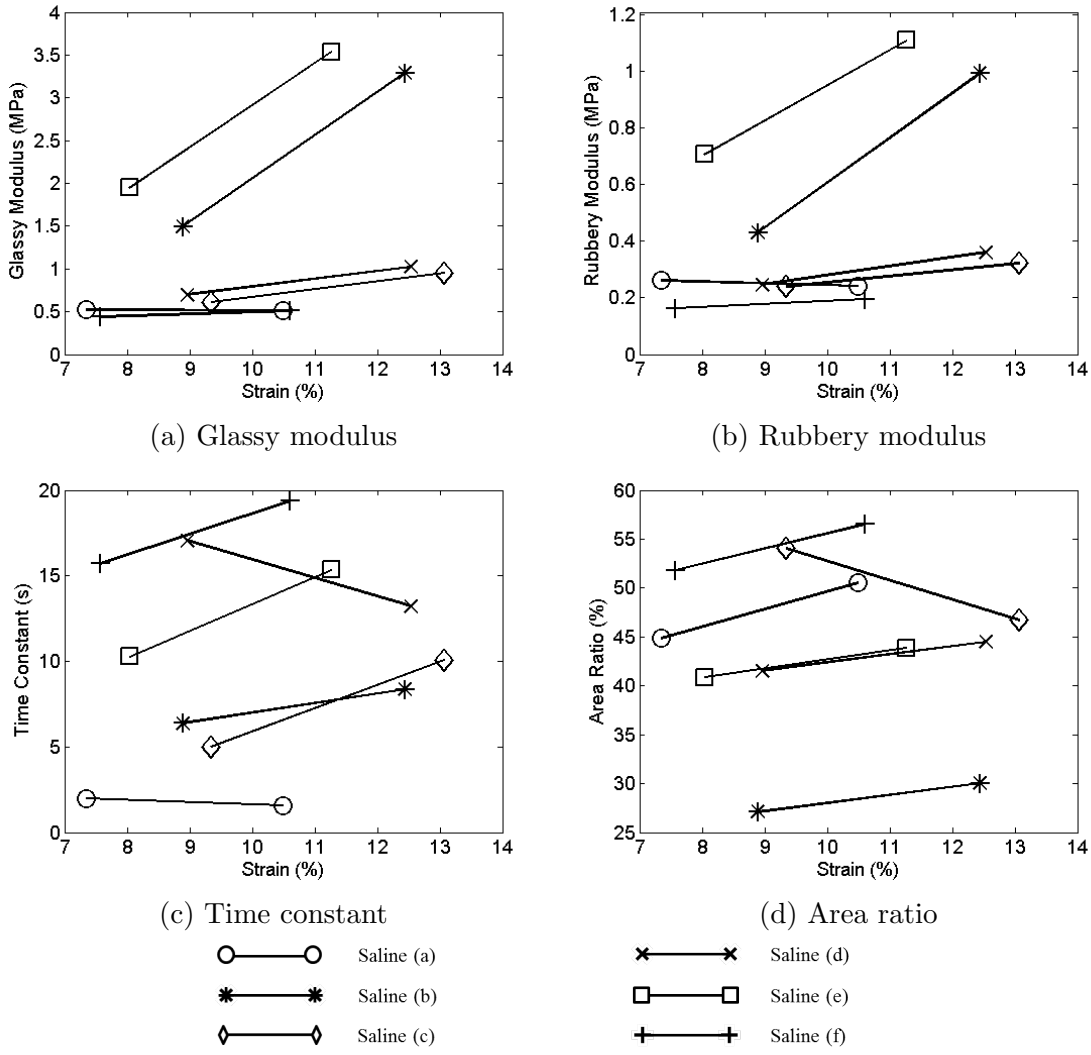

(a) Glassy modulus

(b) Rubbery modulus

(c) Time constant

(d) Area ratio

Figure 7.1: Results of stress relaxation experiments in saline

Table 7.1: Compiled glassy and rubbery modulus data for saline cases

Fluid Bath	Saline	
Number of Samples	12	
Degrees of Freedom	11	
Strain Range	7.35-13.08%	
	Glassy Modulus	Rubbery Modulus
Avg. Modulus (MPa)	**1.294**	**0.439**
Std.	1.088	0.321
SE	0.314	0.093
Two-Tailed, 95% Student's t test	2.201	
Confidence Interval +/-	0.692	0.204
Lower Mean (MPa)	**0.603**	**0.235**
Upper Mean (MPa)	**1.986**	**0.643**

Table 7.2: Compiled time data for saline cases

Fluid Bath	Saline	
Number of Samples	12	
Degrees of Freedom	11	
Strain Range	7.35-13.08%	
	Time Constant (s)	Area Ratio
Avg.	**10.36**	**44.36%**
Std.	5.91	8.86%
SE	1.71	2.56%
Two-Tailed, 95% Student's t test	2.201	
Confidence Interval +/-	3.755	5.63%
Lower Mean	**6.61**	**38.73%**
Upper Mean	**14.12**	**49.99%**

Both metrics relating to the time constant show no strain dependency for the combined cases. The time constant, found numerically from the four-term Prony series, has no distinguishable trend when considering the samples in saline, as shown in Fig. 7.1c. Likewise, the area ratio of the relaxation curve is not dependent on strain in general, which is shown in Fig. 7.1d. For a given sample, the time constant and area ratio typically increase with higher strain. The lines linking individual samples together show this phenomenon. One exception exists for both cases. In Table 7.2, each metric is averaged, and the 95% confidence intervals are given. The absence of a strong trend indicates that cartilage is unique between samples. A generalization

of all samples is difficult for this reason. The strain-dependent increase in modulus and time constant seen in most of the individual samples does not appear in the compiled data. In a particular sample, function, weight, age, and other physiological variables likely influence the cartilage response more than strain. The combined results represent a range of likely cartilage behavior, and each sample is said to have certain strain-dependent properties. More exhaustive testing and additional data should be used to corroborate this finding.

The same metrics used for the saline cases are used for the synovial fluid and synthetic fluid studies. Figure 7.2a shows the instantaneous modulus for the alternative fluids. Compared to the saline information, the alternative fluids have a stronger correlation between strain and instantaneous modulus ($R^2 = 0.557$). Individually, all of the instantaneous moduli increase as the strain increases, with one exception (Synovial (a), 06/13/2012). The rubbery modulus has a similar trend, as shown in Fig. 7.2b. The slopes of the four cases that show strain-dependency are very similar. In general, the rubbery modulus has a positive correlation with strain ($R^2 = 0.629$). Table 7.3 shows the statistical analysis of the glassy and rubbery modulus.

The time constant information is shown in Figs. 7.2c and 7.2d. Lumped together as "alternative fluids," the time constant is unchanged for the alternative fluids and saline. Clearly, not enough information exists to ascertain the effects that synthetic and synovial fluids have on cartilage mechanics. For the individual cases, the area ratio of the decay remains relatively unchanged based on strain. This trend is also shown in the saline cases. The combined information for the alternative fluid area ratio is presented in Table 7.4. The modulus and time constant do not appear to correlate in general, e.g. a higher glassy or rubbery modulus does not indicate a higher (or lower) time constant or time constant area ratio.

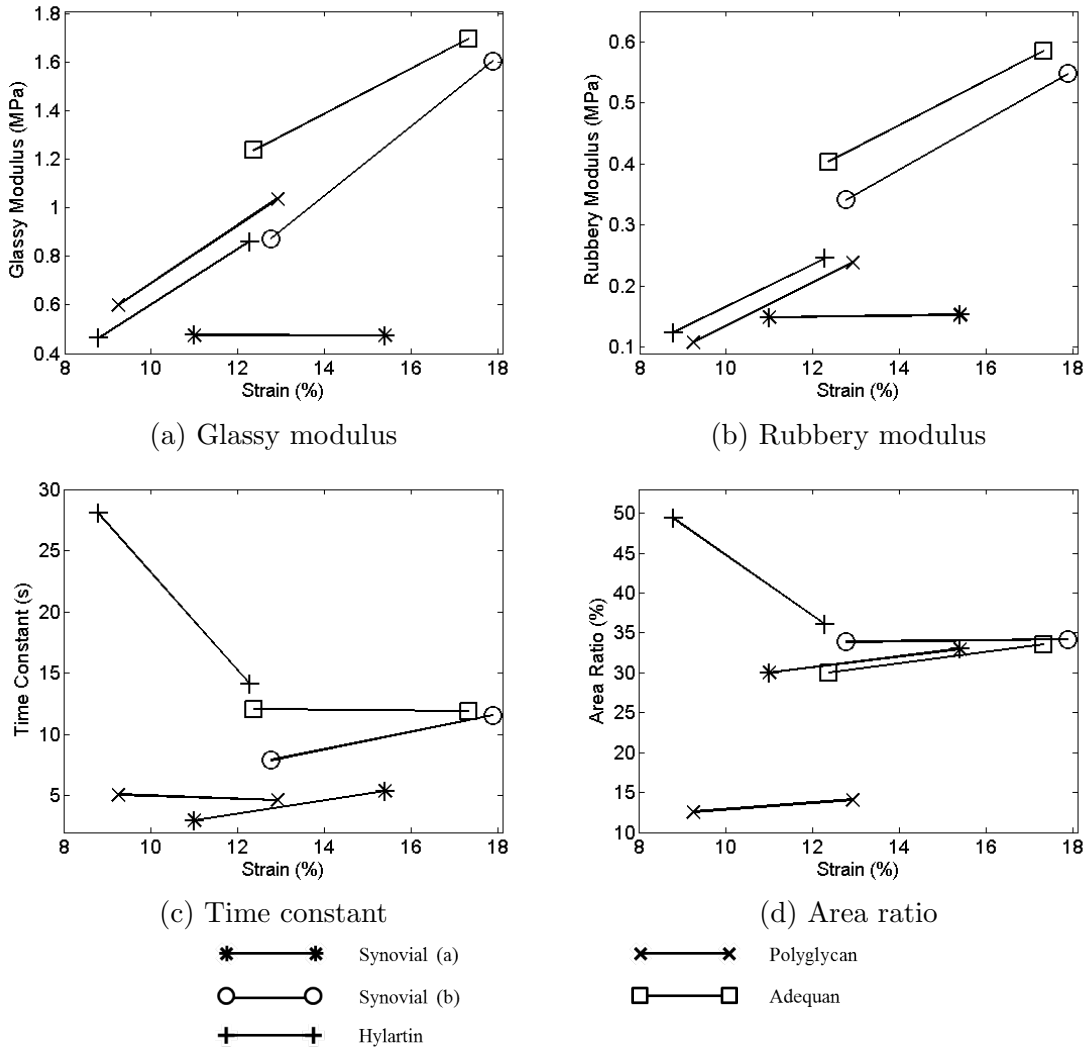

(a) Glassy modulus

(b) Rubbery modulus

(c) Time constant

(d) Area ratio

Figure 7.2: Results of stress relaxation experiments in the alternative fluids

Table 7.3: Compiled glassy and rubbery modulus data for alternative cases

Fluid Bath	Alternative	
Number of Samples	10	
Degrees of Freedom	9	
Strain Range	8.77-17.89%	
	Glassy Modulus	Rubbery Modulus
Avg. Modulus (MPa)	**0.932**	**0.290**
Std.	0.459	0.174
SE	0.145	0.055
Two-Tailed, 95% Student's t test	2.262	
Confidence Interval +/-	0.329	0.125
Lower Mean (MPa)	**0.604**	**0.165**
Upper Mean (MPa)	**1.261**	**0.414**

Table 7.4: Compiled time data for alternative cases

Fluid Bath	Alternative	
Number of Samples	10	
Degrees of Freedom	9	
Strain Range	8.77-17.89%	
	Time Constant (s)	Area Ratio
Avg.	**10.36**	**30.68%**
Std.	7.31	10.64%
SE	2.31	3.37%
Two-Tailed, 95% Student's t test	2.262	
Confidence Interval +/-	5.236	7.61%
Lower Mean	**5.137**	**23.07%**
Upper Mean	**15.590**	**38.29%**

The direction of the current study is to prove that viscoelastic models can be used to analyze cartilage. A significant number of additional tests are required to quantitatively describe the behavior of equine cartilage in the stifle joint in general. The results that are presented are preliminary to a full characterization of cartilage. However, the trends that are seen, such as a different glassy and rubbery modulus based on the type of fluid bath, are promising. More tests are needed to follow up on the results shown.

7.3 Fractional Time Constant

The fractional modeling data also contains a characteristic time parameter, μ. The fractional time constant is perhaps less intuitive than the time constant used in exponential decay. Nevertheless, the fractional time constant is an important characteristic of the mechanical behavior of cartilage. For the saline and alternative cases, μ has an average value of 0.12 and 0.07 $s^{1/2}$, respectively. The standard deviation is 0.12 and 0.075 respectively. Clearly, without a much larger number of samples, a statistical conclusion cannot be drawn about the fractional time constant. Additional work is needed to determine if the fractional time constant provides a useful metric for the analysis of cartilage.

7.4 General Characteristics

The preliminary results obtained for the eleven samples should justify additional study into cartilage viscoelasticity. Although more cartilage samples are required to give statistical significance, the experimental data obtained at this point indicates a few interesting trends. The first is that the bulk mechanical response of articular cartilage to a fixed displacement is viscoelastic in nature. Furthermore, the viscoelastic behavior can be characterized with a Prony series or a complementary error function model. This conclusion may seem trivial, but it is important to note that the mechanical response of cartilage is well captured with viscoelastic theory. A second observation is that cartilage exhibits a correlation between modulus and strain in individual samples. However, when multiple samples are combined, in saline the trend towards a higher modulus disappears, while in the alternative fluids it does not. In the individual saline cases, with one exception, the time constant and area ratio increase with strain, but the combined information does not. The alternative fluids are less predictable in general for the time information. This is not surprising as four different fluid types were used in the alternative cases.

What can be concluded from the data synthesis is that cartilage is uniquely adapted to the user. General ranges can be reported for metrics like the time constant and the glassy and rubbery modulus. These metrics have utility in the analysis of samples; however, it is imperative to remember that biological tissues will inherently have variations. The advantage of viscoelasticity is that as few as three terms are needed to characterize the bulk mechanical response of cartilage. No experimental "fudge-factors" are required for fitting the data. The disadvantage of viscoelasticity is that it reduces cartilage to a homogeneous material, which may be a physiological oversimplification. In general, mechanical modeling is used to simplify a complex system of interactions. With a material as complex as cartilage, models that can capture the majority of the mechanical response with relatively few parameters are very useful. Viscoelasticity has proven capable in this realm.

CHAPTER VIII

CLOSURE

This chapter concludes the work and gives direction for future study into the mechanics of cartilage.

8.1 Conclusions

The current work is focused on linking cartilage mechanics to viscoelastic theory. Many previous researchers have noted that cartilage displays viscoelastic behavior, but a full characterization has not occurred. The majority of viscoelastic tests being performed are creep tests, which are typically easier to execute. However, stress-relaxation experiments are more analogous to movements experienced during exercise, and are a valuable tool for characterizing a viscoelastic substance. The focus of this study has been to characterize the viscoelastic behavior of cartilage utilizing stress-relaxation experiments.

Equine articular cartilage is chosen for study because of its similarity to human cartilage [54], among other reasons. Within the equine skeleton, the stifle joint is harvested for its regions of thick, flat cartilage and for the mechanical similarity to the human knee. Stress-relaxation experiments, which mimic biological function during exercise such as walking or running, are executed utilizing a tribometer. Although an instantaneous displacement can not be obtained during actual experimentation, the CETR-UMT-3 tribometer is capable of producing a sufficiently fast displacement for the study. The resulting relaxation in the cartilage is captured and fit with the Prony and CERF viscoelastic models. Both models can be analytically transferred to the frequency domain, and studied as the storage and loss moduli. Therefore, the cartilage samples are tested in the time-domain with a relaxation experiment, and analyzed in

the frequency domain as a function of gait. This is an important advantage of linear viscoelasticity, and the Boltzmann convolution integral that describes it.

The viscoelastic transition range of cartilage from a rubbery to glassy modulus was found to be directly in the physiological range of gaits that humans and horses experience. Cartilage is likely either inherently designed to operate in this manner, or it adapts to meet the needs of the user. In either case, this shows another unique aspect of cartilage that helps to protect joints and facilitate motion. The tailored nature of cartilage makes it difficult to draw comparisons between samples; however, a general range for the instantaneous modulus is between 0.747 and 1.512 MPa for all of the samples combined. For the equilibrium modulus, the range is between 0.252 and 0.491 MPa. The time constant and area ratios are: 10.363 s +/- 2.844 s, 38.14% +/- 5.21%, respectively. The strain varied in the tests from 7.35% to 17.89%. Certainly, additional tests are needed to make more robust characterizations; however, cartilage's viscoelastic nature is established.

Experimentally repeatable relaxation patterns in cartilage show strong viscoelastic characteristics. Although the relaxation appears to be strain-dependent, the variation due to strain could be small enough to characterize within the limits of linear viscoelastic theory. The advantage of linear viscoelasticity is the model simplicity. For the fractional model, three parameters are capable of characterizing the viscoelasticity in cartilage. A trade-off exists between the number of material parameters used, and complete specificity of the model. Viscoelasticity can provide critical information about the mechanical capabilities of cartilage. This can be used for major comparisons between species, or between healthy and diseased cartilage. Perhaps an entire picture of the mechanics of cartilage cannot be described with viscoelasticity; however, it is an important piece of the puzzle. Additional refinement of the models used in the current study could extend the flexibility of viscoelastic theory for cartilage.

8.2 Future Work

The current study is an initial foray into the mechanical nature of articular cartilage. A lot of additional aspects of cartilage remain to be studied. Based on the information from the current study, some potential modeling changes are proposed for future work and consideration.

First, additional tests should be performed to reduce the statistical variance seen in the current study. A wider range of strains should be studied as well. The ability of cartilage to recover from *in vitro* testing procedures needs further analysis too. These studies should be performed to develop a benchmark for healthy articular cartilage. Tests of other articulating joints should be performed for comparison purposes. Previous work on the surface morphology of cartilage indicates that the type of loading and motion affects the structure of the medium [60, 61]. It is likely that different joints have different mechanical responses as well.

In the viscoelastic model, the strain-dependent behavior should be considered. It is hypothesized that the strain dependency of articular cartilage could be non-linear in general, but the actual viscoelastic contribution could be linear with time (linear viscoelasticity). Equations 8.1 and 8.2 describe the standard linear viscoelastic models with nonlinear strain dependency. It is likely that this hypothesis is valid for a limited range of strains.

$$E(t,\epsilon) = E_0(\epsilon) + \sum_{n=1}^{\infty} E_n(\epsilon) e^{\lambda_n t} \tag{8.1}$$

$$E(t,\epsilon) = E_0(\epsilon) + \sum_{n=1}^{\infty} E_n(\epsilon) e^{\left(\mu_n{}^2 t\right)} erfc\ (\mu_n \sqrt{t}) \tag{8.2}$$

The primary driver of viscoelastic dissipation in cartilage is the flow of interstitial fluid from the collagen matrix. High strains cause a more rapid exodus of fluid from the cartilage, which changes the relaxation history. Whether a full range of strains in cartilage can be reliably approximated with linear viscoelasticity remains to be seen.

Future work should certainly extend viscoelastic theory to accommodate the strain information. Similarly, cartilage relaxation should be studied over a wide range of strains (upwards of 20%).

The advantages of linear viscoelasticity make it an attractive theory for extrapolation in modeling applications. However, if the full nature of cartilage cannot be characterized with linear viscoelastic theory, nonlinear theories can be used. Fung also proposed a quasilinear theory for soft tissues that could be explored for modeling cartilage. These models are more challenging to implement and analyze, but they have the potential to capture the entire physiological range of strain seen in cartilage.

Additional research is needed to quantify the mechanical response of cartilage when immersed in different fluids. Research should also determine the time it takes for the bathing fluid to fully saturate the sample. Preliminary results were largely inconclusive in determining the effect of the bathing medium. The cartilage samples showed the same monotonically decreasing behavior, but the amount of energy transferred and stored is likely different based on the immersing fluid. The more viscous fluids are hypothesized to excrete through the cartilage matrix at a slower rate than saline. The slower movement of fluid should correspond to a larger time constant in the response. However, cartilage is a complex medium with many variables. Additional experimental work is required to attribute the noted changes in mechanical behavior to a specific fluid property.

Articular cartilage is an effective medium for the facilitation of motion in mammalian joints. The motivation for studying cartilage is to understand the mechanisms that make it unique. It is desired to constitutively model cartilage with as simple of a model as possible, so that distinctions can be made between healthy and arthritic cartilage, between joints undergoing different motions and loading, and between different species. In evaluating the predictive capabilities of cartilage models, the constitutive

models that are easiest to implement in FEA programs and other predictive packages have the greatest utility. It is a trade-off in determining the model that best captures the behavior of cartilage, and is easiest to implement. The standard linear solid models used in this work are the foundation for more extensive research.

APPENDIX A

VISCOELASTIC-ELASTIC CORRESPONDENCE PRINCIPLE

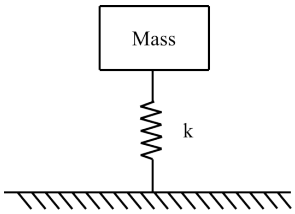

Figure A.1: Spring and mass model for linear elastic solid

A physical foundation of the viscoelastic-elastic correspondence principle is established by considering spring and mass models [48, 47, 57]. A spring is used to represent a linearly elastic solid. For the spring-mass system, shown in Fig. A.1, we write the governing dynamic equation:

$$m\ddot{x} = -kx \tag{A.1}$$

or simply:

$$m\ddot{x} + kx = 0 \tag{A.2}$$

assuming a solution for x:

$$x = \overline{\underline{X}} e^{st} \tag{A.3}$$

where $\overline{\underline{X}}$ is a magnitude and s is a complex eigenvalue, in general. Applying the assumed solution to Eq. A.2, the following result is obtained:

$$(ms^2 + k)\overline{\underline{X}} e^{st} = 0 \tag{A.4}$$

or:

$$ms^2 + k = 0 \tag{A.5}$$

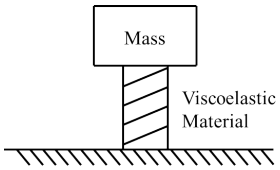

Figure A.2: Viscoelastic material and mass model

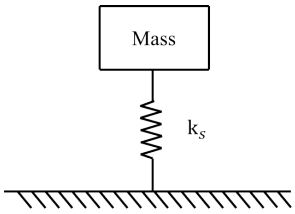

Figure A.3: Pseudo-spring and mass model for viscoelastic solid

Eq. A.5 will be retained for comparison with a viscoelastic material. Consider a mass attached to a viscoelastic material, as shown in Fig. A.2. Now, allow for a replacement of the viscoelastic material with a pseudo-spring, as shown in Fig. A.3. The pseudo-spring represents the relaxation stiffness (see Szumski [47] and Miller [48]), i.e. $k_s(t) = F(t)/x_{step}$, where x_{step} is a step input. The dynamics now appear very similar to those of the elastic material, except that the elastic spring, k, has been replaced with a pseudo-spring, k_s. Applying a similar force balance:

$$m\ddot{x} = -k_s x \tag{A.6}$$

or simply:

$$m\ddot{x} + k_s x = 0 \tag{A.7}$$

using the same assumed solution for x (Eq. A.3), and applying to Eq. A.7:

$$(ms^2 + k_s)\overline{X}e^{st} = 0 \tag{A.8}$$

or:

$$ms^2 + k_s = 0 \tag{A.9}$$

The viscoelastic-elastic correspondence principle essentially states that the pseudo-spring, k_s, that is used to describe the viscoelastic material can be replaced with $sk(s)$. This simply gives:

$$ms^2 + sk(s) = 0 \tag{A.10}$$

The $k(s)$ term is a function of s and has both elastic and dissipative properties. Comparing with Eq. A.5, it is straightforward to see the difference between an elastic and a linear viscoelastic material. As discussed, viscoelastic materials take a form similar to that of Hooke's law in the Laplace domain. The utility of this finding is that the eigenvalue problem is reduced in the dynamic analysis of viscoelastic materials. The relative simplicity of linear viscoelastic theory makes it an attractive model for many materials.

APPENDIX B

PRONY SERIES DERIVED

The derivation for a Prony series is relatively straightforward; however, some preliminary definitions and explanations should be made before continuing. First, it is convenient to define a spring and dashpot in series as a Maxwell element (Fig. B.1). Now, consider a Maxwell element in parallel with a free spring, as shown in Fig. B.2. The configuration shown in Fig. B.2 is known as the standard linear solid, or a one-term Prony series.

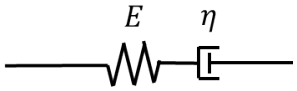

Figure B.1: Maxwell element

Using the notation "one-term Prony series" to define the standard linear solid appears somewhat ambiguous, as the equation actually contains three material parameters- E_0, E_1, and η_1. However, inspection of Eq. 3.9 explains why the label is used. A one-term Prony series refers to $n = 1$, which yields the three material terms expected- E_0, E_1, and η_1. Therefore, a n-term Prony series actually refers to the number of

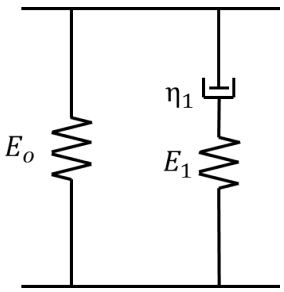

Figure B.2: One Maxwell element Prony series

Maxwell elements in the series, not the total number of material parameters. The number of material parameters in a n-term Prony series is $2n + 1$.

Returning to the standard linear solid, the stress-strain relationship can be determined by noting that the total stress in the model is superimposed while the stain is common:

$$\sigma_T = \sigma_{s_0} + \sigma_M \tag{B.1}$$

$$\epsilon_T = \epsilon_{s_0} = \epsilon_M. \tag{B.2}$$

Here, T denotes the total system, s_0 the free spring, and M the Maxwell element. The total stress in the Prony series is the sum of the free spring and the Maxwell elements, while the total strain is common for all elements. Within the Maxwell element, the stress and strain are as follows:

$$\sigma_M = \sigma_{s_1} = \sigma_D \tag{B.3}$$

$$\epsilon_M = \epsilon_{s_1} + \epsilon_D \tag{B.4}$$

where D denotes the dashpot and s_1 denotes the spring in the Maxwell element. Individually, the stress in a particular spring or dashpot element is:

$$\sigma_{s_1} = E\epsilon_{s_1} \tag{B.5}$$

$$\sigma_D = \eta_1\dot{\epsilon}_D \tag{B.6}$$

Taking the derivative of Eq. B.4 with note of Eq. B.2 yields:

$$\dot{\epsilon}_T = \dot{\epsilon}_{s_1} + \dot{\epsilon}_D \tag{B.7}$$

which can be expressed in terms of strain and stress utilizing Eqs. B.5 and B.6:

$$\dot{\epsilon}_T = \frac{1}{E_1}\dot{\sigma}_{s_1} + \frac{1}{\eta_1}\sigma_D \tag{B.8}$$

or simplified with Eq. B.3:

$$\dot{\epsilon}_T = \frac{1}{E_1}\dot{\sigma}_M + \frac{1}{\eta_1}\sigma_M \tag{B.9}$$

Applying Eq. B.1 yields:

$$\dot{\epsilon}_T = \frac{1}{E_1}(\dot{\sigma}_T - \dot{\sigma}_{S_0}) + \frac{1}{\eta_1}(\sigma_T - \sigma_{S_0}) \tag{B.10}$$

$$\dot{\epsilon}_T = \frac{1}{E_1}(\dot{\sigma}_T - E_0\dot{\epsilon}_{S_0}) + \frac{1}{\eta_1}(\sigma_T - E_0\epsilon_{S_0}) \tag{B.11}$$

$$\dot{\epsilon}_T = \frac{1}{E_1}(\dot{\sigma}_T - E_0\dot{\epsilon}_T) + \frac{1}{\eta_1}(\sigma_T - E_0\epsilon_T) \tag{B.12}$$

Finally arriving at the constitutive equation for a one-term Prony series:

$$\left(1 + \frac{E_0}{E_1}\right)\dot{\epsilon}_T + \frac{E_0}{\eta_1}\epsilon_T = \frac{1}{E_1}\dot{\sigma}_T + \frac{1}{\eta_1}\sigma_T \tag{B.13}$$

For a relaxation experiment ($\dot{\epsilon_T} = 0, \epsilon_T = \epsilon_0$), the Prony series can be solved easily:

$$\frac{E_0}{\eta_1}\epsilon_0 = \frac{1}{E_1}\dot{\sigma}_T + \frac{1}{\eta_1}\sigma_T. \tag{B.14}$$

This is a first-order differential equation, with the particular solution giving the free spring solution:

$$\sigma_T = E_0\epsilon_0 \tag{B.15}$$

and the homogeneous solution giving the Maxwell solution:

$$\sigma_T = C_1 e^{-\frac{E_1}{\eta_1}t} \tag{B.16}$$

solving for the initial condition $\sigma(0) = \sigma_0 = (E_0 + E_1)\epsilon_0$ and combining with the free spring solution gives the solution for the one Maxwell element (one-term) Prony series:

$$\sigma_T = (E_0 + E_1 e^{-\lambda_1 t})\epsilon_0 \tag{B.17}$$

where

$$\lambda_1 = \frac{E_1}{\eta_1} \tag{B.18}$$

and the characteristic time constant is simply:

$$\tau_1 = \frac{1}{\lambda_1} \tag{B.19}$$

When $t = \tau_1 = \frac{1}{\lambda_1}$, the Maxwell element retains only 36.8% of its initial load support. This is typical of a first-order system like the one described by Eq. B.14. The idea of a characteristic time constant is used throughout the thesis, and is extrapolated to the 3 and 4-term Prony series models.

Returning to Eq. B.17, by the principle of linear superposition, the Prony series can be expanded to include more Maxwell elements in parallel. Generalizing Eq. B.17 gives:

$$\sigma_T = \left(E_0 + \sum_{n=1}^{\infty} E_n e^{\lambda_n t} \right) \epsilon_0 \tag{3.9}$$

where the parenthesis encapsulate the relaxation modulus.

$$E(t) \triangleq E_0 + \sum_{n=1}^{\infty} E_n e^{\lambda_n t} \tag{B.20}$$

For a Prony series, the glassy and rubbery moduli are easily determined:

$$E_{glassy}(t \to 0) = E_0 + \sum_{n=1}^{\infty} E_n \tag{B.21}$$

$$E_{rubbery}(t \to \infty) = E_0 \tag{B.22}$$

B.1 Prony Series in Frequency Domain

The definition of a Fourier transform is used to determine the Prony series in the frequency domain:

$$\mathcal{F}\left\{E(t)\right\} = E\left(\omega\right) = \int_{\infty}^{\infty} E(t) e^{-i\omega t}\,\mathrm{d}t \tag{B.23}$$

Consider $E(t)$ to be a one-term Prony series that is zero for all time $t < 0$:

$$E\left(\omega\right) = \int_{0}^{\infty} (E_0 + E_1 e^{-\lambda_1 t}) e^{-i\omega t}\,\mathrm{d}t \tag{B.24}$$

solving Eq. B.24:

$$E\left(\omega\right) = \frac{-E_0}{i\omega} e^{-i\omega t}\Big|_{t=0}^{t=\infty} + \frac{-E_1}{\lambda_1 + i\omega} e^{-(\lambda_1 + i\omega t)}\Big|_{t=0}^{t=\infty} \tag{B.25}$$

and evaluating:

$$E\left(\omega\right) = \frac{E_0}{i\omega} + \frac{E_1}{\lambda_1 + i\omega} \tag{B.26}$$

A multiplication operation on the second term removes the imaginary component from the denominator:

$$E\left(\omega\right) = \frac{E_0}{i\omega} + \frac{E_1}{\lambda_1 + i\omega}\left(\frac{\lambda_1 - i\omega}{\lambda_1 - i\omega}\right) \tag{B.27}$$

yielding:

$$E\left(\omega\right) = \frac{E_0}{i\omega} + E_1\left(\frac{\lambda_1 - i\omega}{\lambda_1^2 + \omega^2}\right) \tag{B.28}$$

A full Prony series in the frequency domain can then be generalized as:

$$E(\omega) = \frac{E_0}{i\omega} + \sum_{n=1}^{\infty} E_n \left(\frac{\lambda_n - i\omega}{\lambda_n^2 + \omega^2} \right) \tag{6.1}$$

By the elastic-viscoelastic correspondence principle, the storage and loss moduli are:

$$E'(\omega) = E_0 + \sum_{n=1}^{\infty} \omega^2 \left(\frac{E_n}{\lambda_n^2 + \omega^2} \right) \tag{6.2}$$

$$E''(\omega) = \sum_{n=1}^{\infty} \left(\frac{E_n \lambda_n \omega}{\lambda_n^2 + \omega^2} \right) \tag{6.3}$$

From the storage and loss moduli, the limits at low and high frequencies are obtained:

$$E'\big|_{\omega\to\infty} = E_0 + \sum_{n=1}^{\infty} E_n \tag{B.29}$$

$$E'\big|_{\omega\to 0} = E_0 \tag{B.30}$$

The loss data approaches zero at both frequency extremes:

$$E''\big|_{\omega\to\infty} = 0 \tag{B.31}$$

$$E''\big|_{\omega\to 0} = 0 \tag{B.32}$$

Therefore, the glassy and rubbery moduli only contain data from the storage (real) moduli.

$$E_{glassy} = E'\big|_{\omega\to\infty} = E_0 + \sum_{n=1}^{\infty} E_n \tag{B.33}$$

$$E_{rubbery} = E'\big|_{\omega\to 0} = E_0 \tag{B.34}$$

This is seen graphically in Fig. 3.2 as well, where the loss moduli approaches zero at the low and high frequency endpoints. However, in the transition region, the loss moduli is clearly non-zero.

APPENDIX C

FRACTIONAL DERIVATIVE MODEL

For a one-element fractional derivative model, the constitutive equation relating stress to strain is similar to that of the one-term Prony model (Eq. B.13), except that the dashpot of the Prony model is replaced with the spring-pot element:

$$\frac{d\epsilon_T}{dt} \longleftarrow \frac{d^\alpha \epsilon_T}{dt^\alpha} \tag{C.1}$$

$$\frac{d\sigma_T}{dt} \longleftarrow \frac{d^\alpha \sigma_T}{dt^\alpha} \tag{C.2}$$

leading to the constitutive equation for the fractional derivative model:

$$\left(1 + \frac{E_0}{E_1}\right) \frac{d^\alpha \epsilon_T}{dt^\alpha} + \frac{E_0}{\eta_1}\epsilon_T = \frac{1}{E_1}\frac{d^\alpha \sigma_T}{dt^\alpha} + \frac{1}{\eta_1}\sigma_T \tag{C.3}$$

In Eq. C.3, if $\alpha = 1$, the constitutive model becomes the standard linear solid (one-term Prony) model. If $\alpha = 0$, the spring-pot simply becomes a spring and the entire model is reduced to an equivalent linear spring. For any fractional valued α between 0 and 1, the spring-pot element has both spring and dashpot behavior.

Equation C.3 is conveniently analyzed in the Laplace domain, which allows for treatment of the fractional power.

$$\left[\left(1 + \frac{E_0}{E_1}\right) s^\alpha + \frac{E_0}{\eta_1}\right] \epsilon(s) = \left(\frac{1}{E_1} s^\alpha + \frac{1}{\eta_1}\right) \sigma(s) \tag{C.4}$$

Rearranging Eq. C.4 and applying the elastic-viscoelastic correspondence principle (Eq. 3.3), the relaxation modulus can be found:

$$E(s) = \frac{\left[\left(1 + \frac{E_0}{E_1}\right) s^{\alpha} + \frac{E_0}{\eta_1}\right]}{\left(\frac{1}{E_1} s^{\alpha} + \frac{1}{\eta_1}\right)} \frac{1}{s} \tag{C.5}$$

The relationship between the Laplace and frequency domains allows for the fractional model to be obtained:

$$E(\omega) = \frac{\left[\left(1 + \frac{E_0}{E_1}\right) (i\omega)^{\alpha} + \frac{E_0}{\eta_1}\right]}{\left[\frac{1}{E_1} (i\omega)^{\alpha} + \frac{1}{\eta_1}\right]} \left(\frac{1}{i\omega}\right) \tag{C.6}$$

With some algebra, Eq. C.6 can be reduced:

$$E(\omega) = \frac{\left[\left(1 + \frac{E_0}{E_1}\right) (i\omega)^{\alpha} + \frac{E_0}{\eta_1}\right]}{\left[\frac{1}{E_1} (i\omega)^{\alpha} + \frac{1}{\eta_1}\right]} \left(\frac{E_1}{E_1}\right) \left(\frac{1}{i\omega}\right) \tag{C.7}$$

$$E(\omega) = \frac{\left[\left(E_1 + E_0\right) (i\omega)^{\alpha} + E_0 \frac{E_1}{\eta_1}\right]}{\left[(i\omega)^{\alpha} + \frac{E_1}{\eta_1}\right]} \left(\frac{1}{i\omega}\right) \tag{C.8}$$

$$E(\omega) = \frac{\left[(i\omega)^{\alpha} + \frac{E_1}{\eta_1}\right]}{\left[(i\omega)^{\alpha} + \frac{E_1}{\eta_1}\right]} \left(\frac{E_0}{i\omega}\right) + \frac{E_1 (i\omega)^{\alpha}}{\left[(i\omega)^{\alpha} + \frac{E_1}{\eta_1}\right]} \left(\frac{1}{i\omega}\right) \tag{C.9}$$

$$E(\omega) = \frac{E_0}{i\omega} + \frac{E_1 (i\omega)^{\alpha}}{\left[(i\omega)^{\alpha} + \frac{E_1}{\eta_1}\right]} \left(\frac{1}{i\omega}\right) \tag{C.10}$$

If required, the fractional model can be generalized as follows:

$$E(\omega) = \frac{E_0}{i\omega} + \sum_{n=1}^{\infty} \frac{E_n (i\omega)^{\alpha}}{\left[(i\omega)^{\alpha} + \frac{E_n}{\eta_n}\right]} \left(\frac{1}{i\omega}\right) \tag{3.11}$$

The complex modulus can be easily found from Eq. 3.11:

$$E^*(\omega) = E_0 + \sum_{n=1}^{\infty} \frac{E_n (i\omega)^{\alpha}}{\left[(i\omega)^{\alpha} + \frac{E_n}{\eta_n}\right]} \tag{C.11}$$

C.1 Simplifications for $\alpha = 1/2$ (special case)

For the special case of $\alpha = 1/2$, the mathematics of the fractional model simplify dramatically. In the time domain, a concise solution appears in the form of a complementary error function multiplied by a decaying exponential. An analytic form of the model can be found for the frequency domain solution as well. Consider a one-term fractional model with $\alpha = 1/2$:

$$E^*(\omega) = E_0 + \frac{E_1 (i\omega)^{1/2}}{\left[(i\omega)^{1/2} + \frac{E_1}{\eta_1}\right]} \tag{C.12}$$

The square root of $i\omega$ can be found from the generalized form of de Moivre's theorem:

$$(i\omega)^{1/2} = \frac{\sqrt{2\omega}}{2}(1+i) \tag{C.13}$$

Two substitutions help clarify the mathematics:

$$\beta = \frac{\sqrt{2\omega}}{2} \tag{C.14}$$

$$\mu_1 = \frac{E_1}{\eta_1} \tag{C.15}$$

Substituting these relations into Eq. C.12 yields:

$$E^*(\omega) = E_0 + \frac{E_1\beta(1+i)}{\mu_1 + \beta(1+i)} \tag{C.16}$$

Simplifying the fraction:

$$E^*(\omega) = E_0 + \frac{E_1\beta(1+i)}{\mu_1 + \beta(1+i)}\left[\frac{\mu_1 - \beta(1+i)}{\mu_1 - \beta(1+i)}\right] \tag{C.17}$$

$$E^*(\omega) = E_0 + \frac{E_1\beta\mu_1(1+i) - E_1\beta^2(1+i)^2}{\mu_1^2 - \beta^2(1+i)^2} \tag{C.18}$$

Which can be simplified with $(1+i)^2 = 2i$

$$E^*(\omega) = E_0 + \frac{E_1\beta\mu_1(1+i) - E_1\beta^2(2i)}{\mu_1^2 - \beta^2(2i)} \tag{C.19}$$

$$E^*(\omega) = E_0 + E_1\beta\left[\frac{\mu_1 - (2\beta - \mu_1)i}{\mu_1^2 - 2\beta^2 i}\right] \tag{C.20}$$

With one additional multiplication, the imaginary part of the denominator can be eliminated:

$$E^*(\omega) = E_0 + E_1\beta\left[\frac{\mu_1 - (2\beta - \mu_1)i}{\mu_1^2 - 2\beta^2 i}\right]\left[\frac{\mu_1^2 + 2\beta^2 i}{\mu_1^2 + 2\beta^2 i}\right] \tag{C.21}$$

$$E^*(\omega) = E_0 + E_1\beta\left[\frac{\mu_1(\mu_1^2 + 2\beta^2 i) - i(2\beta - \mu_1)(\mu_1^2 + 2\beta^2 i)}{\mu_1^4 + 4\beta^4}\right] \tag{C.22}$$

The numerator can be rearranged to separate the real and imaginary components:

$$E^*(\omega) = E_0 + E_1\beta\left[\frac{\mu_1^3 - 2\beta^2\mu_1 + 4\beta^3 + i(\mu_1^3 - 2\beta\mu_1^2 + 2\beta^2\mu_1)}{\mu_1^4 + 4\beta^4}\right] \tag{C.23}$$

Further simplification leads to:

$$E^*(\omega) = E_0 + E_1\beta\left[\frac{(\mu_1 + 2\beta)(\mu_1^2 - 2\mu_1\beta + 2\beta^2) + i\mu_1(\mu_1^2 - 2\mu_1\beta + 2\beta^2)}{(\mu_1^2 - 2\mu_1\beta + 2\beta^2)(\mu_1^2 + 2\mu_1\beta + 2\beta^2)}\right] \tag{C.24}$$

$$E^*(\omega) = E_0 + E_1\beta\left[\frac{\mu_1 + 2\beta}{\mu_1^2 + 2\mu_1\beta + 2\beta^2} + \frac{i\mu_1}{\mu_1^2 + 2\mu_1\beta + 2\beta^2}\right] \tag{C.25}$$

Substitution of Eq. C.14:

$$E^*(\omega) = E_0 + E_1\left[\frac{\left(\frac{\sqrt{2\omega}}{2}\right)\mu_1 + \omega}{\mu_1^2 + \mu_1\sqrt{2\omega} + \omega} + \frac{i\left(\frac{\sqrt{2\omega}}{2}\right)\mu_1}{\mu_1^2 + \mu_1\sqrt{2\omega} + \omega}\right] \tag{C.26}$$

Eq. C.26 can be generalized for any number of fractional terms, although the utility of the fractional model is that few terms typically need to be used to characterize viscoelastic behavior.

$$E^*(\omega) = E_0 + \sum_{n=1}^{\infty} E_n \left[\frac{\left(\frac{\sqrt{2\omega}}{2}\right)\mu_n + \omega}{\mu_n^2 + \mu_n\sqrt{2\omega} + \omega} + \frac{i\left(\frac{\sqrt{2\omega}}{2}\right)\mu_n}{\mu_n^2 + \mu_n\sqrt{2\omega} + \omega} \right] \tag{C.27}$$

$$E'(\omega) = E_0 + \sum_{n=1}^{\infty} E_n \left[\frac{\left(\frac{\sqrt{2\omega}}{2}\right)\mu_n + \omega}{\mu_n^2 + \mu_n\sqrt{2\omega} + \omega} \right] \tag{C.28}$$

$$E''(\omega) = \sum_{n=1}^{\infty} E_n \left[\frac{\left(\frac{\sqrt{2\omega}}{2}\right)\mu_n}{\mu_n^2 + \mu_n\sqrt{2\omega} + \omega} \right] \tag{C.29}$$

For the fractional derivative model where $\alpha = 1/2$, there exists a concise time-domain solution [47]:

$$E(t) = E_0 + \sum_{n=1}^{\infty} E_n e^{(\mu_n{}^2 t)} erfc\ (\mu_n\sqrt{t}) \tag{3.14}$$

which is a decaying complementary error function multiplied by an increasing exponential. To prove that the result of the multiplication of these two functions is a monotonically decreasing function, a comparison is presented in Fig. C.1.

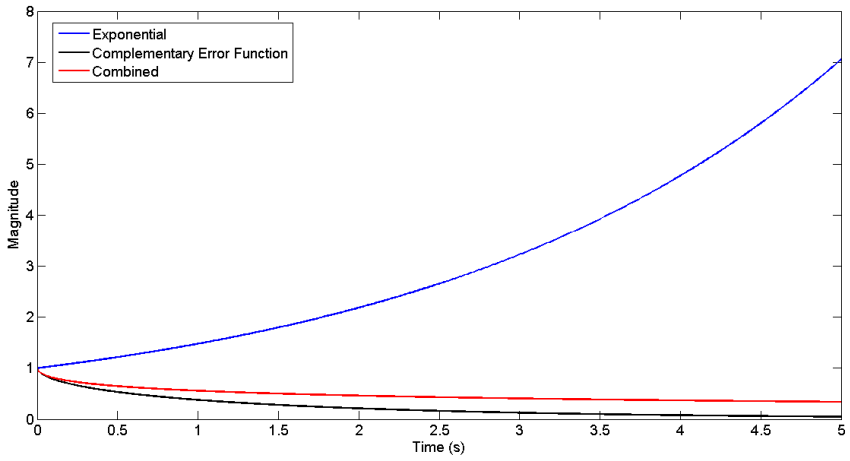

Figure C.1: Comparison of exponential and complementary error function curves

It is clear that the decaying error function dominates the behavior of the fractional viscoelastic model. In this example, the value used for μ is 0.625, which is a reasonable

value for cartilage. However, it should be noted that the monotonically decreasing nature shown in Fig. C.1 does not depend on the value of μ.

APPENDIX D

EQUIPMENT SPECIFICATION

The major pieces of equipment used in the data acquisition process are the bandsaw and tribometer. Company information is provided below:

Grizzly Industrial Inc. G0513P 17 Bandsaw. Grizzly Industrials. Bellingham Washington. 1821 Valencia St. Bellingham, WA 98229[1].

Figure D.1: Grizzly Bandsaw

[1]Figure taken from manufacturer's website

Bruker Technology. CETR-UMT-3 Tribometer. Bruker Nano Surfaces Division. Campbell, CA USA[2]

Figure D.2: CETR UMT-3 Tribometer

Additionally, some small equipment is used for the cartilage plug creating process: an arbor press, Dremel rotary tool, and leather punching kit. The experimental data is reduced with Matlab, the least squares fitting program REGRESS, and Microsoft Excel. The thesis is written in Latex using MikTex.

Various stages of the dissection process are shown in Fig. D.3:

[2]Figure taken from manufacturer's website

(a) Stifle joint after bulk dissection, with the joint capsule intact

(b) Resizing of stifle joint with bandsaw

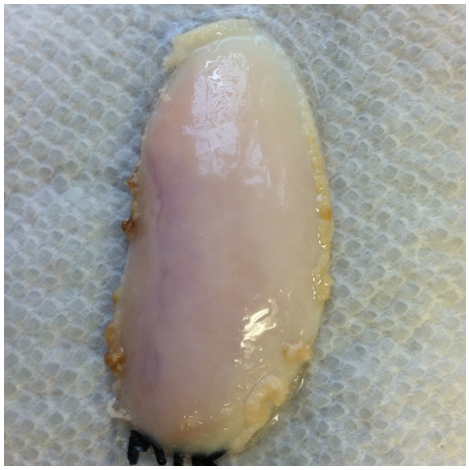

(c) Resized cartilage surface from stifle

(d) Plug created in the cartilage surface

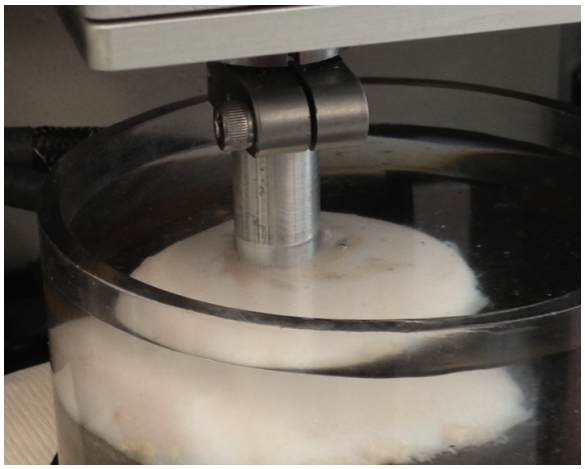

(e) Stress-relaxation analysis of cartilage plug with tribometer

Figure D.3: Steps taken in the dissection process

APPENDIX E

TEST RECORDS FOR EXPERIMENTS

For each of the 11 cases analyzed in the current study, the material modeling parameters are presented for the three and four-term Prony series, as well as the fractional model. The model parameters are located in two columns- one for the lower strain tests, and one for the higher strain tests. Additionally, the biographical and time constant information is presented as well. Recall from Chapter. 5 that the "Normalized Time Constant Area" is the area under the reduced relaxation curve from $t = 0$ to $t = t_{TC}$, normalized by the glassy modulus for convenience. The normalization is merely useful for presentation. The "Area Ratio," defined as:

$$Area\ Ratio = \frac{Normalized\ Time\ Constant\ Area}{Normalized\ Total\ Area}. \tag{E.1}$$

The Area Ratio will be the same regardless of normalization. Of course, the "Normalized Total Area" is the area under the reduced relaxation curve from $t = 0$ to $t = t_{\infty}$.

In the specific model parameter presentations, the "norm" gives an idea of the quality of the fit. The norm is defined as:

$$Norm = \sqrt{\sum_{i=1}^{n} \left(x_{i,exp} - x_{i,model}\right)^2} \tag{E.2}$$

As the norm is dependent on the magnitude of the experimental data, it should not be used to compare between samples. However, within a particular sample, the norm can be used to compare the different viscoelastic models. After the tabulated data, the time-domain fit of the 4-term Prony series and complementary error function (CERF) is presented for both strain levels. Then, the four-term Prony series and

complementary error function models are shown in frequency domain. Interestingly, the viscoelastic transition range for cartilage coincides directly with the range of gaits experienced during common physical exercise, as shown in Figs. E.1 - E.22.

Table E.1: Saline (a): Cartilage information and model parameters

	Strain Level #1	Strain Level #2
Date: 5/22/2012	Case #: 1070752	Fluid Bath: Saline
Age (yrs)	7	
Estimated Weight (kg)	498.96	
Use	Show	
Breed	American Quarter Horse	
Gender	M	
Plug Thickness (mm)	2.374	
Number of Thickness Samples	5	
Standard Dev. (mm)	0.396	
Displacement (mm)	0.249	0.174
Strain	**10.49%**	**7.35%**
Time Constant (s)	**1.57**	**1.98**
Normalized Time Constant Area	2.16	2.97
Normalized Total Area	4.82	5.99
Area Ratio	**44.78%**	**49.63%**
4-Term Prony Model Parameters		
Glassy Modulus (MPa)	**0.514**	**0.520**
E_0 (MPa)	0.060	0.056
E_1 (MPa)	0.072	0.067
E_2 (MPa)	0.064	0.062
E_3 (MPa)	0.077	0.074
E_4 (MPa)	0.241	0.261
λ_1 (1/s)	0.447	0.358
λ_2 (1/s)	21.023	17.044
λ_3 (1/s)	2.524	1.874
λ_4 (1/s)	0.067	0.054
Norm	3.13E+05	4.46E+05
3-Term Prony Model Parameters		
Glassy Modulus (MPa)	**0.497**	**0.506**
E_0 (MPa)	0.093	0.083
E_1 (MPa)	0.077	0.076
E_2 (MPa)	0.083	0.082
E_3 (MPa)	0.243	0.265
λ_1 (1/s)	8.054	7.299
λ_2 (1/s)	0.692	0.649
λ_3 (1/s)	0.077	0.069
Norm	3.35E+05	4.61E+05

Table: E.1 continued:

Fractional Model Parameters		
E_0 (Mpa)	0.271	0.261
E_1 (Mpa)	0.208	0.231
μ^2 (1/s)	0.372	0.316
α	1/2	1/2
Norm	4.36E+05	5.39E+05
Test Notes		
Test Time	4:00 pm	
Approximate Demise to Collection Time	24 hours	
Time from Harvest to Test	<25 min	
This data set was the initial test performed, with the larger strain tests performed first		

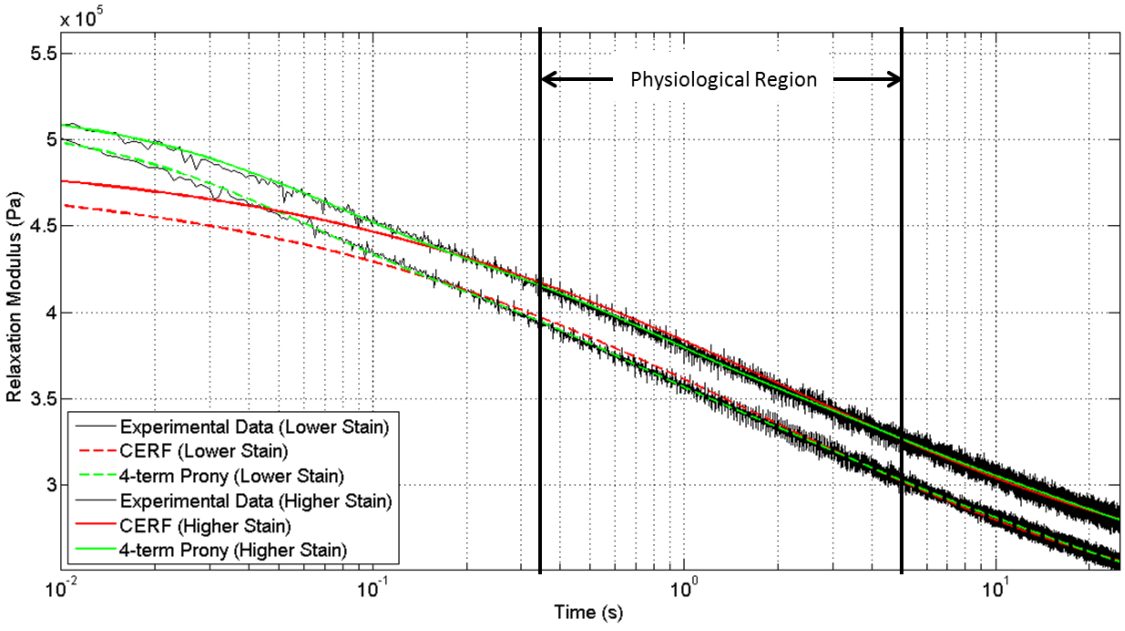

Figure E.1: Time-domain fits of experimental data on semi-log scale for Saline (a)

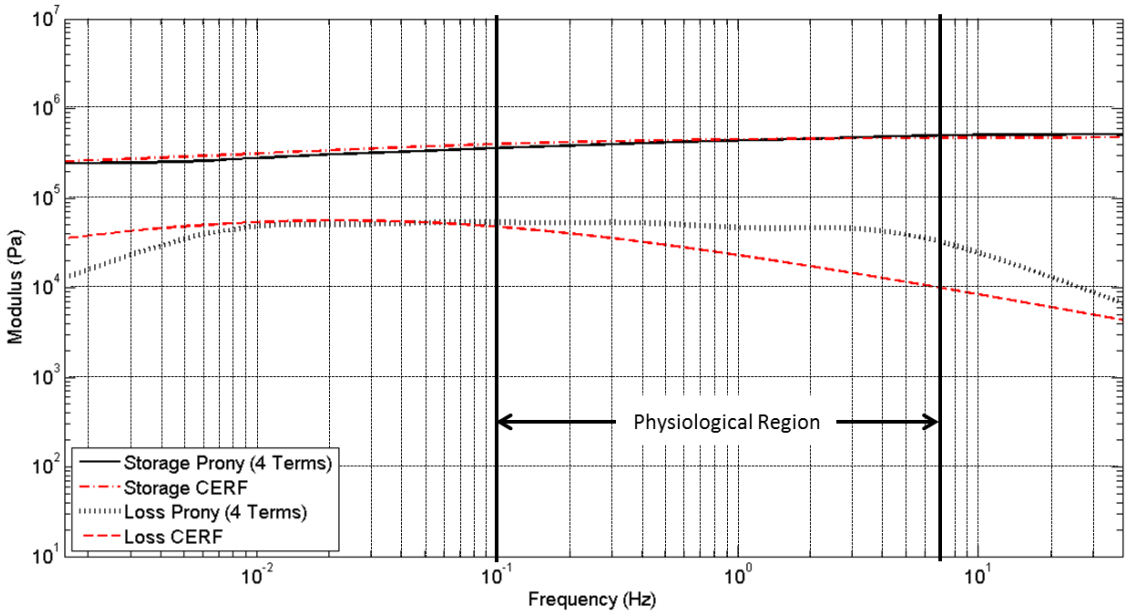

(a) Lower strain (7.35%)

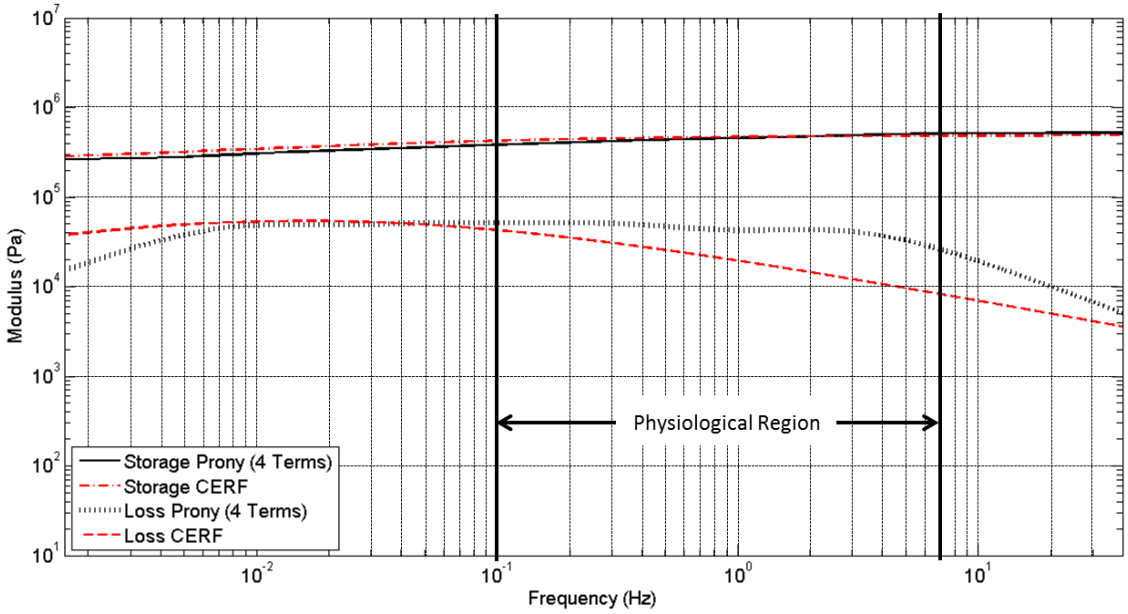

(b) Higher strain (10.49%)

Figure E.2: Compiled frequency domain information for Saline (a)

Table E.2: Saline (b): Cartilage information and model parameters

	Strain Level #1	Strain Level #2
Date: 5/24/2012	Case #: 1102477	Fluid Bath: Saline
Age (yrs)	11	
Estimated Weight (kg)	453.74	
Use	Unknown	
Breed	American Quarter Horse	
Gender	F	
Plug Thickness (mm)	2.805	
Number of Thickness Samples	5	
Standard Dev. (mm)	0.196	
Displacement (mm)	0.249	0.349
Strain	**8.89%**	**12.44%**
Time Constant (s)	**6.38**	**8.36**
Normalized Time Constant Area	5.71	7.75
Normalized Total Area	21.07	25.79
Area Ratio	**27.11%**	**30.04%**
4-Term Prony Model Parameters		
Glassy Modulus (MPa)	**1.492**	**3.290**
E_0 (MPa)	0.248	0.543
E_1 (MPa)	0.277	0.527
E_2 (MPa)	0.259	0.563
E_3 (MPa)	0.278	0.664
E_4 (MPa)	0.430	0.994
λ_1 (1/s)	0.099	0.096
λ_2 (1/s)	7.026	5.282
λ_3 (1/s)	0.609	0.564
λ_4 (1/s)	0.014	0.013
Norm	9.34E+05	1.14E+06
3-Term Prony Model Parameters		
Glassy Modulus (MPa)	**1.389**	**3.114**
E_0 (MPa)	0.336	0.720
E_1 (MPa)	0.306	0.664
E_2 (MPa)	0.304	0.704
E_3 (MPa)	0.443	1.026
λ_1 (1/s)	1.842	1.507
λ_2 (1/s)	0.156	0.144
λ_3 (1/s)	0.018	0.015
Norm	1.45E+06	2.42E+06

Table: E.2 continued:

Fractional Model Parameters		
E_0 (Mpa)	1.034	2.290
E_1 (Mpa)	0.316	0.743
μ^2 (1/s)	0.094	0.077
α	1/2	1/2
Norm	2.26E+06	5.65E+06
Test Notes		
Test Time	5:00 pm	
Approximate Demise to Collection Time	2 hours	
Time from Harvest to Test	<25 min	
Test #5 was performed at the lower strain level		

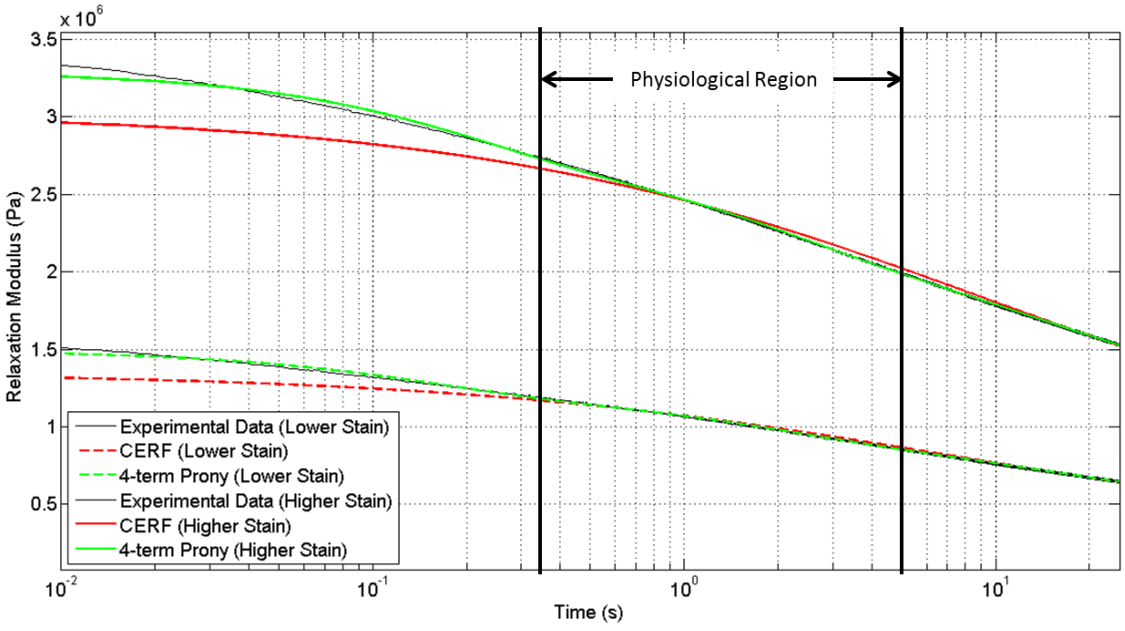

Figure E.3: Time-domain fits of experimental data on semi-log scale for case Saline (b)

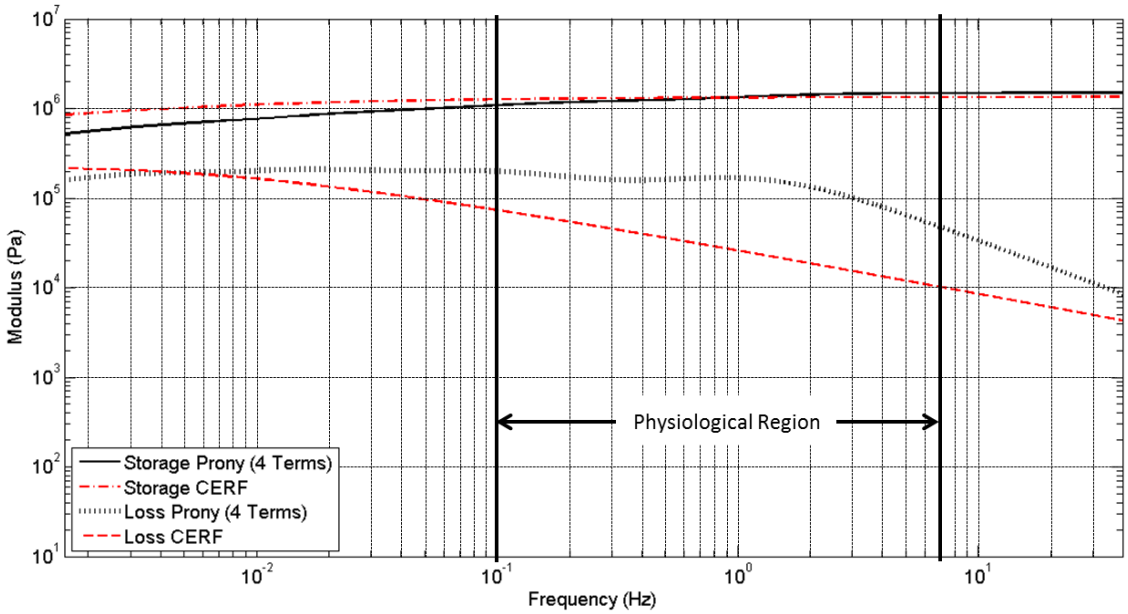

(a) Lower strain (8.89%)

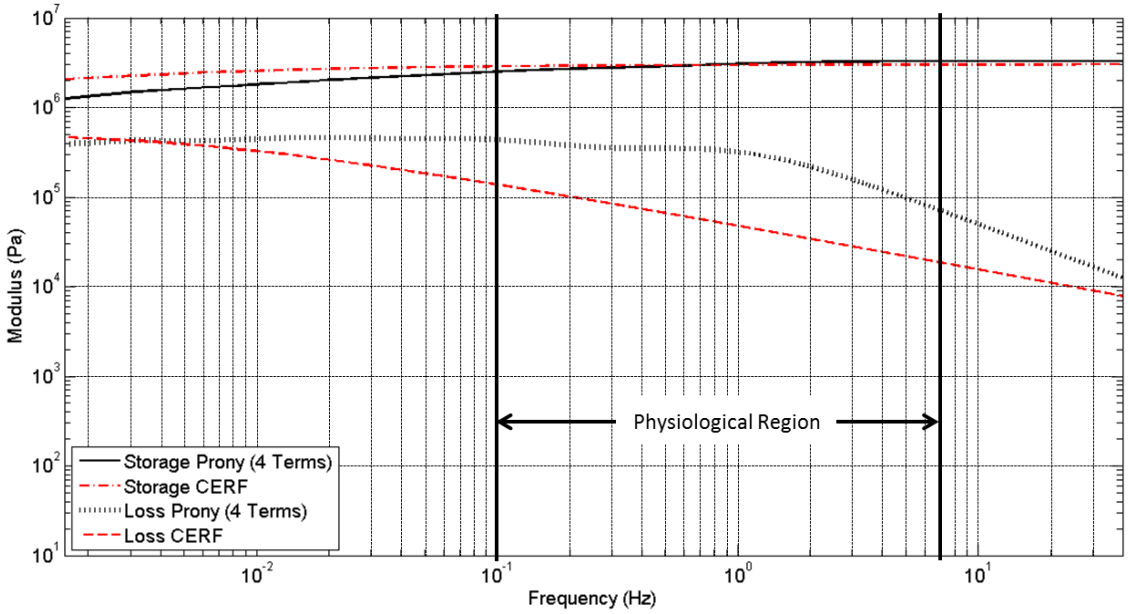

(b) Higher strain (11.55%)

Figure E.4: Compiled frequency domain information for case Saline (b)

Table E.3: Saline (c): Cartilage information and model parameters

	Strain Level #1	Strain Level #2
Date: 5/29/2012	Case #: 1102292	Fluid Bath: Saline
Age (yrs)	17	
Estimated Weight (kg)	544.32	
Use	Teaching	
Breed	American Quarter Horse	
Gender	M	
Plug Thickness (mm)	2.676	
Number of Thickness Samples	3	
Standard Dev. (mm)	0.092	
Displacement (mm)	0.250	0.350
Strain	**9.34%**	**13.08%**
Time Constant (s)	**5.00**	**10.06**
Normalized Time Constant Area	5.76	10.21
Normalized Total Area	10.70	21.86
Area Ratio	**53.89%**	**46.69%**
4-Term Prony Model Parameters		
Glassy Modulus (MPa)	**0.609**	**0.951**
E_0 (MPa)	0.098	0.174
E_1 (MPa)	0.083	0.129
E_2 (MPa)	0.078	0.136
E_3 (MPa)	0.110	0.190
E_4 (MPa)	0.240	0.321
λ_1 (1/s)	0.169	0.091
λ_2 (1/s)	9.106	5.592
λ_3 (1/s)	0.978	0.523
λ_4 (1/s)	0.034	0.016
Norm	1.28E+06	6.57E+05
3-Term Prony Model Parameters		
Glassy Modulus (MPa)	**0.582**	**0.903**
E_0 (MPa)	0.108	0.168
E_1 (MPa)	0.115	0.197
E_2 (MPa)	0.118	0.212
E_3 (MPa)	0.241	0.327
λ_1 (1/s)	2.674	1.470
λ_2 (1/s)	0.225	0.133
λ_3 (1/s)	0.036	0.019
Norm	1.30E+06	8.61E+05

Table: E.3 continued:

Fractional Model Parameters		
E_0 (Mpa)	0.422	0.705
E_1 (Mpa)	0.194	0.221
μ^2 (1/s)	0.213	0.074
α	1/2	1/2
Norm	1.68E+06	8.06E+05
Test Notes		
Test Time	5:00 pm	
Approximate Demise to Collection Time	2 hours	
Time from Harvest to Test	<25 min	
Tests #1-2 were excluded from the analysis due to erroneous behavior		

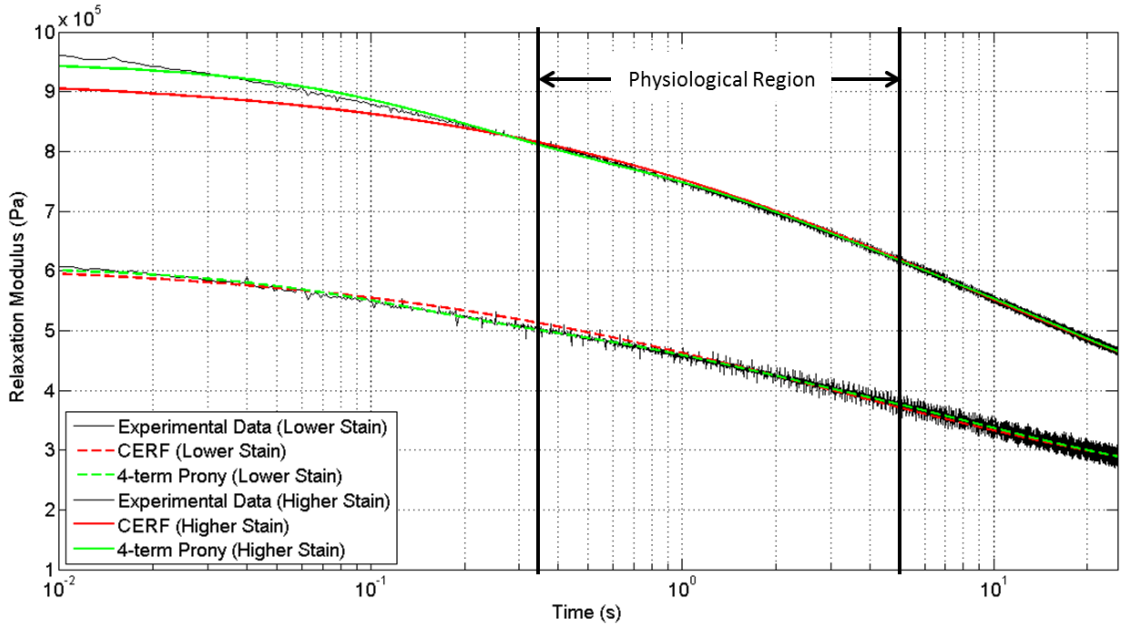

Figure E.5: Time-domain fits of experimental data on semi-log scale for case Saline (c)

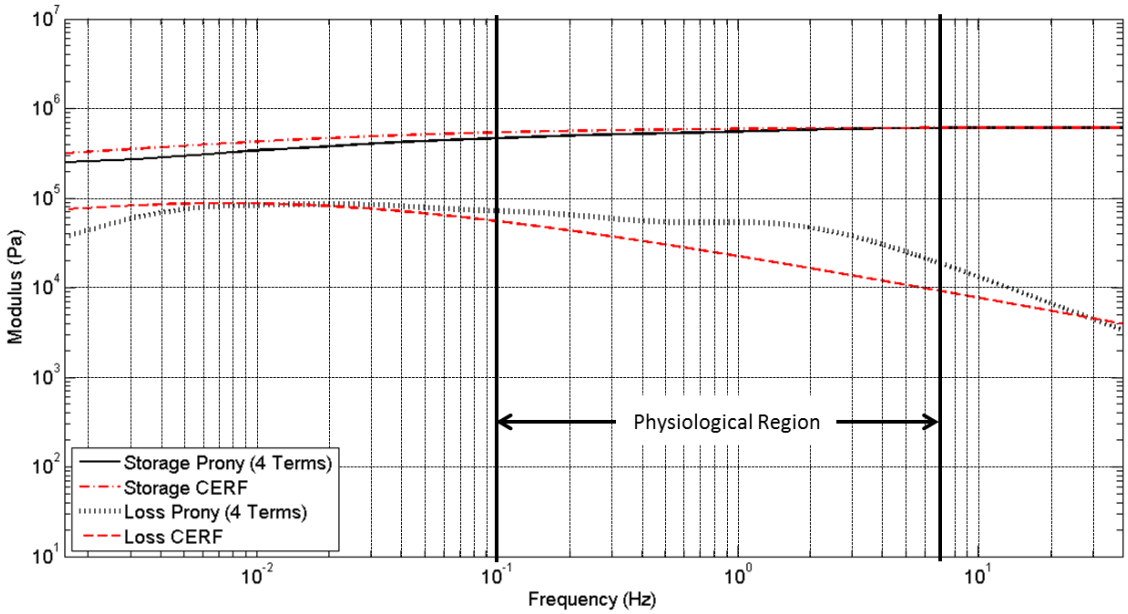

(a) Lower strain (9.34%)

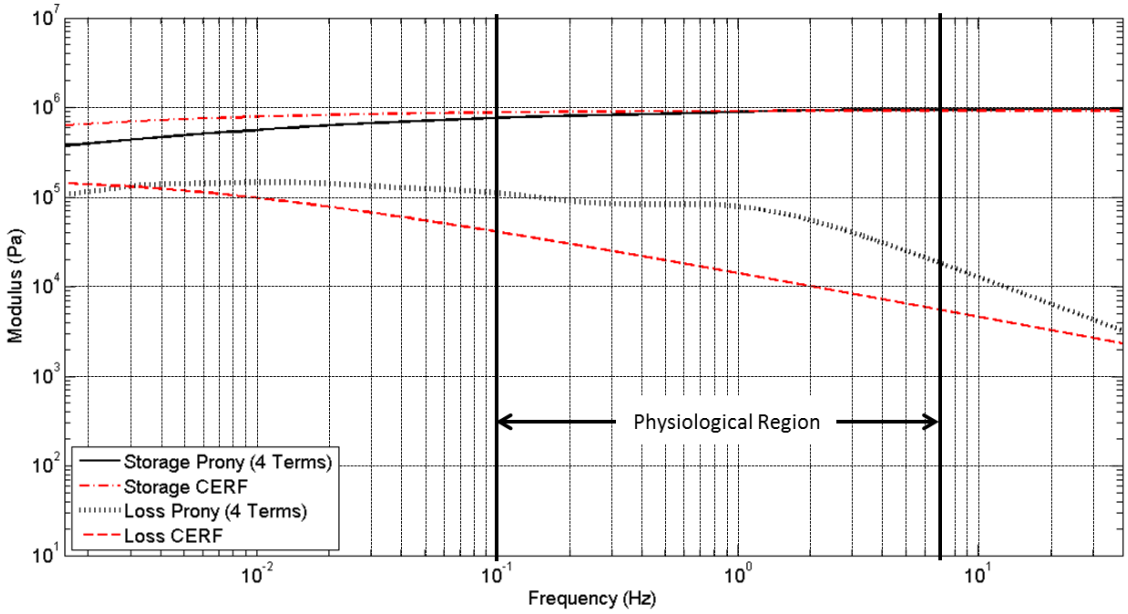

(b) Higher strain (13.08%)

Figure E.6: Compiled frequency domain information for case Saline (c)

Table E.4: Saline (d): Cartilage information and model parameters

	Strain Level #1	Strain Level #2
Date: 5/30/2012	Case #: 1091811	Fluid Bath: Saline
Age (yrs)	14	
Estimated Weight (kg)	535.25	
Use	Teaching	
Breed	American Quarter Horse	
Gender	M	
Plug Thickness (mm)	3.107	
Number of Thickness Samples	3	
Standard Dev. (mm)	0.079	
Displacement (mm)	0.250	0.350
Strain	**8.04%**	**11.27%**
Time Constant (s)	**10.28**	**15.36**
Normalized Time Constant Area	11.12	14.92
Normalized Total Area	24.94	34.02
Area Ratio	**44.57%**	**43.86%**
4-Term Prony Model Parameters		
Glassy Modulus (MPa)	**1.949**	**3.533**
E_0 (MPa)	0.373	0.691
E_1 (MPa)	0.255	0.405
E_2 (MPa)	0.296	0.554
E_3 (MPa)	0.316	0.772
E_4 (MPa)	0.708	1.111
λ_1 (1/s)	0.074	0.070
λ_2 (1/s)	4.568	3.904
λ_3 (1/s)	0.398	0.356
λ_4 (1/s)	0.013	0.011
Norm	1.23E+06	1.18E+06
3-Term Prony Model Parameters		
Glassy Modulus (MPa)	**1.849**	**0.979**
E_0 (MPa)	0.335	0.586
E_1 (MPa)	0.431	0.804
E_2 (MPa)	0.361	0.835
E_3 (MPa)	0.722	1.146
λ_1 (1/s)	1.102	0.878
λ_2 (1/s)	0.110	0.100
λ_3 (1/s)	0.016	0.013
Norm	1.78E+06	2.49E+06

Table: E.4 continued:

Fractional Model Parameters		
E_0 (Mpa)	1.409	2.779
E_1 (Mpa)	0.549	0.741
μ^2 (1/s)	0.093	0.053
α	1/2	1/2
Norm	1.37E+06	1.94E+06

Test Notes	
Test Time	12:00 pm
Approximate Demise to Collection Time	4 hours
Time from Harvest to Test	<20 min

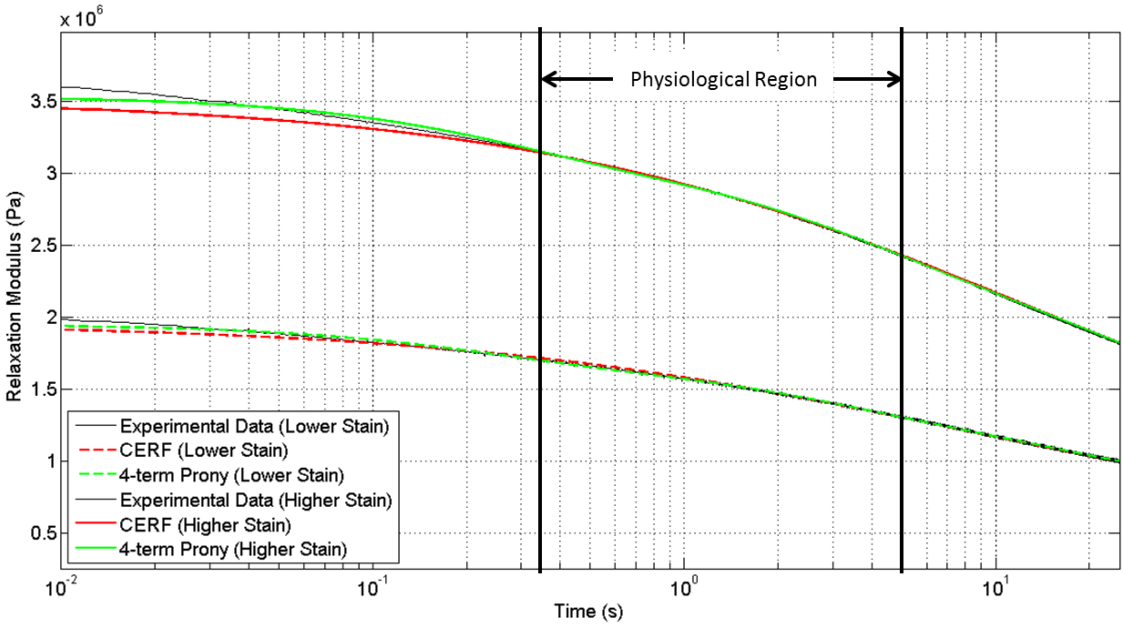

Figure E.7: Time-domain fits of experimental data on semi-log scale for case Saline (d)

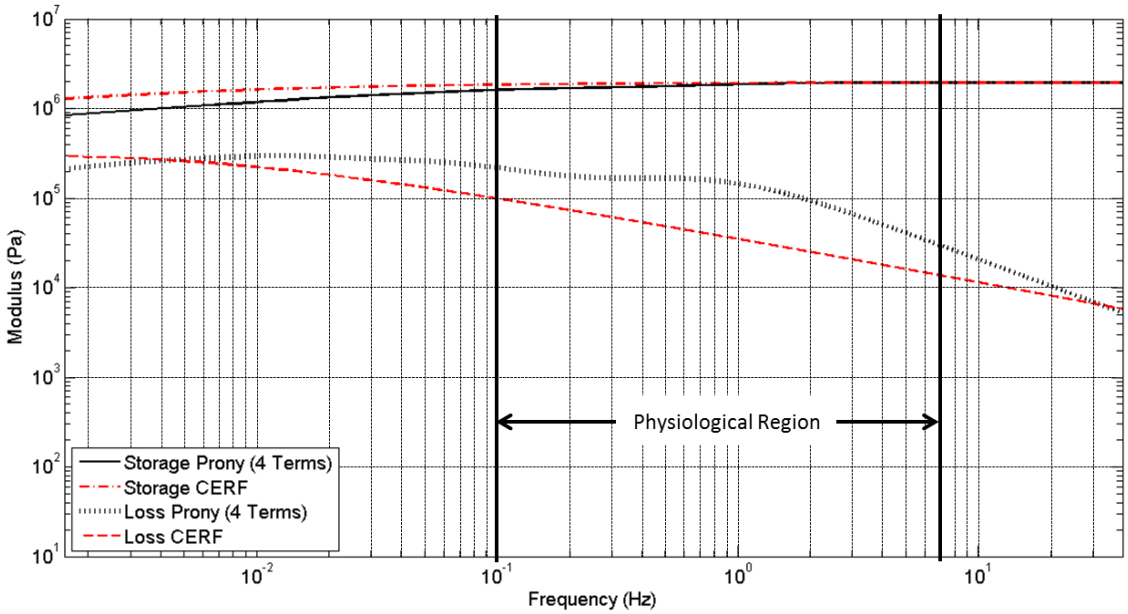

(a) Lower strain (8.04%)

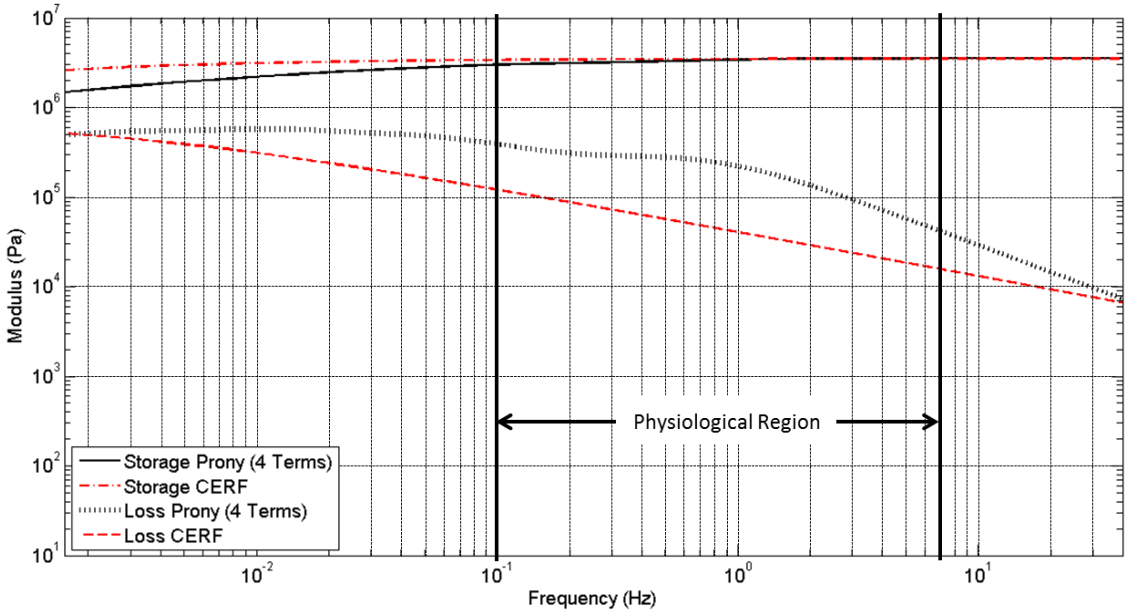

(b) Higher strain (11.27%)

Figure E.8: Compiled frequency domain information for case Saline (d)

Table E.5: Saline (e): Cartilage information and model parameters

	Strain Level #1	Strain Level #2
Date: 5/30/2012	Case #: 1093329	Fluid Bath: Saline
Age (yrs)	11	
Estimated Weight (kg)	534.32	
Use	Teaching	
Breed	Thoroughbred	
Gender	M	
Plug Thickness (mm)	2.785	
Number of Thickness Samples	3	
Standard Dev. (mm)	0.117	
Displacement (mm)	0.250	0.349
Strain	**8.96%**	**12.54%**
Time Constant (s)	**17.06**	**13.23**
Normalized Time Constant Area	17.71	13.81
Normalized Total Area	42.45	31.02
Area Ratio	**44.71%**	**44.51%**
4-Term Prony Model Parameters		
Glassy Modulus (MPa)	**0.698**	**1.025**
E_0 (MPa)	0.113	0.171
E_1 (MPa)	0.098	0.140
E_2 (MPa)	0.095	0.147
E_3 (MPa)	0.146	0.206
E_4 (MPa)	0.247	0.361
λ_1 (1/s)	0.061	0.071
λ_2 (1/s)	4.061	3.950
λ_3 (1/s)	0.381	0.419
λ_4 (1/s)	0.009	0.012
Norm	1.05E+06	7.57E+05
3-Term Prony Model Parameters		
Glassy Modulus (MPa)	**0.665**	**0.979**
E_0 (MPa)	0.123	0.188
E_1 (MPa)	0.126	0.195
E_2 (MPa)	0.156	0.226
E_3 (MPa)	0.260	0.370
λ_1 (1/s)	1.151	1.169
λ_2 (1/s)	0.098	0.107
λ_3 (1/s)	0.012	0.014
Norm	1.15E+06	9.93E+05

Table: E.5 continued:

Fractional Model Parameters		
E_0 (Mpa)	0.465	0.716
E_1 (Mpa)	0.185	0.260
μ^2 (1/s)	0.037	0.051
α	1/2	1/2
Norm	1.39E+06	1.21E+06
Test Notes		
Test Time	12:00 pm	
Approximate Demise to Collection Time	4 hours	
Time from Harvest to Test	<20 min	

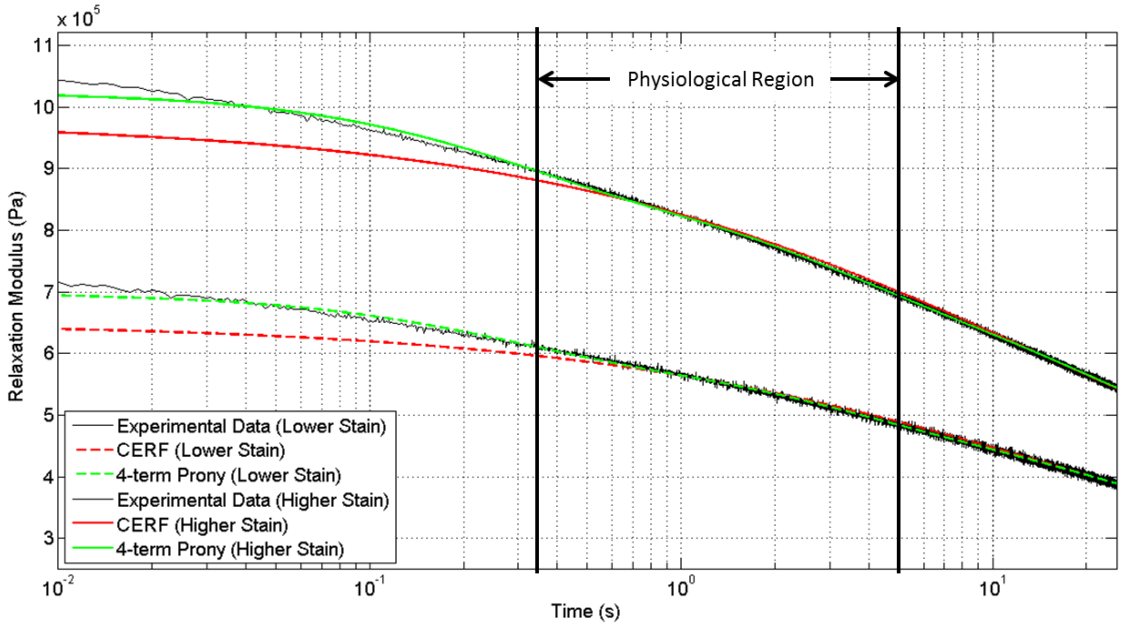

Figure E.9: Time-domain fits of experimental data on semi-log scale for case Saline (e)

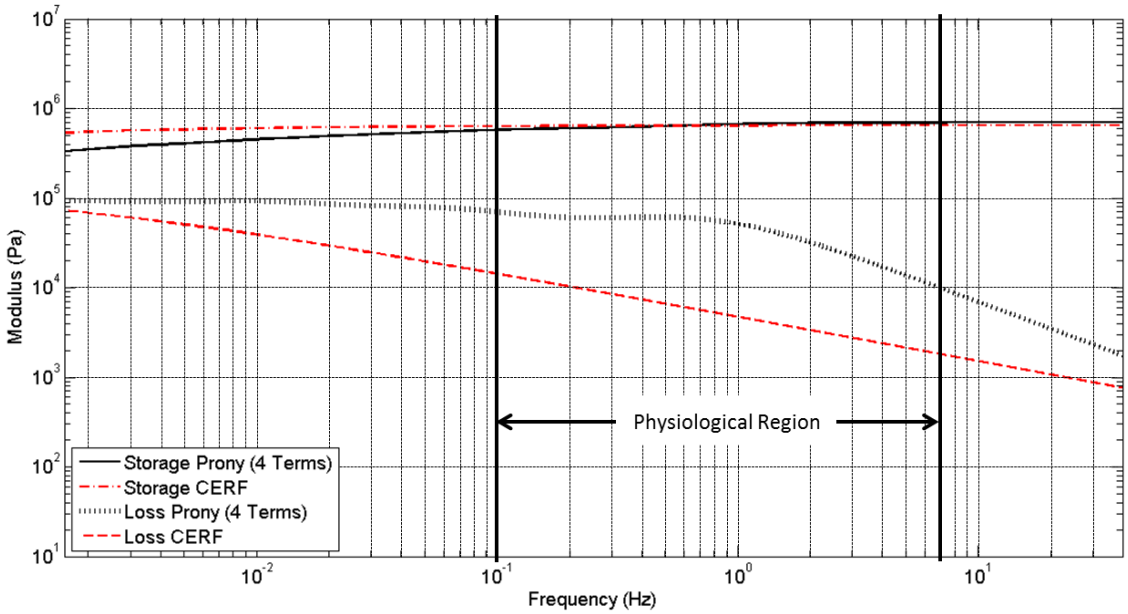

(a) Lower strain (8.96%)

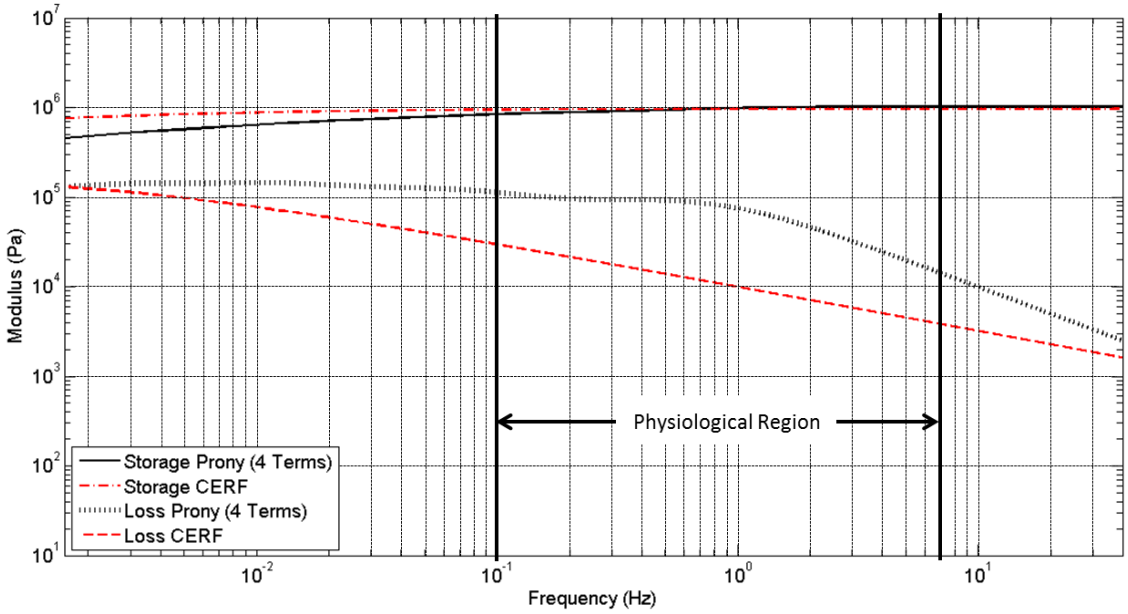

(b) Higher strain (12.54%)

Figure E.10: Compiled frequency domain information for case Saline (e)

Table E.6: Synovial (a): Cartilage information and model parameters

	Strain Level #1	Strain Level #2
Date: 6/13/2012	Case #: 1102568	Fluid Bath: Synovial
Age (yrs)	6	
Estimated Weight (kg)	453.6	
Use	Teaching	
Breed	American Warmblood	
Gender	F	
Plug Thickness (mm)	2.275	
Number of Thickness Samples	4	
Standard Dev. (mm)	0.173	
Displacement (mm)	0.250	0.350
Strain	**11.00%**	**15.40%**
Time Constant (s)	**2.99**	**5.37**
Normalized Time Constant Area	2.82	5.21
Normalized Total Area	9.38	15.79
Area Ratio	**30.04%**	**32.97%**
4-Term Prony Model Parameters		
Glassy Modulus (MPa)	**0.476**	**0.473**
E_0 (MPa)	0.149	0.153
E_1 (MPa)	0.071	0.076
E_2 (MPa)	0.098	0.090
E_3 (MPa)	0.073	0.075
E_4 (MPa)	0.085	0.078
λ_1 (1/s)	0.185	0.101
λ_2 (1/s)	11.730	7.396
λ_3 (1/s)	1.155	0.633
λ_4 (1/s)	0.032	0.019
Norm	8.94E+05	5.51E+05
3-Term Prony Model Parameters		
Glassy Modulus (MPa)	**0.501**	**0.442**
E_0 (MPa)	0.145	0.105
E_1 (MPa)	0.107	0.093
E_2 (MPa)	0.098	0.090
E_3 (MPa)	0.150	0.155
λ_1 (1/s)	14.357	2.095
λ_2 (1/s)	0.389	0.159
λ_3 (1/s)	0.037	0.022
Norm	1.00E+06	6.49E+05

Table: E.6 continued:

Fractional Model Parameters		
E_0 (Mpa)	0.327	0.324
E_1 (Mpa)	0.119	0.117
μ^2 (1/s)	0.261	0.127
α	1/2	1/2
Norm	1.34E+06	7.33E+05

Test Notes	
Test Time	5:39 pm
Approximate Demise to Collection Time	1 hour
Time from Harvest to Test	10 min
Plug was rinsed with saline during harvest, but given approx. 5 minutes in pooled synovial fluid before testing was performed Test #1 was excluded from the analysis due to erroneous behavior	

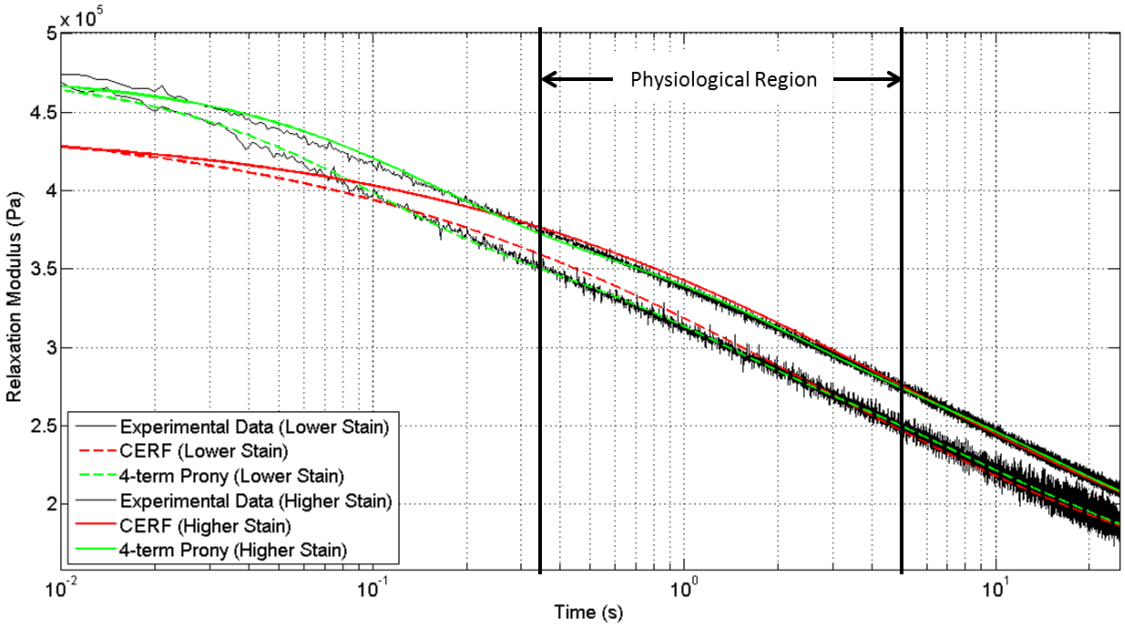

Figure E.11: Time-domain fits of experimental data on semi-log scale for case Synovial (a)

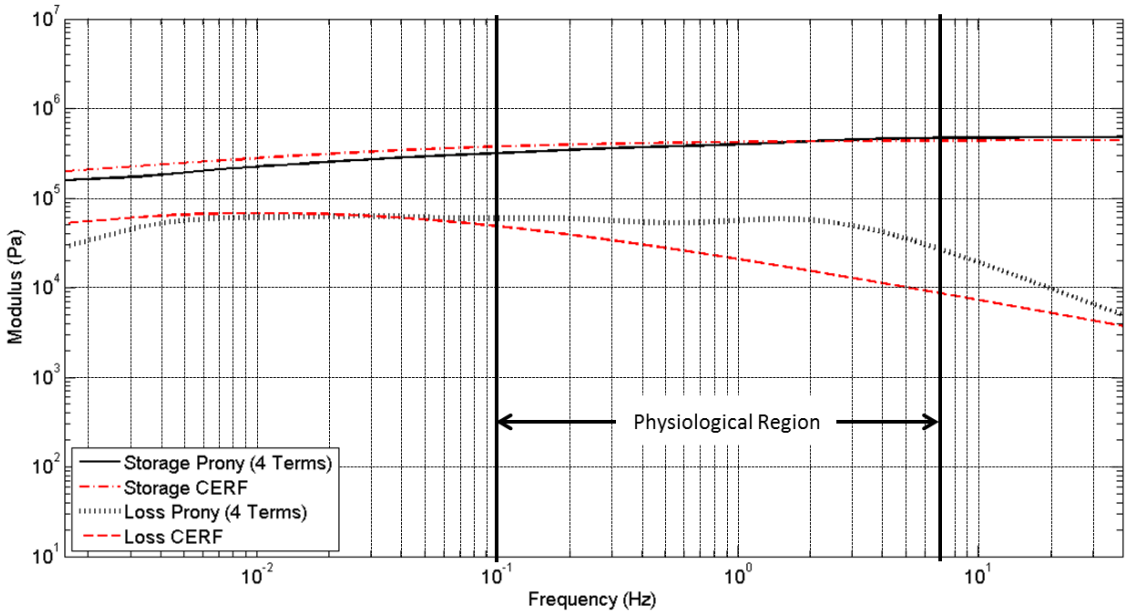

(a) Lower strain (11.00%)

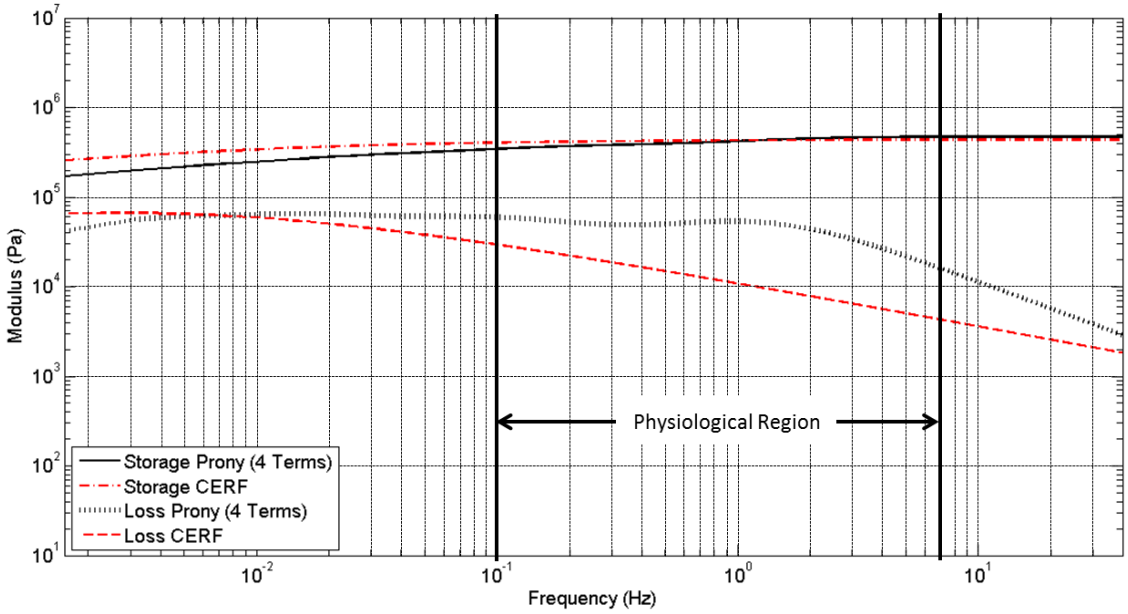

(b) Higher strain (15.40%)

Figure E.12: Compiled frequency domain information for case Synovial (a)

Table E.7: Synovial (b): Cartilage information and model parameters

	Strain Level #1	Strain Level #2
Date: 6/19/2012	Case #: 1075979	Fluid Bath: Synovial
Age (yrs)	12	
Estimated Weight (kg)	498.96	
Use	Unknown	
Breed	Thoroughbred	
Gender	M	
Plug Thickness (mm)	1.955	
Number of Thickness Samples	3	
Standard Dev. (mm)	0.494	
Displacement (mm)	0.250	0.350
Strain	**12.76%**	**17.89%**
Time Constant (s)	**7.89**	**11.54**
Normalized Time Constant Area	9.01	11.78
Normalized Total Area	26.61	34.46
Area Ratio	**33.85%**	**34.18%**
4-Term Prony Model Parameters		
Glassy Modulus (MPa)	**0.873**	**1.605**
E_0 (MPa)	0.131	0.270
E_1 (MPa)	0.127	0.212
E_2 (MPa)	0.137	0.271
E_3 (MPa)	0.137	0.304
E_4 (MPa)	0.342	0.548
λ_1 (1/s)	0.085	0.075
λ_2 (1/s)	5.196	3.693
λ_3 (1/s)	0.466	0.409
λ_4 (1/s)	0.011	0.009
Norm	8.51E+05	7.01E+05
3-Term Prony Model Parameters		
Glassy Modulus (MPa)	**0.826**	**1.532**
E_0 (MPa)	0.163	0.318
E_1 (MPa)	0.168	0.327
E_2 (MPa)	0.147	0.320
E_3 (MPa)	0.349	0.567
λ_1 (1/s)	1.343	0.990
λ_2 (1/s)	0.131	0.109
λ_3 (1/s)	0.014	0.012
Norm	1.03E+06	1.25E+06

Table: E.7 continued:

Fractional Model Parameters		
E_0 (Mpa)	0.537	1.106
E_1 (Mpa)	0.292	0.444
μ^2 (1/s)	0.096	0.072
α	1/2	1/2
Norm	1.39E+06	2.49E+05

Test Notes	
Test Time	4:00 pm
Approximate Demise to Collection Time	<8 hour
Time from Harvest to Test	<30 min
Plug was rinsed with synovial fluid during harvest Six tests were performed overall because additional time was given in the recovery phase (5 minutes)	

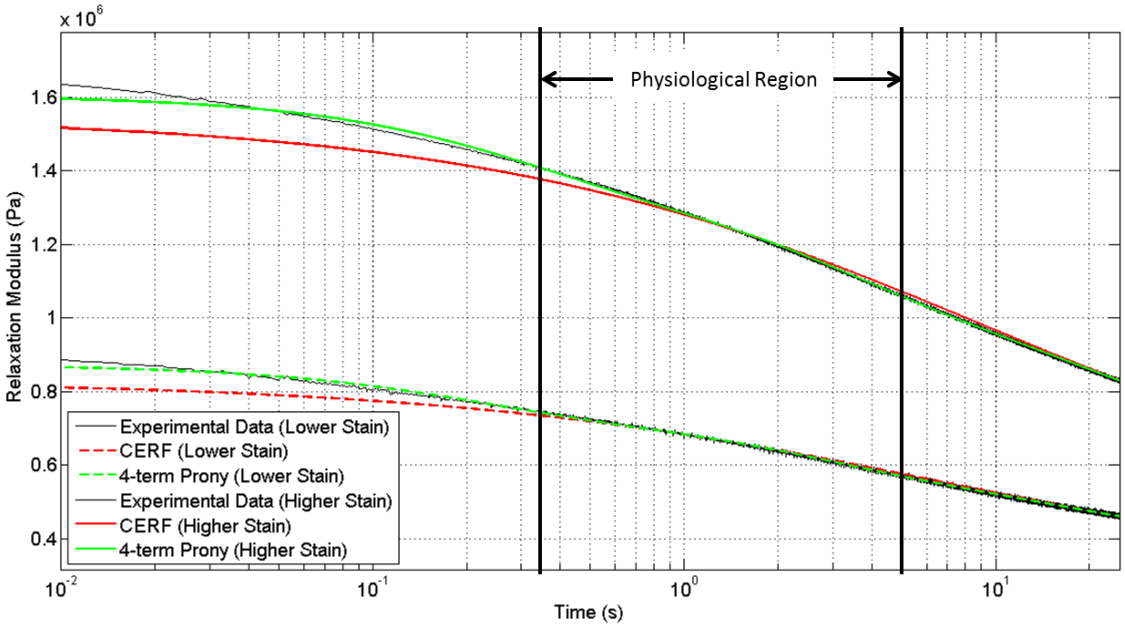

Figure E.13: Time-domain fits of experimental data on semi-log scale for case Synovial (b)

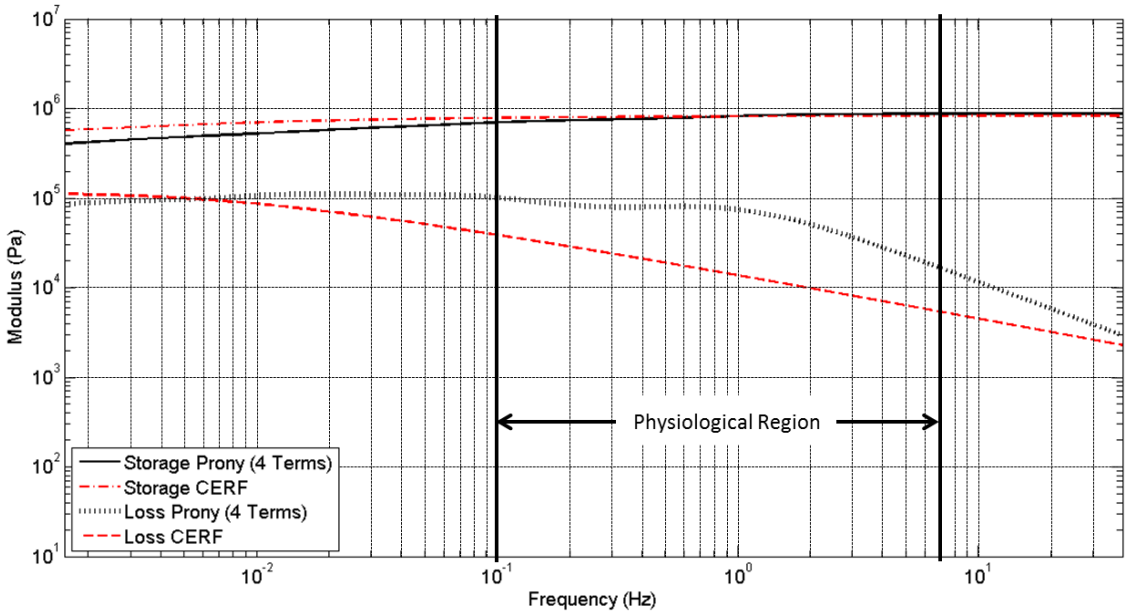

(a) Lower strain (12.76%)

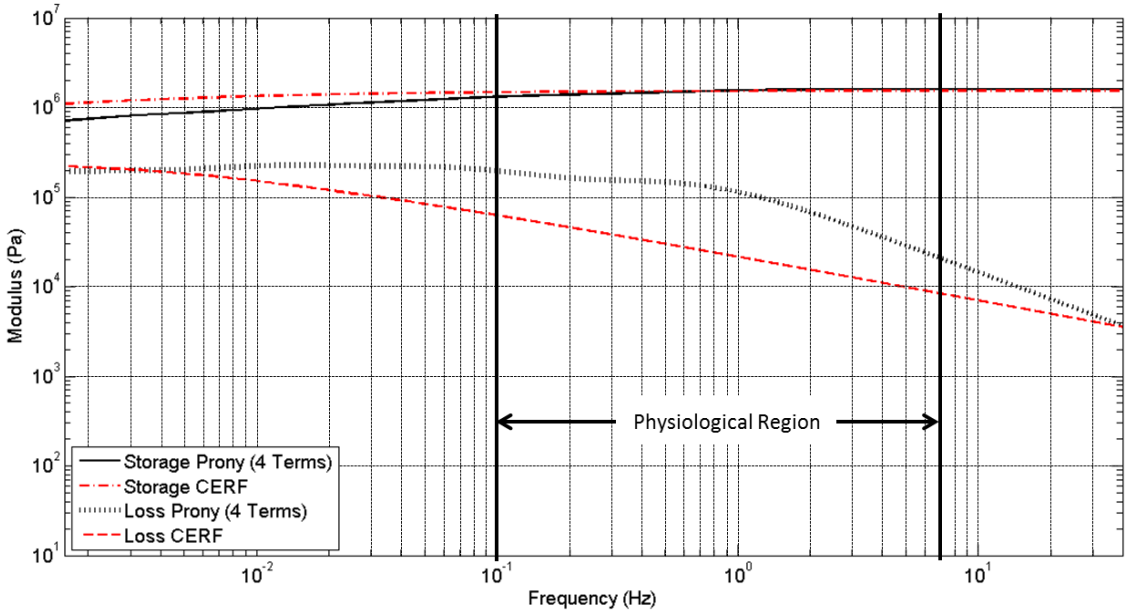

(b) Higher strain (17.89%)

Figure E.14: Compiled frequency domain information for case Synovial (b)

Table E.8: Hylartin: Cartilage information and model parameters

	Strain Level #1	Strain Level #2
Date: 6/20/2012	Case #: 1050005	Fluid Bath: Hylartin
Age (yrs)	22	
Estimated Weight (kg)	498.96	
Use	Unknown	
Breed	TN Walking	
Gender	M	
Plug Thickness (mm)	2.851	
Number of Thickness Samples	5	
Standard Dev. (mm)	0.584	
Displacement (mm)	0.250	0.350
Strain	**8.77%**	**12.27%**
Time Constant (s)	**28.07**	**14.08**
Normalized Time Constant Area	24.45	12.36
Normalized Total Area	49.53	34.22
Area Ratio	**49.37%**	**36.12%**
4-Term Prony Model Parameters		
Glassy Modulus (MPa)	**0.463**	**0.861**
E_0 (MPa)	0.085	0.145
E_1 (MPa)	0.058	0.151
E_2 (MPa)	0.048	0.113
E_3 (MPa)	0.148	0.207
E_4 (MPa)	0.125	0.245
λ_1 (1/s)	0.071	0.077
λ_2 (1/s)	6.040	9.171
λ_3 (1/s)	0.466	0.604
λ_4 (1/s)	0.010	0.011
Norm	1.18E+06	8.32E+05
3-Term Prony Model Parameters		
Glassy Modulus (MPa)	**0.438**	**0.783**
E_0 (MPa)	0.066	0.157
E_1 (MPa)	0.090	0.153
E_2 (MPa)	0.151	0.217
E_3 (MPa)	0.130	0.253
λ_1 (1/s)	1.326	1.570
λ_2 (1/s)	0.092	0.104
λ_3 (1/s)	0.011	0.013
Norm	1.21E+06	1.06E+06

Table: E.8 continued:

Fractional Model Parameters		
E_0 (Mpa)	0.396	0.608
E_1 (Mpa)	0.032	0.136
μ^2 (1/s)	0.015	0.029
α	1/2	1/2
Norm	1.26E+06	1.41E+06

Test Notes	
Test Time	3:30 pm
Approximate Demise to Collection Time	2 hours
Time from Harvest to Test	<30 min

Horse had moderate degenerative joint disease in the stifle
Test #1 released after the preload, and then imposed a displacement of 0.35 mm, and was included in the larger strain information
Test #6 had additional recovery time of approx. 2 minutes
Test #8 was started immediately following Test #7

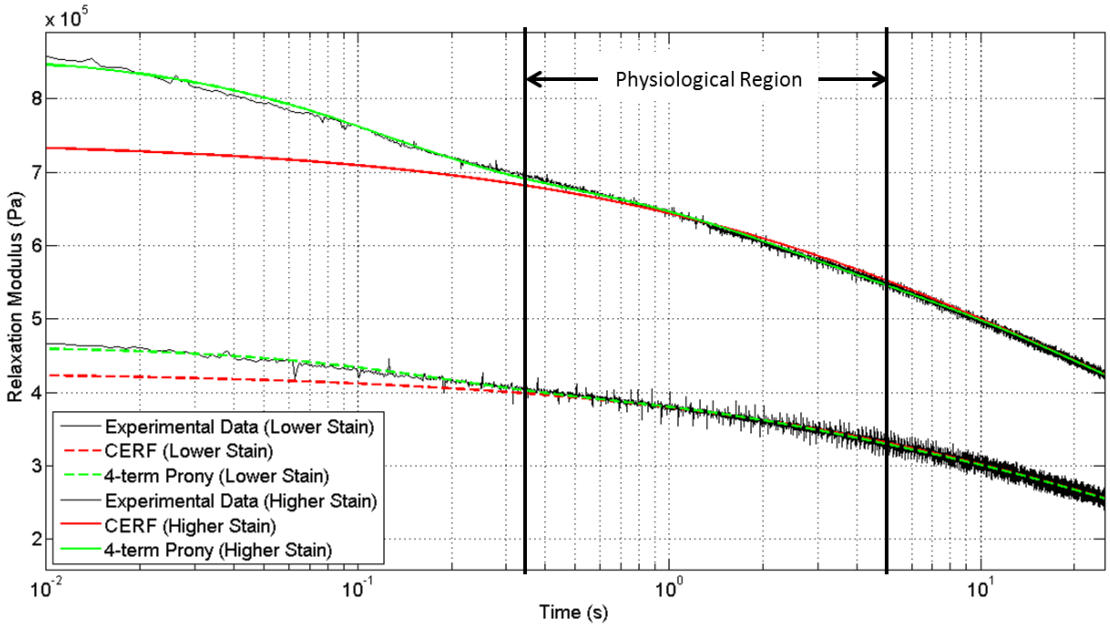

Figure E.15: Time-domain fits of experimental data on semi-log scale for case Hylartin

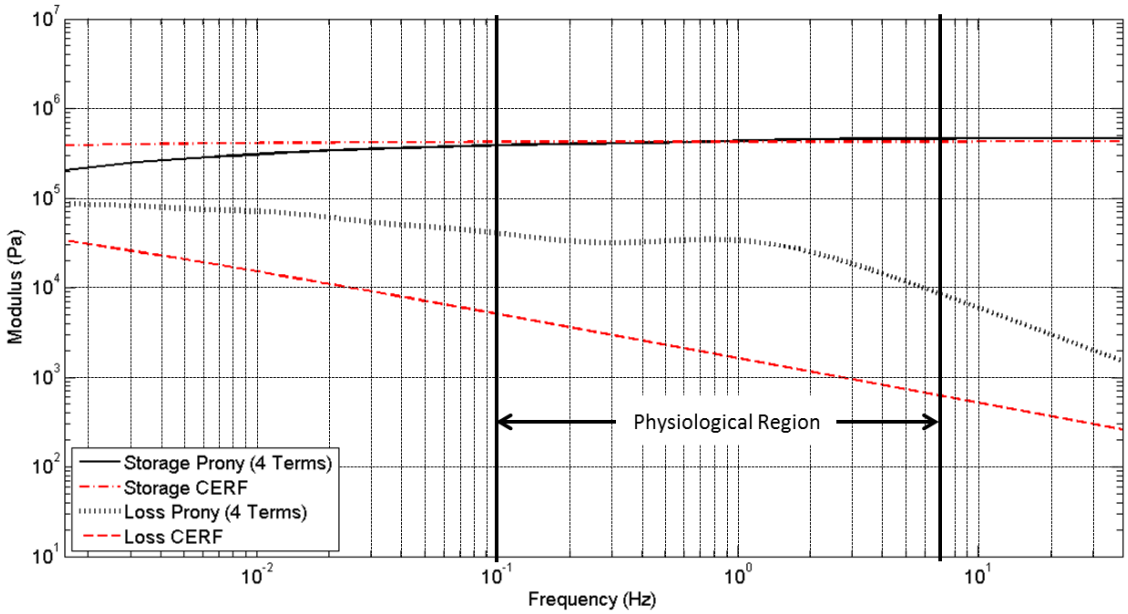

(a) Lower strain (8.77%)

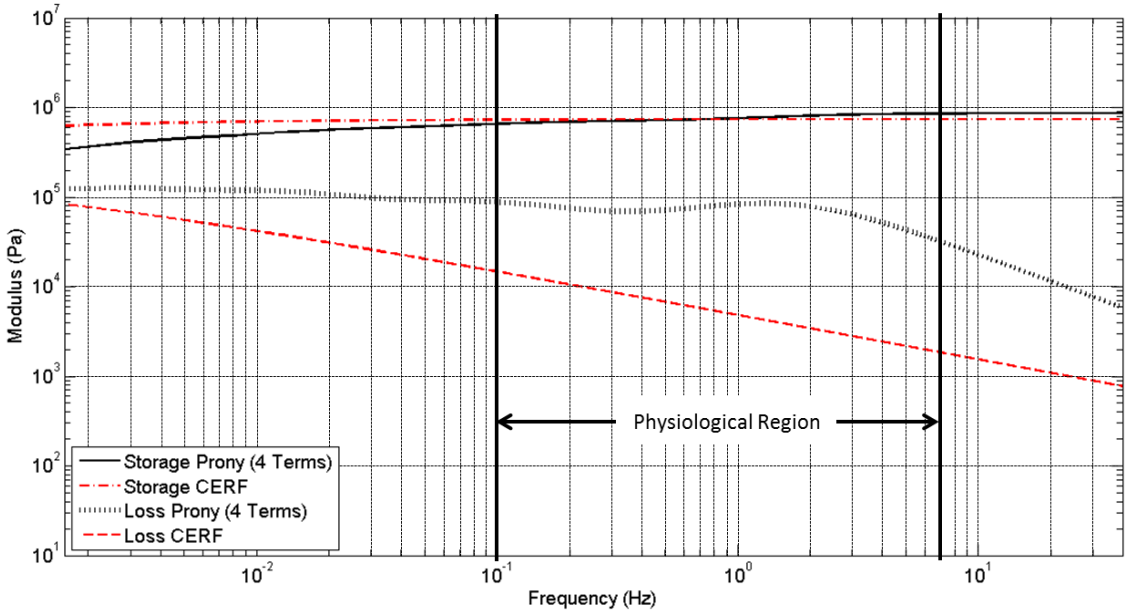

(b) Higher strain (12.27%)

Figure E.16: Compiled frequency domain information for case Hylartin

Table E.9: Polyglycan: Cartilage information and model parameters

	Strain Level #1	Strain Level #2
Date: 6/20/2012	Case #: 1102054	Fluid: Polyglycan
Age (yrs)	16	
Estimated Weight (kg)	481.81	
Use	Unknown	
Breed	American Quarter Horse	
Gender	F	
Plug Thickness (mm)	2.708	
Number of Thickness Samples	5	
Standard Dev. (mm)	0.06	
Displacement (mm)	0.250	0.350
Strain	**9.24%**	**12.92%**
Time Constant (s)	**5.07**	**4.64**
Normalized Time Constant Area	3.41	3.49
Normalized Total Area	27.11	24.81
Area Ratio	**12.57%**	**14.09%**
4-Term Prony Model Parameters		
Glassy Modulus (MPa)	**0.600**	**1.037**
E_0 (MPa)	0.083	0.143
E_1 (MPa)	0.182	0.302
E_2 (MPa)	0.095	0.150
E_3 (MPa)	0.132	0.203
E_4 (MPa)	0.108	0.239
λ_1 (1/s)	0.085	0.085
λ_2 (1/s)	12.206	12.942
λ_3 (1/s)	0.774	0.755
λ_4 (1/s)	0.011	0.011
Norm	1.03E+06	8.30E+05
3-Term Prony Model Parameters		
Glassy Modulus (MPa)	**0.528**	**0.917**
E_0 (MPa)	0.173	0.279
E_1 (MPa)	0.100	0.169
E_2 (MPa)	0.140	0.219
E_3 (MPa)	0.115	0.250
λ_1 (1/s)	3.253	3.455
λ_2 (1/s)	0.146	0.145
λ_3 (1/s)	0.013	0.014
Norm	1.20E+06	1.32E+06

Table: E.9 continued:

Fractional Model Parameters		
E_0 (Mpa)	0.373	0.608
E_1 (Mpa)	0.046	0.145
μ^2 (1/s)	0.031	0.038
α	1/2	1/2
Norm	1.90E+06	2.46E+06

Test Notes	
Test Time	5:25 pm
Approximate Demise to Collection Time	3 hours
Time from Harvest to Test	15 min
Sample was immersed in Polyglycan for approximately 10 minutes prior to testing Test #1 released after the preload, but appeared to function fine	

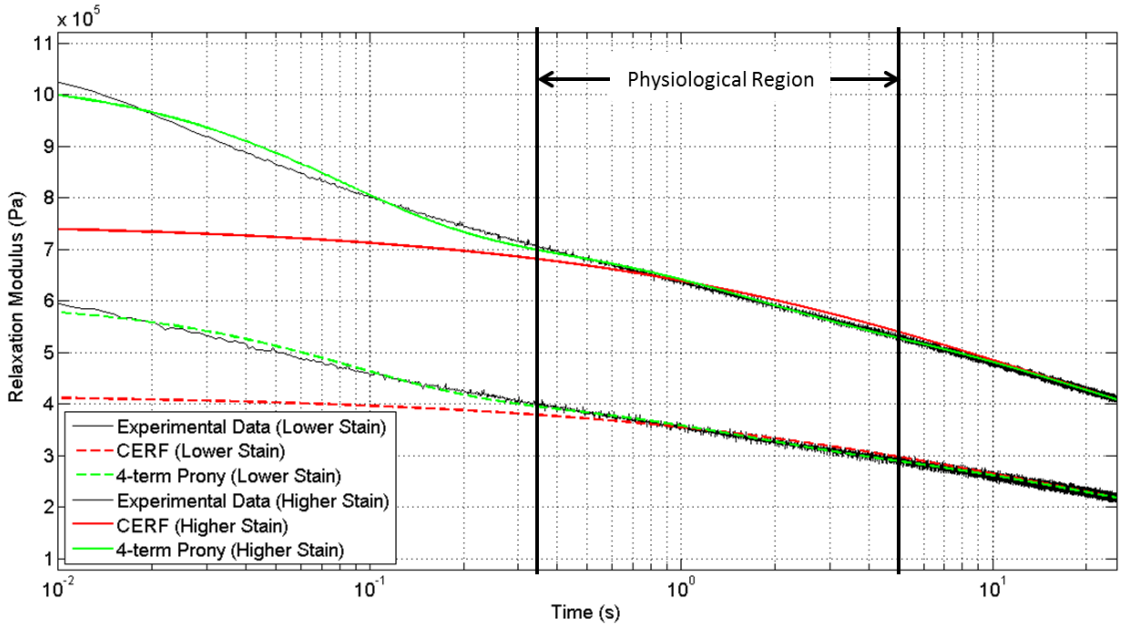

Figure E.17: Time-domain fits of experimental data on semi-log scale for case Polyglycan

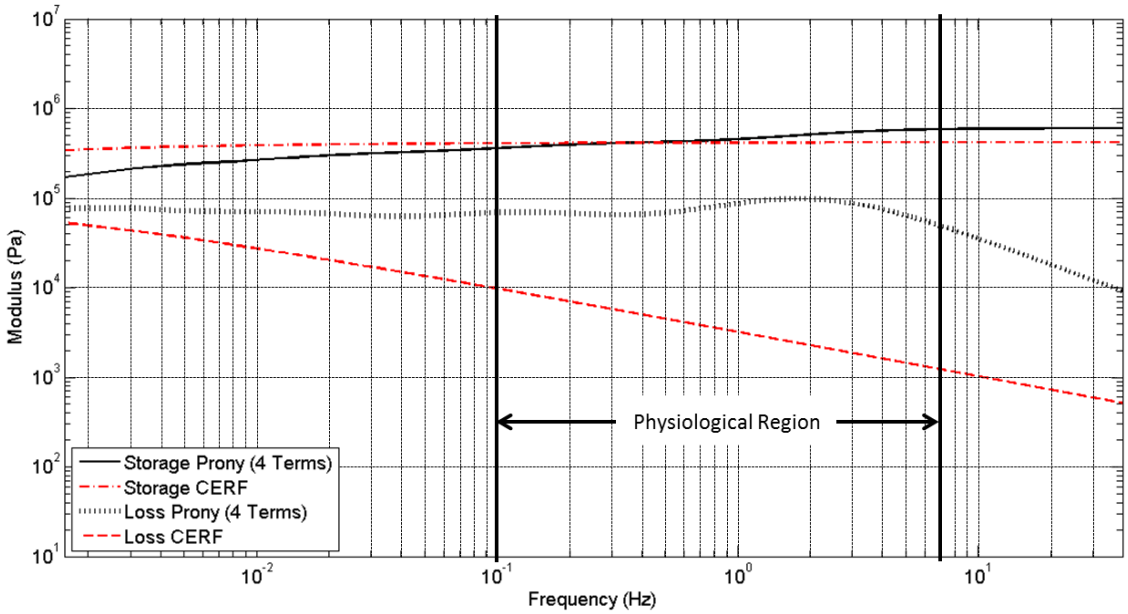

(a) Lower strain (9.24%)

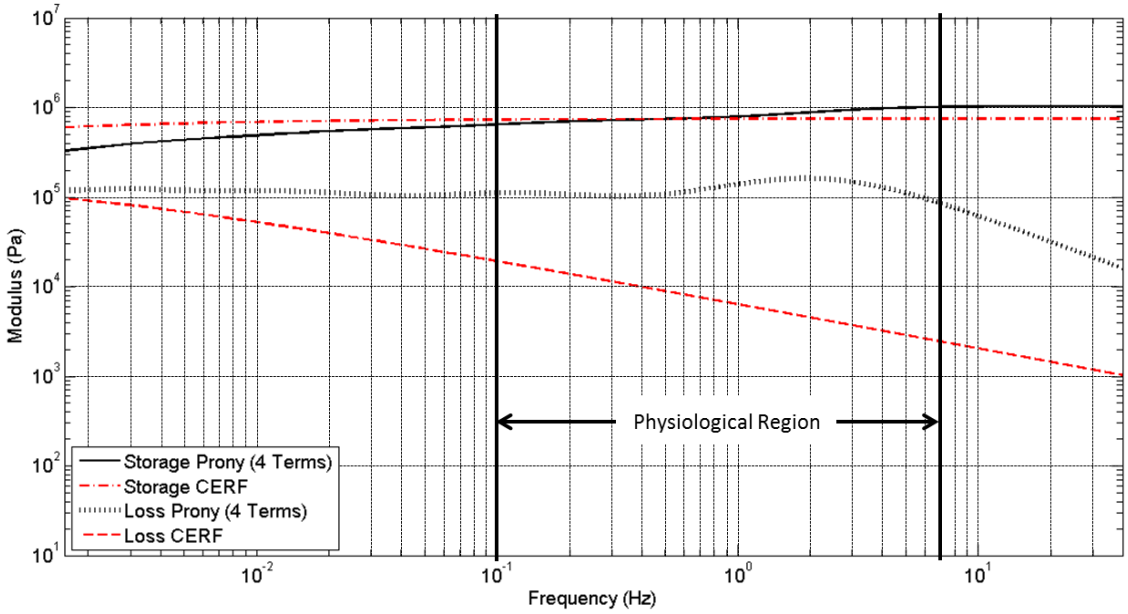

(b) Higher strain (12.92%)

Figure E.18: Compiled frequency domain information for case Polyglycan

Table E.10: Adequan: Cartilage information and model parameters

	Strain Level #1	Strain Level #2
Date: 6/21/2012	Case #: 1100301	Fluid Bath: Adequan
Age (yrs)	Unknown	
Estimated Weight (kg)	Unknown	
Use	Unknown	
Breed	Unknown	
Gender	Unknown	
Plug Thickness (mm)	2.021	
Number of Thickness Samples	4	
Standard Dev. (mm)	0.291	
Displacement (mm)	0.250	0.350
Strain	**12.36%**	**17.32%**
Time Constant (s)	**12.06**	**11.90**
Normalized Time Constant Area	11.55	11.97
Normalized Total Area	38.46	35.70
Area Ratio	**30.02%**	**33.53%**
4-Term Prony Model Parameters		
Glassy Modulus (MPa)	**1.238**	**1.696**
E_0 (MPa)	0.173	0.244
E_1 (MPa)	0.221	0.282
E_2 (MPa)	0.180	0.239
E_3 (MPa)	0.261	0.346
E_4 (MPa)	0.403	0.585
λ_1 (1/s)	0.073	0.075
λ_2 (1/s)	6.206	6.269
λ_3 (1/s)	0.497	0.497
λ_4 (1/s)	0.009	0.010
Norm	8.16E+05	7.23E+05
3-Term Prony Model Parameters		
Glassy Modulus (MPa)	**1.153**	**1.583**
E_0 (MPa)	0.250	0.323
E_1 (MPa)	0.208	0.291
E_2 (MPa)	0.272	0.363
E_3 (MPa)	0.423	0.606
λ_1 (1/s)	1.600	1.531
λ_2 (1/s)	0.118	0.117
λ_3 (1/s)	0.011	0.012
Norm	1.27E+06	1.45E+06

Table: E.10 continued:

Fractional Model Parameters		
E_0 (Mpa)	0.758	1.044
E_1 (Mpa)	0.302	0.443
μ^2 (1/s)	0.034	0.038
α	1/2	1/2
Norm	2.82E+06	3.22E+06

Test Notes	
Test Time	9:15 am
Approximate Demise to Collection Time	19 hours
Time from Harvest to Test	<20 min

Sample was an unexpected case, and the horse biographical information was not obtained
Sample was refrigerated overnight
Sample was immersed in Adequan for approx. 10 minutes
Test #1 was performed at the higher strain level
Test #5 was performed at the lower strain level

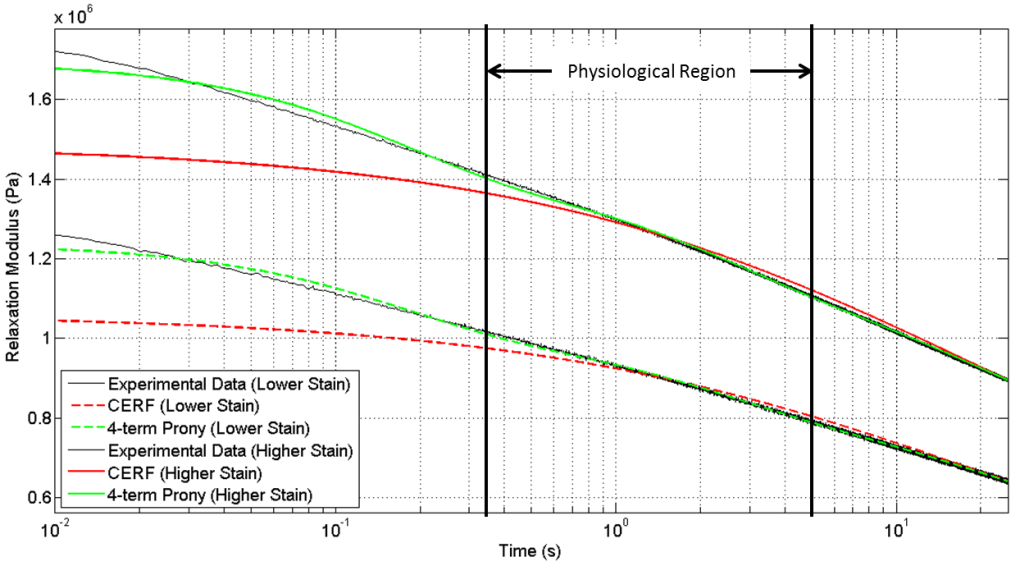

Figure E.19: Time-domain fits of experimental data on semi-log scale for case Adequan

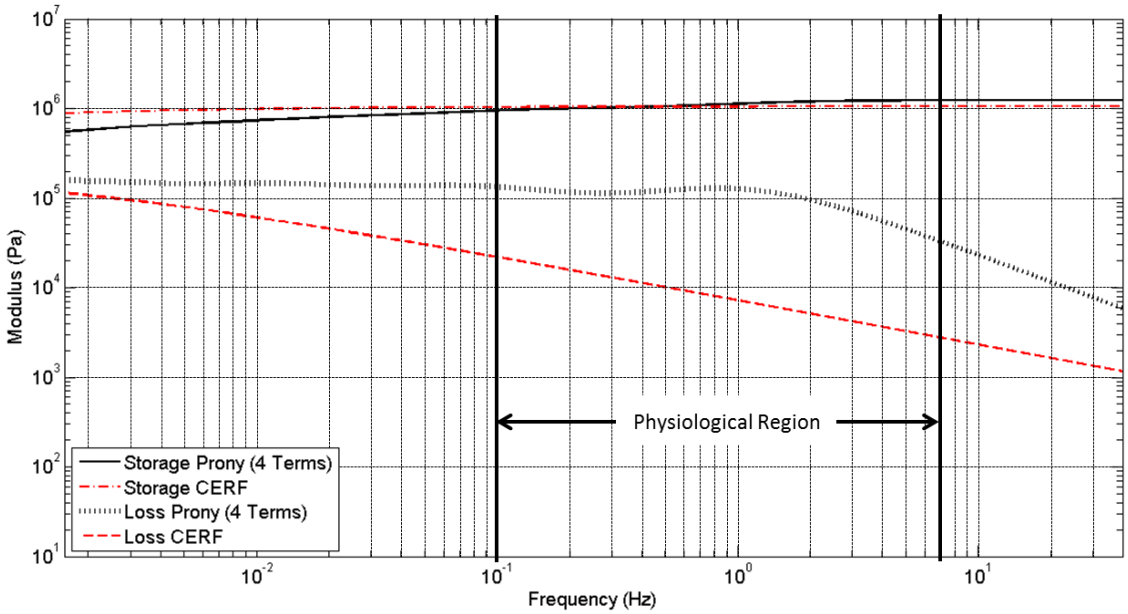

(a) Lower strain (12.36%)

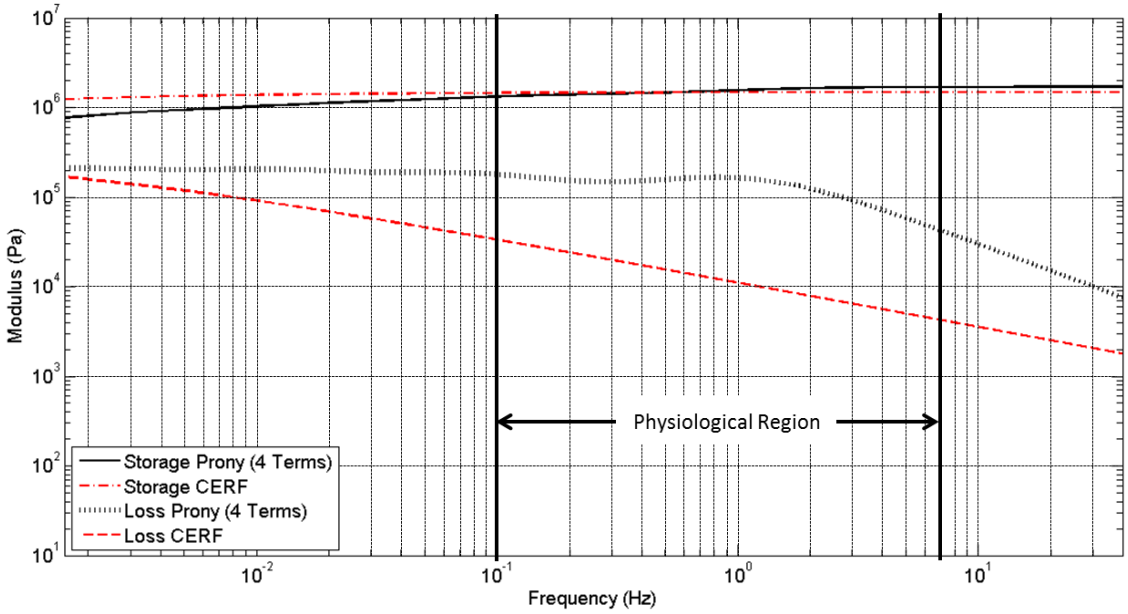

(b) Higher strain (17.32%)

Figure E.20: Compiled frequency domain information for case Adequan

Table E.11: Saline (f): Cartilage information and model parameters

	Strain Level #1	Strain Level #2
Date: 6/26/2012	Case #: 1102570	Fluid Bath: Saline
Age (yrs)	12	
Estimated Weight (kg)	453.6	
Use	Field	
Breed	American Quarter Horse	
Gender	M	
Plug Thickness (mm)	3.296	
Number of Thickness Samples	5	
Standard Dev. (mm)	0.102	
Displacement (mm)	0.250	0.350
Strain	**7.58%**	**10.60%**
Time Constant (s)	**15.71**	**19.37**
Normalized Time Constant Area	17.04	21.51
Normalized Total Area	32.86	38.17
Area Ratio	**51.85%**	**56.36%**
4-Term Prony Model Parameters		
Glassy Modulus (MPa)	**0.437**	**0.512**
E_0 (MPa)	0.064	0.072
E_1 (MPa)	0.062	0.067
E_2 (MPa)	0.051	0.059
E_3 (MPa)	0.097	0.119
E_4 (MPa)	0.163	0.196
λ_1 (1/s)	0.072	0.066
λ_2 (1/s)	5.590	4.913
λ_3 (1/s)	0.470	0.423
λ_4 (1/s)	0.012	0.011
Norm	1.17E+06	8.28E+05
3-Term Prony Model Parameters		
Glassy Modulus (MPa)	**0.473**	**0.488**
E_0 (MPa)	0.106	0.079
E_1 (MPa)	0.083	0.080
E_2 (MPa)	0.114	0.129
E_3 (MPa)	0.170	0.201
λ_1 (1/s)	14.315	1.363
λ_2 (1/s)	0.191	0.105
λ_3 (1/s)	0.017	0.013
Norm	1.30E+06	8.84E+05

Table: E.11 continued:

Fractional Model Parameters		
E_0 (Mpa)	0.293	0.348
E_1 (Mpa)	0.108	0.125
μ^2 (1/s)	0.030	0.023
α	1/2	1/2
Norm	1.25E+06	9.87E+05
Test Notes		
Test Time	9:15 am	
Approximate Demise to Collection Time	19 hours	
Time from Harvest to Test	<20 min	
Needle testing was performed before relaxation testing Test #2 was performed at the higher strain lever Test #5 was performed at the lower strain level		

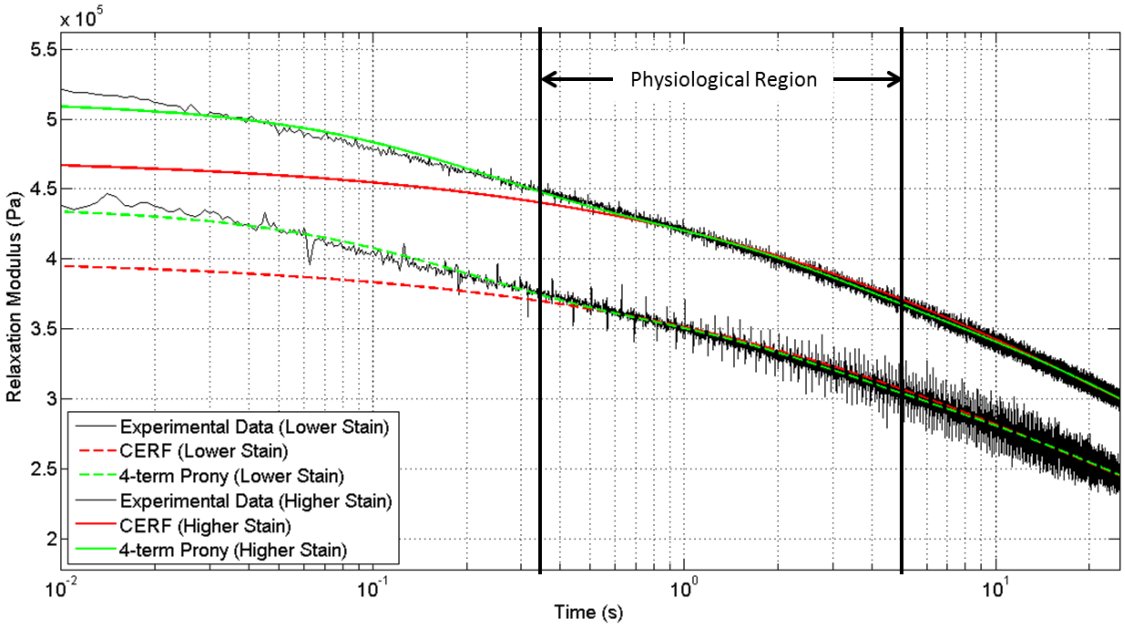

Figure E.21: Time-domain fits of experimental data on semi-log scale for case Saline (f)

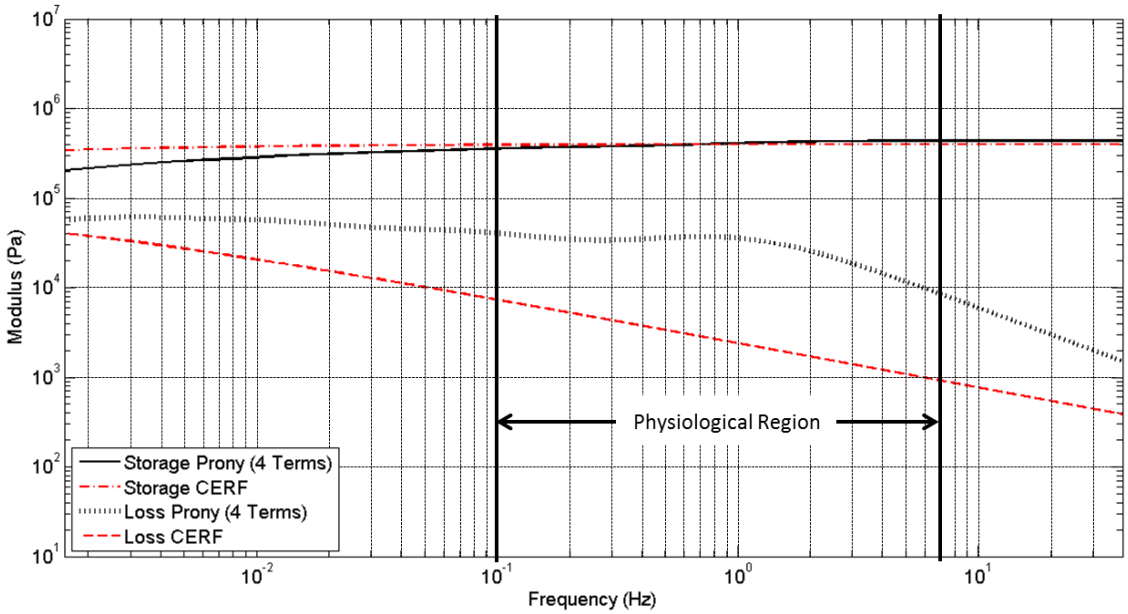

(a) Lower strain (7.58%)

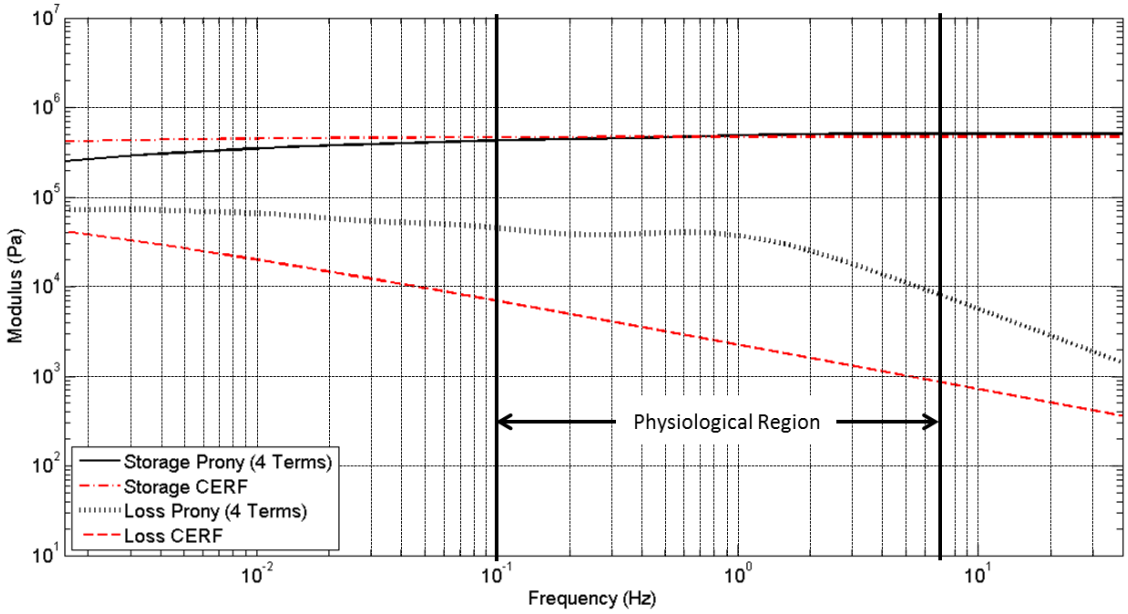

(b) Higher strain (10.60%)

Figure E.22: Compiled frequency domain information for case Saline (f)

REFERENCES

[1] Carolina, B. B. o. N., 2011. "Straight Talk About Health Care Costs".

[2] Bren, L., 2004. "Joint Replacement: An Inside Look". *FDA Consumer*(March-April).

[3] Grybos, G. R., 1991. "The dynamics of a viscoelastic rotor in flexible bearings". *Archive of Applied Mechanics,* ***61***(1), pp. 479–487.

[4] Friswell, M., 2007. "The Response of Rotating Machines on Viscoelastic Supports". *International Review of Mechanical Engineering,* ***1***(1), pp. 32–40.

[5] Elsharkawy, A. A., and Nassar, M. M., 1996. "Hydrodynamic lubrication of squeeze-film porous bearings". *Acta Mechanica,* ***118***, pp. 121–134.

[6] Hirsch, C., and Frey, H. D., 1944. "A contribution to the pathogenesis of chondromalacia of the patella; a physical, histologic and chemical study". PhD thesis, Karolinska institutet, Stockholm.

[7] Mow, V., Gu, W., and Chen, F., 2005. *Basic Orthopaedic Biomechanics & Mechano-biology*, 3. ed. Lippincott Williams & Wilkins, Philadelphia, PA, ch. Structure and function of articular cartilage and meniscus, pp. 181–258.

[8] Charnley, J., 1960. "The lubrication of animal joints in relation to surgical reconstruction by arthroplasty". *Annals of the rheumatic diseases,* ***19***, pp. 10–9.

[9] McCutchen, C. W., 1962. "The frictional properties of animal joints". *Wear,* ***5***(1), pp. 1–17.

[10] Ateshian, G. A., 2009. "The role of interstitial fluid pressurization in articular cartilage lubrication". *J Biomech,* ***42***(9), pp. 1163–76.

[11] Ateshian, G. A., Wang, H., and Lai, W. M., 1998. "The Role of Interstitial Fluid Pressurization and Surface Porosities on the Boundary Friction of Articular Cartilage". *Journal of Tribology,* ***120***(2), pp. 241–248.

[12] Ateshian, G. A., Warden, W. H., Kim, J. J., Grelsamer, R. P., and Mow, V. C., 1997. "Finite deformation biphasic material properties of bovine articular cartilage from confined compression experiments". *Journal of Biomechanics,* ***30***(11-12), pp. 1157–1164.

[13] Mow, V. C., Kuei, S. C., Lai, W. M., and Armstrong, C. G., 1980. "Biphasic Creep and Stress Relaxation of Articular Cartilage in Compression: Theory and Experiments". *Journal of Biomechanical Engineering,* ***102***(1), pp. 73–84.

[14] Lai, W. M., Mow, V. C., and Roth, V., 1981. "Effects of Nonlinear Strain-Dependent Permeability and Rate of Compression on the Stress Behavior of Articular Cartilage". *Journal of Biomechanical Engineering,* ***103***(2), pp. 61–66.

[15] Alford, J. W., and Cole, B. J., 2005. "Cartilage Restoration, Part 1". *The American Journal of Sports Medicine,* ***33***(2), pp. 295–306.

[16] McCutchen, C. W., 1959. "Mechanism of Animal Joints: Sponge-hydrostatic and Weeping Bearings". *Nature,* ***184***(4695), pp. 1284–1285.

[17] Fung, Y. C., 1967. "Elasticity of soft tissues in simple elongation". *Am J Physiol,* ***213***(6), pp. 1532–44.

[18] Kempson, G. E., Freeman, M. A. R., and Swanson, S. A. V., 1971. "The determination of a creep modulus for articular cartilage from indentation tests on the human femoral head". *Journal of Biomechanics,* ***4***(4), pp. 239–250.

[19] Mow, V. C., and Mansour, J. M., 1977. "The nonlinear interaction between cartilage deformation and interstitial fluid flow". *Journal of Biomechanics,* ***10***(1), pp. 31–39.

[20] Lipshitz, H., Mow, V. C., Torzilli, P. A., Eisenfeld, J., and Glimcher, M. J., 1976. "On the stress relaxation of articular cartilage during confined compression". In VII International Congress of Rheology, C. K. Kubat and J., eds., pp. 198–199.

[21] Eisenfeld, J., Mow, V. C., and Lipshitz, H., 1978. "Mathematical analysis of stress relaxation in articular cartilage during compression". *Mathematical Biosciences,* ***39***(1-2), pp. 97–112.

[22] Mow, V. C., Lipshitz, H., and Glimcher, M. J., 1977. "Mechanisms for Stress Relaxation in Articular Cartilage". In 23rd Annual Meeting of The Orthopaedic Research Society, T. O. R. Society, ed., Vol. 2, The Orthopaedic Research Society, p. 71.

[23] Armstrong, C. G., Lai, W. M., and Mow, V. C., 1984. "An Analysis of the Unconfined Compression of Articular Cartilage". *Journal of Biomechanical Engineering,* ***106***(2), pp. 165–173.

[24] Mak, A. F., 1986. "The Apparent Viscoelastic Behavior of Articular Cartilage—The Contributions From the Intrinsic Matrix Viscoelasticity and Interstitial Fluid Flows". *Journal of Biomechanical Engineering,* ***108***(2), pp. 123–130.

[25] Holmes, M. H., and Mow, V. C., 1990. "The nonlinear characteristics of soft gels and hydrated connective tissues in ultrafiltration". *Journal of Biomechanics,* ***23***(11), pp. 1145–1156.

[26] Suh, J. K., and DiSilvestro, M. R., 1999. "Biphasic Poroviscoelastic Behavior of Hydrated Biological Soft Tissue". *Journal of Applied Mechanics,* ***66***(2), pp. 528–535.

[27] DiSilvestro, M. R., Zhu, Q., and Suh, J.-K. F., 2001. "Biphasic Poroviscoelastic Simulation of the Unconfined Compression of Articular Cartilage: II—Effect of Variable Strain Rates". *Journal of Biomechanical Engineering,* ***123***(2), pp. 198–200.

[28] Lai, W. M., Hou, J. S., and Mow, V. C., 1991. "A triphasic theory for the swelling and deformation behaviors of articular cartilage". *J Biomech Eng,* ***113***(3), pp. 245–58.

[29] Desai, C. S., and Abel, J. F., 1972. *Introduction to the Finite Element Method*. Van Nostrand Reinhold Company.

[30] Coletti, J. M., Akeson, W. H., and Woo, S. L. Y., 1972. "A Comparison of the Physical Behavior of Normal Articular Cartilage and the Arthroplasty Surface". *The Journal of Bone and Joint Surgery,* ***54-A***(1), pp. 147–160.

[31] Woo, S. L. Y., Akeson, W. H., and Jemmott, G. F., 1976. "Measurements of nonhomogeneous, directional mechanical properties of articular cartilage in tension". *Journal of Biomechanics,* ***9***(12), pp. 785–791.

[32] Parsons, J. R., and Black, J., 1977. "The viscoelastic shear behavior of normal rabbit articular cartilage". *Journal of Biomechanics,* ***10***(1), pp. 21–29.

[33] Parsons, J. R., and Black, J., 1979. "Mechanical behavior of articular cartilage: Quantitative changes with alteration of ionic environment". *Journal of Biomechanics,* ***12***(10), pp. 765–773.

[34] Woo, S. L. Y., Simon, B. R., Kuei, S. C., and Akeson, W. H., 1980. "Quasi-Linear Viscoelastic Properties of Normal Articular Cartilage". *Journal of Biomechanical Engineering,* ***102***(2), pp. 85–90.

[35] Simon, B. R., Coats, R. S., and Woo, S. L. Y., 1984. "Relaxation and Creep Quasilinear Viscoelastic Models for Normal Articular Cartilage". *Journal of Biomechanical Engineering,* ***106***(2), pp. 159–164.

[36] Ehlers, W., and Markert, B., 2000. "A Linear Viscoelastic Two-Phase Model for Soft Tissues.: Application to Articular Cartilage". *ZAMM - Journal of Applied Mathematics and Mechanics / Zeitschrift fr Angewandte Mathematik und Mechanik,* ***80***(S1), pp. 149–152.

[37] Ehlers, W., and Markert, B., 2001. "A Linear Viscoelastic Biphasic Model for Soft Tissues Based on the Theory of Porous Media". *Journal of Biomechanical Engineering,* ***123***(5), pp. 418–424.

[38] Wilson, W., van Donkelaar, C. C., van Rietbergen, B., Ito, K., and Huiskes, R., 2004. "Stresses in the local collagen network of articular cartilage: a poroviscoelastic fibril-reinforced finite element study". *Journal of Biomechanics,* ***37***(3), pp. 357–366.

[39] Wilson, W., van Donkelaar, C. C., van Rietbergen, B., and Huiskes, R., 2005. "A fibril-reinforced poroviscoelastic swelling model for articular cartilage". *Journal of Biomechanics,* ***38***(6), pp. 1195–1204.

[40] Wang, J. L., Parnianpour, M., ShiraziAdl, A., and Engin, A. E., 1997. "Failure criterion of collagen fiber: Viscoelastic behavior simulated by using load control data". *Theoretical and Applied Fracture Mechanics,* ***27***(1), pp. 1–12.

[41] DiSilvestro, M. R., and Suh, J.-K. F., 2001. "A cross-validation of the biphasic poroviscoelastic model of articular cartilage in unconfined compression, indentation, and confined compression". *Journal of Biomechanics,* ***34***(4), pp. 519–525.

[42] Garcia, J. J., and Cortes, D. H., 2006. "A nonlinear biphasic viscohyperelastic model for articular cartilage". *J Biomech,* ***39***(16), pp. 2991–8.

[43] Julkunen, P., Wilson, W., Jurvelin, J. S., Rieppo, J., Qu, C.-J., Lammi, M. J., and Korhonen, R. K., 2008. "Stress relaxation of human patellar articular cartilage in unconfined compression: Prediction of mechanical response by tissue composition and structure". *Journal of Biomechanics,* ***41***(9), pp. 1978–1986.

[44] June, R. K., Ly, S., and Fyhrie, D. P., 2009. "Cartilage stress-relaxation proceeds slower at higher compressive strains". *Archives of Biochemistry and Biophysics,* ***483***(1), pp. 75–80.

[45] June, R. K., Mejia, K. L., Barone, J. R., and Fyhrie, D. P., 2009. "Cartilage stress relaxation is affected by both the charge concentration and valence of solution cations". *Osteoarthritis and Cartilage,* ***17***(5), pp. 669–676.

[46] Gurtin, M. E., and Sternberg, E., 1962. "On the linear theory of viscoelasticity". *Archive for Rational Mechanics and Analysis,* ***11***(1), pp. 291–356.

[47] Szumski, R. G., and Green, I., 1991. "Constitutive Laws in Time and Frequency Domains for Linear Viscoelastic Materials". *J. Acoustical Soc. of America,* ***90***(40), p. 2292.

[48] Miller, B., and Green, I., 1997. "On the stability of gas lubricated triboelements using the step jump method". *Journal of Tribology-Transactions of the Asme,* ***119***(1), pp. 193–199.

[49] Bagley, R. L., 1989. "Power law and fractional calculus model of viscoelasticity". *American Institute of Aeronautics and Astronautics,* ***27***(10), p. 6.

[50] Kisela, T., 2009. "Fractional Generalization of the Classical Viscoelasticity Models". *Aplimat 2009: 8th International Conference, Proceedings*, pp. 593–600.

[51] A. Erdelyi, W. Magnus, F. O., and Tricomi, F., eds., 1955. *Higher Transcendental Functions*, Vol. III. McGraw-Hill, New York.

[52] Szumski, R. G., 1993. "A Finite Element Formulation for the Time Domain Vibration Analysis of an Elastic-Viscoelastic Structure". PhD thesis, Georgia Institute of Technology.

[53] Abramowitz, M., and Stegun, I. A., eds., 1972. *Handbook of Mathematical Functions*. Dover Publications.

[54] Malda, J., Benders, K. E. M., Klein, T. J., de Grauw, J. C., Kik, M. J. L., Hutmacher, D. W., Saris, D. B. F., van Weeren, P. R., and Dhert, W. J. A., 2012. "Comparative study of depth-dependent characteristics of equine and human osteochondral tissue from the medial and lateral femoral condyles". *Osteoarthritis and Cartilage,* ***20***(10), pp. 1147–1151.

[55] Kestin, J., Sokolov, M., and Wakeham, W. A., 1978. "Viscosity of Liquid Water in the Range -8 C to 150 C". *J.Phys. Chem. Ref. Data,* ***7***(3), pp. 941–948.

[56] Tew, W. P., and Hotchkiss, R. N., 1981. "Synovial Fluid Analysis and Equine Joint Disorders". *Equine Veterinary Science*, pp. 163–170.

[57] Miller, B., and Green, I., 1998. "Constitutive Equations and the Correspondence Principle for the Dynamics of Gas Lubricated Triboelements". *Journal of Tribology,* ***120***(2), pp. 345–352.

[58] Hildebrand, F. B., 1987. *Introduction to Numerical Analysis*. Dover Publications.

[59] Green, I., 2012. Personal Communication.

[60] Smyth, P. A., Rifkin, R. E., Jackson, R. L., and Hanson, R. R., 2012. "A surface roughness comparison of cartilage in different types of synovial joints". *Journal of Biomechanical Engineering,* ***134***(2), p. 021006.

[61] Smyth, P. A., Rifkin, R. E., Jackson, R. L., and Reid Hanson, R., 2012. "The Fractal Structure of Equine Articular Cartilage". *Scanning*.

[62] Miller, B. A., 1996. "Constitutive Laws for Gas Lubricated Triboelements". Master's thesis, Georgia Institute of Technology.

[63] Mow, V. C., Ateshian, G. A., and Spilker, R. L., 1993. "Biomechanics of diarthrodial joints: a review of twenty years of progress". *Journal of Biomechanical Engineering,* ***115***(4B), pp. 460–7.

[64] Mow, V. C., Mak, A. F., Lai, W. M., Rosenberg, L. C., and Tang, L. H., 1984. "Viscoelastic properties of proteoglycan subunits and aggregates in varying solution concentrations". *Journal of Biomechanics,* ***17***(5), pp. 325–338.

[65] Vena, P., Gastaldi, D., and Contro, R., 2006. "A Constituent-Based Model for the Nonlinear Viscoelastic Behavior of Ligaments". *Journal of Biomechanical Engineering,* ***128***(3), pp. 449–457.